

NEUTRINOLESS DOUBLE BETA DECAY IN DEFORMED
NUCLEI: ITS IMPLICATIONS IN PARTICLE AND NUCLEAR
PHYSICS

DISSERTATION

zur Erlangung des Grades eines
Doktors der Naturwissenschaften

der Mathematisch-Naturwissenschaftliche Fakultät
der Eberhard–Karls–Universität zu Tübingen

vorgelegt von

FANG DONG-LIANG
aus Nantong, China

2010

Tag der mündlichen Prüfung:

28/01/2011

Dekan:

Prof. Dr. Wolfgang Rosenstiel

1. Berichterstatter:

Prof. Dr. Dr. h.c. mult. Amand Fäßler

2. Berichterstatter:

Prof. Dr. Josef Jochum

Ad patrem meum, Requiscat in Pace

Contents

Abstract	v
1 Introduction	1
2 New Physics and Emission Mechanism for $0\nu\beta\beta$	9
2.1 Neutrinos	9
2.1.1 Neutrino Oscillation and mixing	10
2.1.2 see-saw mechanism	12
2.2 Majorana Neutrinos in Neutrinoless Double-Beta-Decay	13
2.2.1 Simple Addition to SM	13
2.2.2 Grand Unification Theory	20
2.2.3 Sterile Kaluza-Klein Neutrinos in Extra Dimensions	25
2.3 R Parity Violated SuperSymmetry	29
2.3.1 SuperSymmetry Theories and MSSM	29
2.3.2 R Parity and Lepton Number Conservation	32
3 Decay Width and Nuclear Matrix Element for Double Beta Decay	39
3.1 General Results of Decay Widths	40
3.1.1 Decay width for $2\nu\beta\beta$	40
3.1.2 Half-lives for the $0\nu\beta\beta$	41
3.2 Nuclear Matrix Element For $0\nu\beta\beta$	44
4 Many Body Approaches for Calculation of NME	45
4.1 Quasi-particle RPA	45
4.1.1 Introduction of the pn-QRPA	48
4.1.2 pn-QRPA for deformed Nuclei	48
4.1.3 Final Expression for NME	50
4.1.4 Modification and Improvement for QRPA	52
4.2 Nuclear Shell Model	54
4.3 Other Methods	56
5 Results and Outlook	57
5.1 Choice of Model Parameters	58
5.2 Illustration of the Results for $M^{2\nu}$ and $M^{0\nu}$	65

5.2.1	Multipole Transition Strength from pn-QRPA	66
5.2.2	NME for $2\nu\beta\beta$	70
5.2.3	NME for $0\nu\beta\beta$	73
5.3	Prospect of Neutrinoless Double Beta Decay	89
6	Summary and Conclusions	93
7	Zusammenfassung	97
A	Brief Introduction to Superfield Formulation	101
B	Nuclear Mean Field	103
B.1	Nuclear Mean Field Potential for deformed nuclei	103
B.1.1	Harmonic Oscillators	103
B.2	Deformed Woods-Saxon Potential	104
	Bibliography	107

Abstract

This thesis is mainly devoted to the calculation of nuclear matrix element for neutrinoless double beta decay (hereafter $0\nu\beta\beta$). In addition to the calculations with spherical QRPA (Quasi-particle Random Phase Approximation) methods and other methods previously used by many groups, we develop the deformed version of QRPA, using the deformed wave-functions derived from the Woods-Saxon potential. We adopt a realistic force as the residual interaction, in order to get reliable intermediate states which are very important in the QRPA formalism. This generalization makes the QRPA method applicable to all nuclei either spherical or deformed.

In chapter 2, a detailed derivation and illustration of different possible emission mechanisms for $0\nu\beta\beta$ are demonstrated. We introduce different new physics models which will produce new phenomena beyond the Standard Model (SM). We give the Lagrangians which are related to lepton-number violation and weak interaction. With these terms we describe possible inner processes of the $0\nu\beta\beta$ by Feynman Diagrams.

In Chapter 3, we go on with realistic calculations of this process and deduce the half-lives from the underlying mechanisms. We transform the interactions originally between quarks to that of nucleons by the so-called hadronization process, and the non-relativistic approximation for nuclei is justified. A derivation of the complete expressions for both $2\nu\beta\beta$ and $0\nu\beta\beta$ NME is given.

In chapter 4, we introduce the many-body techniques which are required in the calculations, such as QRPA, NSM (Nuclear Shell Model) and others. Our focus is on the pn-QRPA (proton-neutron Quasi-particle Random Phase Approximations), we give the numerical details of the method and the modifications to treat deformed calculations. Finally we give also a derivation of the formulae for the NME (Nuclear Matrix Elements).

In the last chapter 5, we give our detailed results on this calculation. First some details of the wave-functions derived from the mean field approximations and also the pairings are discussed. Then we solve the QRPA equations. With these solutions we can give the multipole transition strength distributions as well as NMEs for $0\nu\beta\beta$ and $2\nu\beta\beta$. The distributions then can be compared with experiments to assess the reliability of our approach. The NME is what one really needs. It is the most important step on the final determinations of neutrino mass $\langle m \rangle_{ee}$. Our calculation is the calculation of $0\nu\beta\beta$ decay with realistic forces in deformed nuclei. The results for ^{150}Nd show that the general structure of the $0\nu\beta\beta$, such as the g_{pp} dependence and the dependence on the angular momenta of the neutron pairs, changed into proton pairs, have not been modified drastically except for a suppression from the overlaps between the BCS vacua for the parent and daughter nuclei. Our results give optimistic predictions, that ^{150}Nd should have the shortest $0\nu\beta\beta$ half-life. And with this achievement we may now have all $0\nu\beta\beta$ NMEs available. We wait now for the breakthroughs

from the experiments with values for $0\nu\beta\beta$ lifetimes. This will bring us further to the new era of physics beyond the Standard Models.

Chapter 1

Introduction

The establishment of the electroweak theory [1, 2] is one of the greatest achievements of physics in the last century. Together with the $SU(3)$ Quantum Chromodynamics (QCD) for strong interaction [3], physicists finally built the so called Standard Model (SM) based on quantum field theory developed in the middle of 20th century by Feynman, Schwinger *et. al.* [4, 5]. Experiments afterwards at the energy scales below several hundred GeV proved the success of the model except the lack of observation of the Higgs particle [6] which is responsible for the mass of various fermions and weak bosons. However, the faith of the existence of one unified interaction which incorporates all known interactions (electromagnetic, weak, strong and gravitation) pushed particle physics forward to search for new physics beyond standard model. There are experimental indications for this: The neutrino oscillations which proved the massive nature of the neutrinos. These ask for new theories: either modification of the standard model or for new physics beyond the SM. After the first decade of the new century, the LHC experiments started the search for not only the Higgs particle predicted by the SM but also other particles implicated by new physics models competing with the SM. But for the search of new physics, LHC experiments are the most promising but not the only ones. In fact the search for new particles from cosmic rays have already started, together with the search for lepton number violating processes in nuclei. All these experiments and observations will surely open a new era of physics and broaden our view of the universe further.

The economically cheapest way to detect physics beyond the SM, however, may be the confirmation of the $0\nu\beta\beta$, although these experiments are supposed to be time-consuming in account of the long half-life of the $0\nu\beta\beta$. But once the $0\nu\beta\beta$ is observed, this surely gives evidence of the incompleteness of the standard model and further data can also give us clues about new physics. Nonetheless, despite the claim of events for $0\nu\beta\beta$ from the Heidelberg-Moscow experiments [7], there is still not enough direct evidence whether the lepton-number and/or lepton-flavor violating processes truly exist in nature. Double beta-decay is a kind of special nuclear β decay first proposed by Mayer [8], which is originating from the energy difference between odd-odd and even even nuclei as shown in fig.1.1. These differences stem from the nuclear pairing which makes the even-even nuclei much more stable, because pairing between neutron or/and proton pairs will lower the energy of the ground state, the energy difference is the so called pairing energy (named gap) described in the BCS theory. So in this case, the emission with two electrons is possible since the neighboring odd-

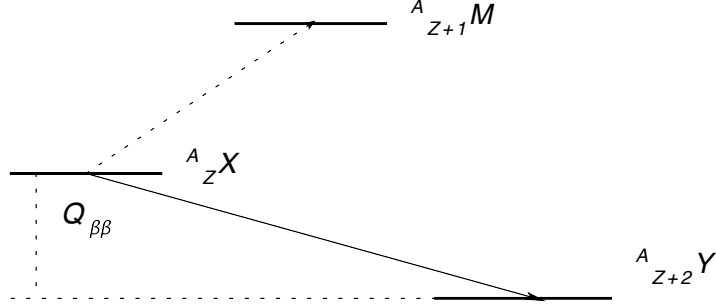


Figure 1.1: Graphical sketch of the energy levels for $\beta\beta$ -emitters. They(X) are even-even nuclei, and more stable than their neighboring odd-odd nucleus M. So single β -decay is forbidden, but decay to a neighboring even-even nucleus Y with $Z+2, A$.

odd nuclei is less stable compared to neighboring even-even nuclei with the same nucleon number A . Thus the even-even mass parent nucleus can decay to a neighboring even-even nucleus with $Z+2$ and $N-2$:

$$(A, Z) \rightarrow (A, Z + 2) + 2e^- + 2\bar{\nu} \quad (1.1)$$

Usually, in the SM, this process will emit two electrons together with two anti-electron neutrinos just as two successive single beta decays except the intermediate nucleus being replaced by intermediate virtual states. But, if the neutrinos are of Majorana nature, things will become more interesting. In this case, neutrinos are antiparticles of themselves, this makes it possible that the neutrino produced in double beta decay be reabsorbed, so no neutrinos will be observed. This is called neutrinoless double beta decay($0\nu\beta\beta$):

$$(A, Z) \rightarrow (A, Z + 2) + 2e^- \quad (1.2)$$

This process violates the conservation of lepton number which is thought to be an accidental symmetry but conserved in the SM. And this is important for the creation of baryons in the Big Bang. Present observation suggests a large excess of baryons over anti-baryons. Through the so-called leptogenesis mechanism [9], the non-conservation of lepton number will finally make our universe to be matter dominant.

Lepton number violation is not possible in the SM, so modifications or new theories beyond the SM are needed. This can be done by introducing lepton number violating interactions. We shall check different new physics theories for this. In fact, even for the SM, the lepton number as well as the baryon number are not conserved separately. $B - L$ should be instead a much more fundamental symmetry. In many new physics theories, the lepton number symmetry is violated. This allows the $0\nu\beta\beta$.

The easiest way of extending the SM to include the neutrino mass is to add a mass term of Majorana neutrinos which spontaneously violates the lepton number conservation. But this will not answer the question why the neutrino is so light (Current experiments from β decay and neutrino oscillations tell us that the mass of the electron neutrino is smaller than $1eV$, compared with

$0.5MeV$ of the lightest charged lepton, the electron). So new mechanisms were proposed to explain this mass hierarchy, of which the most promising one is the so-called "See-Saw" mechanism[10], with prediction of heavy right-handed neutrinos, together with Dirac and Majorana mass terms this can explain the smallness of the left-handed neutrino mass. There are different types of See-Saw depending on the types of Higgs particles which are responsible for all the mass terms. They are also closely related with the vacuum structure. These new Higgs particles are usually singlets of the SM but are multiplets of extra symmetries beyond the SM.

It has long been a dream of Grand Unification Theory (GUT) to unify electroweak and strong interactions into one[11] force. In this way, a larger gauge group is needed to be introduced as well as more Higgs particles responsible for the spontaneous symmetry breaking (SSB) at a higher energy scale above the SSB of electroweak interactions. In GUT theories of $SO(10)$, in certain SSB patterns [12], a left-right symmetric subgroup ($SU_L(2) \times SU_R(2)$) is predicted and hence the possible existence of right-handed neutrinos. This scenario will also give the appearance of a See-Saw model. The mass of left- and right- handed neutrinos in this model can be quite different due to the structure of the scalar vacuum. This will also affect the $0\nu\beta\beta$ due to neutrino mixings between the left- and right-handed ones. But considering the heavy mass of the right-handed gauge bosons (Must larger than W and Z bosons), this contribution should be small with the ratio $\kappa = M_L/M_R$. The $L - R$ symmetric model with suitable Higgs sectors will automatically give the see-saw mechanism with the lepton number violation (only $B - L$ is conserved). But new problems may emerge such as the proton decay and the hierarchy problem due to the huge difference between the broken energy scales.

To realize the see-saw mechanism, there are also other possibilities such as that of the existence of extra dimensions[13] which are warped with a small radius. This will lower the Planck scale and solve the naturalness problem of the SM by the hierarchy between the mass scales of electroweak and gravity. In this scenario, if we introduce sterile neutrinos[14] (not the neutrinos of the SM) which can travel in this short warped interval while SM particles are stucked to a 3-brane (our world) located somewhere in the fifth dimension. This is an attractive proposal, as we need only to add one single sterile neutrino and this new five dimensional particle will automatically give the smallness of the left-handed neutrinos like that in See-Saw. In this case, after the compactification of the fifth dimension, we can get many resonant states of neutrinos called Klein-Kaluza particles which act as the right-handed neutrinos in see-saw. And with certain boundary conditions we will find the lightest states to be left-handed states and also the smallness of neutrino mass can be explained. By adjusting the position of the brane in the fifth dimension and the compactified radius we can get the correct magnitude of the decay width of the $0\nu\beta\beta$ as from GUT without the annoyance of many extra heavy gauge bosons and Higgs particles.

Above we discussed the mediating neutrinos which must be Majorana particles. Are there possibilities that the mediating particle can be something other than neutrinos? The answer is perhaps yes. In the supersymmetry if the R parity, which is +1 for SM particles and -1 for their SUSY partners, is violated. Then there is the possibility for heavy SUSY particles to decay into SM particles and also quarks into leptons which allows $0\nu\beta\beta$. SUSY theory[15] is considered to be one of the most promising theories beyond the SM, it relates the fermions with the bosons by supersymmetry, and the equality of boson and fermion degrees of freedom may solve many problems in

the SM and GUT such as the axial symmetry anomaly from introductions of new particles and the hierarchy problem. Because of the non-observation of these superpartners of the SM particles, it is suggested that the symmetry is broken, and if we introduce the R-parity and its conservation, we will have the lightest SUSY particle (LSP) which is stable with heavy mass served as the candidate for Dark matter. However, to incorporate lepton and baryon number violation, we must take into consideration the violation of R-parity. But in addition to $0\nu\beta\beta$, this will also give rise to the existence of proton decay, so this violation should be well constrained by recent experiments. For $0\nu\beta\beta$, in this case, weak bosons and mediating neutrinos are replaced by SUSY particles.

The above mechanisms should not be the only possibilities for the $0\nu\beta\beta$. Actually new theories beyond the SM may contribute, especially those, which contain lepton number violating terms. If these mechanisms co-exist, the important task is to determine whether one is dominant or if they contribute of comparable weight. The nature of these mechanisms can be a proof of new physics beyond SM. So we need first to calculate the experimental observables from the realistic, effective theories instead of interactions from first principles. Usually one replaces then quarks by nucleons and one integrates out the heavy mediating particles as in weak interactions the W and Z bosons. In the $0\nu\beta\beta$ we expect that the weak interactions are most important, since comparing with other new particles from theories beyond the SM, weak bosons should have the lightest masses hence give the largest interaction strength at an effective four-fermion vertex. So if the neutrinos are truly Majorana, then we can take the most simple emission mechanism of Majorana neutrinos to be the leading contribution. Besides these mechanisms for $0\nu\beta\beta$ discussed above, we should be aware that the nuclear environment which guarantees this process should also be carefully examined.

So we need well established nuclear structure theories which could well interpret both $0\nu\beta\beta$ and $2\nu\beta\beta$. As $2\nu\beta\beta$ is well observed for various nuclei and contains only physics we know, it can serve as a good test for nuclear theories which can then be applied to the $0\nu\beta\beta$. After decades of development, from the early simple treatment by the time of discovery of the $2\nu\beta\beta$, we now have several tools for the calculation of $\beta\beta$ -decay.

The $\beta\beta$ emitters lie in the medium and heavy atomic mass region with nucleon numbers from tens to hundred, the lightest one is ^{48}Ca , with 20 protons and 28 neutrons. So we are dealing with nuclear many-body systems which are complicated to deal with not only because of the many-body problems but also the troublesome and mainly unknown nucleon-nucleon interactions. Nucleons are bound systems of quarks and feel the strong interactions. The strong interaction are described by quantum chromodynamics(QCD). The important feature of this theory is asymptotic freedom and color confinement. This poses great difficulties for the calculations of the nucleon properties from first principles. In spite of some non-perturbative attempts such as "Lattice QCD", we resort here to nuclear models. In nuclear structure theories, these models can be classified into different categories as empirical or phenomenological. The empirical models are constructed from the bare nuclear force, such as the Brückner G-matrix [16]. These realistic nucleon-nucleon interactions are then suitable for describing the nuclei. The phenomenological ones are constructed with some analytic expressions with several parameters which are adjusted to reproduce the properties of nuclei, i.e. the Skyrme force [18] or the Gogny force [17]. The nuclear many-body problems are usually dealt with the Hatree-Fock(HF) approach or its generalization Hatree-Fock-Bogoliubov (HFB) taking into consideration also nuclear pairing.

Table 1.1: Half-life and experimental nuclear matrix element values for the two neutrino double beta decay [28]

Isotope	$T_{1/2}(2\nu)$, yr	$M^{2\nu}$
^{48}Ca	$4.4^{+0.6}_{-0.5} \times 10^{19}$	$0.0238^{+0.0015}_{-0.0017}$
^{76}Ge	$(1.5 \pm 0.1) \times 10^{21}$	$0.0716^{+0.0025}_{-0.0023}$
^{82}Se	$(0.92 \pm 0.07) \times 10^{20}$	$0.0503^{+0.0020}_{-0.0018}$
^{96}Zr	$(2.3 \pm 0.2) \times 10^{19}$	$0.0491^{+0.0023}_{-0.0020}$
^{100}Mo	$(7.1 \pm 0.4) \times 10^{18}$	$0.1258^{+0.0037}_{-0.0034}$
$^{100}\text{Mo}-^{100}\text{Ru}(0_1^+)$	$5.9^{+0.8}_{-0.6} \times 10^{20}$	$0.1017^{+0.0056}_{-0.0063}$
^{116}Cd	$(2.8 \pm 0.2) \times 10^{19}$	$0.0695^{+0.0025}_{-0.0024}$
^{128}Te	$(1.9 \pm 0.4) \times 10^{24}$	$0.0249^{+0.0031}_{-0.0023}$
^{130}Te	$(6.8^{+1.2}_{-1.1}) \times 10^{20}$	$0.0175^{+0.0016}_{-0.0014}$
^{150}Nd	$(8.2 \pm 0.9) \times 10^{18}$	$0.0320^{+0.0018}_{-0.0017}$
$^{150}\text{Nd}-^{150}\text{Sm}(0_1^+)$	$1.33^{+0.45}_{-0.26} \times 10^{20}$	$0.0250^{+0.0029}_{-0.0034}$
^{238}U	$(2.0 \pm 0.6) \times 10^{21}$	$0.0271^{+0.0053}_{-0.0033}$
^{130}Ba ; ECEC(2ν)	$(2.2 \pm 0.5) \times 10^{21}$	$0.105^{+0.014}_{-0.010}$

The approaches used commonly for the $0\nu\beta\beta$ are the nuclear shell model(NSM) and the Quasi-particle Random Phase Approximations(QRPA). The shell model gives a very good description of the observed properties of nuclei. In principle, it can be the most reliable method, however, for the medium and heavy nuclei involved in $\beta\beta$ -decay, the basis space increases so drastically, that it makes the numerical calculations beyond pf -shell impossible. Only for the candidate ^{48}Ca a full pf -shell calculation has been performed [19], for other $\beta\beta$ decay nuclei, severe truncations are used. This makes the calculation less reliable. But for $QRPA$ these severe truncations can be avoided with however limited many-body configurations included. The pn -QRPA is an approximation to the nuclear many body problems, which uses the groundstates derived from the HF meanfield with pairing and constructs the states of the intermediate nucleus by neutron-proton quasiparticle excitations. It is the most popular method for calculating the $\beta\beta$ -decay. However, there are also drawbacks: The matrix elements become extremely sensitive at the physically acceptable region to the particle-particle strength (g_{pp}), this is due to the overestimation of the ground state correlations which lead for increased particle-particle force to a collapse of the QRPA ground states. Since QRPA uses the Quasiboson approximation(QBA), which violates the Pauli exclusion principle. So generalizations are made to remove this violation. This is the so-called Renormalized QRPA(RQRPA)[21, 22, 23]. pn -RQRPA largely reduces the overestimated groundstate correlations and prevents the collapse of pn -QRPA solutions and makes the matrix element less sensitive to g_{pp} . But it has also shortcomings. It violates of the Ikeda sum rule and the particle number conservation. This was further investigated and the Fully Renormalize QRPA(FRQRPA)[24] was proposed to overcome these problems. Besides these two methods, a bunch of other methods are also used for the calculations, such as pseudo-SU(3)[25], the projected HFB[26], and the IBM-2[27].

These methods are good cross checks for the calculations.

Currently, over 10 $2\nu\beta\beta$ nuclei have been observed. Their half-lives range from 10^{19} up to 10^{24} years(see table.1.1). Despite of the quite different half-lives, the matrix elements $M^{2\nu}$ are somehow of the same magnitude. So the difference comes largely from the difference of the phase space factor related to the decay energy. We expect this to be similar for the $0\nu\beta\beta$ -decay. From table1.1, we see that ^{150}Nd has the shortest $2\nu\beta\beta$ life time. From table1.2, we see that it has also the largest phase space factors for both $0\nu\beta\beta$ and $2\nu\beta\beta$. One can expect it has also the shortest half-life for the $0\nu\beta\beta$. This expectation can be verified with a reliable calculation of the nuclear matrix element. But we have also a new challenge as ^{150}Nd is heavier and also known to be deformed. All the discussion above are based on the assumption, that the nuclei are spherical. This in fact may be true for most of the medium mass nuclei, since the measured deformations are rather small, but for ^{150}Nd , this could be a different story. As ^{150}Nd seems to be the best candidate for the $0\nu\beta\beta$, we need also reliable calculations for it. Thus realistic calculations for deformed nuclei are needed. The basic idea here is to generalize the spherical calculations to the deformed case by abandoning certain symmetries such as the rotational symmetry. Then the angular momentum is no longer a good quantum number and the degeneracy of states with different angular momentum projections is destroyed. This increases the number of separate energy levels. So for the shell model, it becomes even more impossible to do realistic calculations, while for QRPA we can avoid this difficulty. The deformed pn-QRPA approach, was developed by ref.[29] for $2\nu\beta\beta$,and good agreement has been achieved with experiments. In this work we will extend this approach to the calculations of the $0\nu\beta\beta$ and predict the half-life of ^{150}Nd .

Table 1.2: characteristics of $2\nu\beta\beta$ candidates [28]

Isotope	T_0 , keV	$(G^{2\nu})^{-1}$, yr	$(G^{0\nu})^{-1}$, yr
^{48}Ca	4274 ± 4	2.52×10^{16}	4.10×10^{24}
^{76}Ge	2039.00 ± 0.05	7.66×10^{18}	4.09×10^{25}
^{82}Se	2995.5 ± 1.9	2.30×10^{17}	9.27×10^{24}
^{96}Zr	1142.9 ± 1.9	4.34×10^{20}	1.57×10^{26}
^{100}Mo	3030 ± 6	1.06×10^{17}	5.70×10^{24}
^{116}Cd	2809 ± 4	1.25×10^{17}	5.28×10^{24}
^{128}Te	868.0 ± 1.5	1.18×10^{21}	1.43×10^{26}
^{130}Te	2533.3 ± 2.0	2.08×10^{17}	5.89×10^{24}
^{150}Nd	3367.7 ± 2.2	8.41×10^{15}	1.25×10^{24}
^{238}U	1144.2 ± 1.2	1.47×10^{18}	1.68×10^{24}

The thesis is arranged as follows: in chapter 2 we will discuss the underlying new physics which may govern the $0\nu\beta\beta$ process. Various models with new physics beyond the SM are introduced and the $0\nu\beta\beta$ Feynman diagrams are constructed, which show how the processes take place at the fundamental level. In chapter 3, we are dealing with the problem of how to realize this process at the nucleon and nuclear level and perform the actual calculations. In Chapter 4, different many

body approaches are introduced with the details of how to finalize the calculations of $\beta\beta$ NME; and in the last chapter we show the results of our calculation and make some predictions on the $0\nu\beta\beta$ for ^{150}Nd .

Chapter 2

New Physics and Emission Mechanism for $0\nu\beta\beta$

In this chapter, we will present the possible underlying physics behind the $0\nu\beta\beta$, since in the SM the lepton number violation is strictly forbidden. Nevertheless, for various models beyond the SM, the $B - L$ (Baryon minus Lepton number) symmetry instead of separate lepton and baryon conservations are commonly considered as intrinsic symmetries. In this sense, many new physics models may be eyed as underlying theories for the $0\nu\beta\beta$ from GUT to SUSY. We will present these theories and also demonstrate how these theories can be realized in the actual $0\nu\beta\beta$ process. In this chapter we study first the underlying emission mechanisms, these are at the level of quarks which are thought to be the basic constituent of hadronic matter. In the next chapter we will describe the realization of these mechanisms at the levels of hadrons and nuclei. This will involve many effective theories. So in this chapter we will try to construct the Feynman diagrams. To do this, we notice that at the underlying level, this process is due to two d quarks decaying into two u quarks with two electrons e^- emitted (for $2\nu\beta\beta$ also two neutrinos), as illustrated in fig.2.3. What we need now is the structure inside the black box in fig.2.3. Usually the decay has an energy of several MeV. It is therefore impossible for massive decay products but perhaps for massless particles. We will in the following explore all these possibilities of the underlying emission mechanisms.

2.1 Neutrinos

The simplest theory for lepton number violation is that the neutrinos are Majorana particles. A Majorana mass term will yield the lepton number violation. In this case we can construct the $0\nu\beta\beta$ process with a virtual intermediate neutrino, as we shall see in this section. To deal with Majorana neutrinos, first we must have some basic knowledges on neutrinos.

Neutrinos were first proposed by Pauli [30] in 1930's in order to explain the continuum electron energy spectrum of β decay, and only later it was discovered [31]. It has no electric charge, and thus is only engaged in weak interaction. In the SM, it is the up component of left-handed lepton doublet which interact with W and Z bosons with assigned hypercharge $Y = -1$. There exists a one-to-one correspondence for neutrinos and charged leptons: $e - \nu_e$, $\mu - \nu_\mu$, $\tau - \nu_\tau$, From the Z^0

	Reps.	Y	mass range
$\begin{pmatrix} U \\ D \end{pmatrix}_L$	(3,3,1)	1/3	1MeV-100GeV
U_R	(3,1,1)	4/3	1MeV-100GeV
D_R	(3,1,1)	-2/3	1MeV-100GeV
$\begin{pmatrix} N \\ E \end{pmatrix}_L$	(1,3,1)	-1	eV-GeV
E_R	(1,1,1)	-2	MeV-GeV
$N_R(?)$	(1,1,0)	0	(?)

Table 2.1: Fermions in Standard Models with symmetry $SU(3)_c \times SU(2)_L \times U(1)_Y$, where quarks undergo both strong and electroweak interactions, while leptons participate in electroweak interactions. We have no direct experimental evidence for the right-handed neutrinos, so we have no idea whether they exist nor how heavy they are.

decay experiments [32] we can derive, that only 3 generations of neutrinos (below 45GeV) exist just as quarks and charged leptons, which engage in weak interactions (see table.2.1). If we add the right handed neutrinos into this model, then they are just singlets for all gauge interactions in the SM. This means they will not interact with other SM particles. In the SM, Higgs particles, which are thought to be the origin of masses for heavy weak bosons and leptons, will not give mass to neutrinos. So, in the SM, neutrinos are massless Dirac fermions. This is supposed so until the discoveries of the neutrino oscillations.

2.1.1 Neutrino Oscillation and mixing

Neutrino Oscillations were first proposed by Pontecorvo [33] to explain the deviation between the theory and observed flux of solar neutrinos. Instead of modifying the the nuclear fusion model for stars, the loss of the observed neutrinos is assigned to the mixing among different flavors of neutrinos, just as the so-called Cabbibo angle [34] for quarks. This process requires two conditions: the massive nature of neutrinos with inequality of their masses and different eigenvectors for mass and weak eigenstates in Hilbert space. As with the CKM [34, 35] matrix for quarks, the weak neutrino eigenstates can be expressed as decompositions of mass eigenstates:

$$\nu_L = \sum_i V_{Li} \nu_i \quad (2.1)$$

where L is the family index for weak interaction and i 's are the mass indices. V_{Li} is the mixing matrix, which is unitary as for quark mixing. This matrix is called $PMNS$ (Pontecorvo-Maki-Nakagawa-Sakata) matrix [33, 36]. For three generations, the $PMNS$ matrix is 3×3 , which has 8 parameters, if it is unitary. But some of the parameters can be absorbed into the phases of the fermions. If neutrinos are Dirac particles, then 3 phases (one for each generation) and one overall phase can be absorbed, so 4 parameters are left for the CKM and the PMNS matrices, 3 are rotational angles from the mass eigenstate basis to that of weak interactions, and one phase as for quarks is responsible for CP violations. But if neutrinos are Majorana particles, 2 more phases will

be present in the PMNS matrix, and it will play an important role in the calculations of effective neutrino mass in the $0\nu\beta\beta$ as we shall see. In literature, the most frequently used parameterization has the form as [37]:

$$V = R_{23}U_{13}R_{12}P_{12} \quad (2.2)$$

R_{23} and R_{12} are just rotation matrix between the three mass eigenvector space:

$$R_{12} = \begin{pmatrix} \cos \theta_{12} & \sin \theta_{12} & 0 \\ -\sin \theta_{12} & \cos \theta_{12} & 0 \\ 0 & 0 & 1 \end{pmatrix} \quad R_{23} = \begin{pmatrix} 1 & 0 & 0 \\ 0 & \cos \theta_{23} & \sin \theta_{23} \\ 0 & -\sin \theta_{23} & \cos \theta_{23} \end{pmatrix}$$

and U_{13} is similar but combined with one dirac phase and P_{12} pure phase matrix:

$$U_{13} = \begin{pmatrix} \cos \theta_{13} & 0 & \sin \theta_{13}e^{-i\delta} \\ 0 & 1 & 0 \\ -\sin \theta_{13}e^{i\delta} & 0 & \cos \theta_{13} \end{pmatrix} \quad P_{12} = \begin{pmatrix} e^{i\beta_1} & 0 & 0 \\ 0 & e^{i\beta_2} & 0 \\ 0 & 0 & 1 \end{pmatrix}$$

where β_1 and β_2 are Majorana phases which equal to 0 if neutrinos are Dirac particles and δ is the Dirac phase. This is the most apparent parameterization which shows the essentials of the neutrino mixing. But it is more convenient to adopt the following one:

$$V = U_{23}U_{13}U_{12} \quad (2.3)$$

where the phases are absorbed into rotation matrix with:

$$\begin{aligned} U_{23} &= \begin{pmatrix} 1 & 0 & 0 \\ 0 & \cos \theta_{23} & \sin \theta_{23}e^{-2i\delta_{23}} \\ 0 & -\sin \theta_{23}e^{i\delta_{23}} & \cos \theta_{23} \end{pmatrix} \\ U_{13} &= \begin{pmatrix} \cos \theta_{13} & 0 & \sin \theta_{13}e^{-i\delta_{13}} \\ 0 & 1 & 0 \\ -\sin \theta_{13}e^{i\delta_{13}} & 0 & \cos \theta_{13} \end{pmatrix} \\ U_{12} &= \begin{pmatrix} \cos \theta_{12} & \sin \theta_{12}e^{-i\delta_{12}} & 0 \\ -\sin \theta_{12}e^{i\delta_{12}} & \cos \theta_{12} & 0 \\ 0 & 0 & 1 \end{pmatrix} \end{aligned} \quad (2.4)$$

Here the phases are related to the Dirac and Majorana phases as: $\delta_{23} = \beta_2$, $\delta_{13} = \delta + \beta_1$ and $\delta_{12} = \beta_1 - \beta_2$. With these matrix we can show how the oscillation takes place.

In quantum mechanics, the free neutrinos propagate in vacuum as plane waves $|\nu_i(t)\rangle = e^{-i(E_i t - \vec{p} \cdot \vec{x})} |\nu_i(0)\rangle$. If the neutrino has a very small mass, then the energy $E_i = \sqrt{p^2 + m_i^2} \approx p + \frac{m_i^2}{2p}$, and thus $p \approx E$. The neutrino travels with nearly the velocity of light. So when neutrino travels for a distance L , the evolution of the neutrino wave function has the form

$$|\nu_i(t)\rangle \approx e^{-ipL} e^{-\frac{im_i^2 L}{2E}} |\nu_i(0)\rangle \quad (2.5)$$

Apart from a common irrelevant phase e^{-ipL} , which drops out, if one calculates probabilities. Because of the mixing among different weak eigenstates, the flavor eigenstates can be expanded as

$$|\nu_L(t)\rangle = \sum_i U_{Li} |\nu_i(t)\rangle = e^{-ipL} \sum_i U_{Li} e^{-\frac{im_i^2 L}{2E}} |\nu_i\rangle \quad (2.6)$$

during the propagation. As we know, only anti-electron neutrino can be produced at the core of the sun with the reaction $4H \rightarrow 4He + 2e^- + 2\bar{\nu}_e$, however, if we observe it from the earth and neglect the effect of the medium of the solar and earth sphere, the probability is

$$P_{e'e} = |\langle \nu_e | \nu_{e(solar)} \rangle|^2 = \left| \sum_i U_{ei}^* U_{ei} e^{-\frac{im_i^2 L}{2E}} \right|^2 \quad (2.7)$$

Here L is the distance from the sun to the earth. If we make a simple assumption that only two generations of neutrinos exist, we reduce the $PMNS$ matrix to:

$$\begin{pmatrix} \cos \theta & \sin \theta \\ -\sin \theta & \cos \theta \end{pmatrix} \quad (2.8)$$

with $V_{e1} = \cos \theta$ and $V_{e2} = \sin \theta$. Then we can get the probability of observing an $\bar{\nu}_e$ originally emitted from the sun as:

$$P_{e'e} = \left| \cos^2 \theta e^{-\frac{im_1^2 L}{2E}} + \sin^2 \theta e^{-\frac{im_2^2 L}{2E}} \right|^2 = 1 - \sin^2 \theta \sin \frac{\Delta m_{12}^2 L}{4E} \quad (2.9)$$

here Δm_{12}^2 is defined as $\Delta m_{12}^2 \equiv m_2^2 - m_1^2$. As we can see here the measured number of neutrinos at earth will not equal to the numbers produced in the sun unless that $\frac{\Delta m_{12}^2 L}{4E} = 2n\pi (n \in \mathbb{Z})$. This perfectly explains the missing neutrinos. If we generalize this to three generations, the expression will become complicated, the expression are given in ref.[37].

Current experimental results for mixing parameters are [38]: the mixing angles with $\theta_{23} \approx \pi/4$, $\theta_{13} \leq \pi/13$, $\theta_{12} \approx \pi/5.4$ and the square mass difference $\delta m_{21}^2 \approx 7.65 \times 10^{-5} eV^2$, $|\delta m_{23}^2| \approx 2.4 \times 10^{-3} eV^2$. These are derived from solar neutrino and also atmospheric neutrino experiments. As we saw above, the neutrino oscillation experiments give us only the differences of the squared masses but not the absolute magnitude. So from the current results of Δm_{ij}^2 , we still can have different schemes for neutrino masses:

- i) Normal hierarchy: $m_1, m_2 \ll m_3$. In this case the three masses have a normal order as the flavor states, and the mass of $m_3 \approx \sqrt{\delta m_{23}^2}$. There may be two different cases as well, that is $m_1 \approx m_2$ or the full hierarchy case $m_1 \ll m_2$.
- ii) Inverted hierarchy: $m_1 \approx m_2 \gg m_3$. In this case the heaviest neutrinos are ν_1 and ν_2 , since $m_{12}^2 \ll m_{23}^2$, so we can say that ν_1 and ν_2 have nearly degenerate masses.
- iii) Degenerate masses: $m_1 \approx m_2 \approx m_3$. in order to realize this relation, we should have the inequality as $m_3^2 \approx m_2^2 \gg m_{23}^2$.

The improvement of the precision of the experiments will not help us to distinguish among above possibilities, instead we need other experiments besides the oscillations. These can be the single and double beta decays which measure the absolute mass scale of the neutrino mass. The single β decay measures the neutrino mass as $m_e = \sqrt{\sum_j |U_{ej}|^2 m_j^2}$ directly from the electron spectrum's end point. In this work we will discuss the $0\nu\beta\beta$, which will give us also an effective mass of the electron neutrino in the form of $|\langle m_{\beta\beta} \rangle| = |\sum_j V_{ej}^2 m_j|$ as well as the Dirac or Majorana nature of neutrino.

2.1.2 see-saw mechanism

The main question concerning the neutrino mass is that it is too small compared even to the electron, the lightest electrically charged fermion in the SM. For the degenerate case, the mass

scale for neutrinos is of about 1eV , while the electron has a mass of 0.5MeV , the τ 1.777GeV and the top quark 174GeV . This large mass hierarchy is somehow very unnatural, so various theories were proposed. For the top quark mass there is the top see-saw, and for neutrinos the neutrino see-saw [39] model. The general idea of the see-saw mechanism is that the low mass of the particle we observe is due to the existence of another superheavy particle which mixes with the former, after diagonalisation, the tiny mass will appear. We assume also the existence of right-handed neutrinos. The mass is a mixture of both Dirac and Majorana masses. So in the mass Lagrangian, both terms will be present

$$\mathcal{L}_{mass} = m_L \nu_L^c \nu_L + m_D \bar{\nu}_L \nu_R + M_R \nu_R^c \nu_R + h.c. \quad (2.10)$$

so we have the mass matrix as:

$$\begin{pmatrix} m_L & m_D \\ m_D^T & M_R \end{pmatrix} \quad (2.11)$$

By dignolization, we can have the mass eigenvalues, for the light neutrinos:

$$m_\nu = m_L - m_D M_R^{-1} (M_D)^T \quad (2.12)$$

Depending on whether the first or the second terms dominate in the expression, the see-saw mechanism can be divided into two types: Type I which is usually without the m_L term and Type II which usually has the first terms by the introductions of the triplet Higgs particles [40] as we shall see later.

Besides these possibilities, it is also possible to introduce a singlet neutrino which can have interactions with the right handed neutrinos, in this case, the left- and right- handed neutrinos are both Dirac particles with definite mass, and the Majorana mass term originates from the singlet neutrino, the mass matrix may have the form:

$$\begin{pmatrix} 0 & m_{LR} & 0 \\ m_{LR} & 0 & M_{RS} \\ 0 & M_{RS}^T & M_{SS} \end{pmatrix} \quad (2.13)$$

this is called the double see-saw mechanism [41].

All these mechanisms assume that the small masses of the neutrinos come from a large mass scale from neutrinos which are singlets in the SM, but the origin of the neutrino mixing is still unclear. Theories concerning the mixing usually related it to the family symmetry, which is global and broken by a Goldstone boson [42].

2.2 Majorana Neutrinos in Neutrinoless Double-Beta-Decay

2.2.1 Simple Addition to SM

In the SM, the electroweak interaction is mediated by electroweak gauge bosons which span the *adjoint representation* of the $SU(2)_L \times U(1)_Y$ symmetry group. Left handed fermions form the *fundamental representation* of the $SU(2)_L$ (For the first generation, the quark doublet $\psi_L^T = (u_L, d_L)$ and lepton doublet (ν_L, e_L)). The right handed fermions are the singlets of $SU(2)_L$ such

as e_R , u_R and d_R (notice that the right-handed neutrinos have zero hypercharge). Under gauge symmetry, the Lagrangian for fermions can be written as:

$$\mathcal{L} = -\frac{1}{4}(G_{\mu\nu}^a G^{a\mu\nu} + B_{\mu\nu} B^{\mu\nu}) + \bar{\psi}_L i \not{D} \psi_L + \bar{\psi}_R i \not{D} \psi_R \quad (2.14)$$

Here, $G_{\mu\nu}^a \equiv \partial_\mu W_\nu^a - \partial_\nu W_\mu^a - g_2 \epsilon^{abc} W_\mu^b W_\nu^c$ and $B_{\mu\nu} \equiv \partial_\mu B_\nu - \partial_\nu B_\mu$ are field strength for the non-Abelian $SU(2)_L$ and Abelian $U(1)_Y$ electroweak gauge bosons, and the gauge covariant derivative for the doublet is $\not{D} \psi_L \equiv \gamma^\mu (\partial_\mu + i \frac{g_1}{2} Y B_\mu + i g_2 \frac{\tau^a}{2} W_\mu^a) \psi_L$ while for singlet $\not{D} \psi_R \equiv \gamma^\mu (\partial_\mu + i \frac{g_1}{2} Y B_\mu) \psi_R$. Here Y is the so called hypercharge listed in table 2.1 for different particles in the SM and we can see from table 2.1, that right handed neutrinos have a hypercharge zero. They will not interact with the standard model gauge bosons.

From the above Lagrangian, we see that in gauge theory, no mass term can be presented due to the gauge invariance. However, if there exists a complex scalar doublet (named after Higgs[6]) which interacts with gauge bosons like:

$$\mathcal{L}_H = (D^\mu \Phi)^* D_\mu \Phi - V(\Phi) \quad (2.15)$$

where $D_\mu \Phi = (\partial_\mu + i \frac{g_1}{2} B_\mu + i g_2 \frac{\tau^a}{2} W_\mu^a)$ is the gauge covariant derivative for the scalar field and if this Higgs particle has the potential of the form $V(\Phi) = -\mu^2 \Phi^\dagger \Phi + \lambda (\Phi^\dagger \Phi)^2$, with the minimum of this potential not at the point $\Phi = 0$. Then the Higgs field has a nonzero vacuum expectation value $\langle \Phi \rangle^T = (0, v)$ with $v \equiv \sqrt{\mu^2/\lambda}$ corresponding to this minimum of the potential. If we expand the Higgs field around the minimum, then the vacuum expectation value will give the gauge boson mass.

$$\begin{aligned} \mathcal{L}_{mass} &= \left(\frac{v g_2}{2}\right)^2 W_\mu^+ W^{-\mu} + \frac{v^2}{8} \begin{pmatrix} W_\mu^3 & B_\mu \end{pmatrix} \begin{pmatrix} g_2^2 & -g_1 g_2 \\ -g_1 g_2 & g_1^2 \end{pmatrix} \begin{pmatrix} W^{3\mu} \\ B^\mu \end{pmatrix} \\ &= \left(\frac{v g_2}{2}\right)^2 W_\mu^+ W^{-\mu} + \frac{v^2}{8} \begin{pmatrix} Z_\mu^0 & A_\mu \end{pmatrix} \begin{pmatrix} g_1^2 + g_2^2 & 0 \\ 0 & 0 \end{pmatrix} \begin{pmatrix} Z^{0\mu} \\ A^\mu \end{pmatrix} \end{aligned} \quad (2.16)$$

In this case the charged weak bosons ($W^+ = \sqrt{1/2}(W_1 - iW_2)$ and $W^- = \sqrt{1/2}(W_1 + iW_2)$) get mass of about hundred GeV. The combination of a left-handed boson W^3 with the hypercharged boson B yields a massive boson $Z^0 = \cos \theta_W W_3 - \sin \theta_W B$ with a mass around hundred GeV, and one massless boson combination, which we call photon $A = \sin \theta_W W_3 + \cos \theta_W B$. Here $\theta_W = \tan^{-1}(g_1/g_2)$ is the Weinberg angle. Three of the four scalar field components are absorbed by the gauge bosons with one left being the massive Higgs particle we are looking for. Also from the Yukawa coupling between scalar particles and fermions, fermions acquire mass.

$$\mathcal{L}_{Yukawa} = -\frac{v}{\sqrt{2}}(f_u \bar{u}u + f_d \bar{d}d + f_e \bar{e}e) = -m_u \bar{u}u - m_d \bar{d}d - m_e \bar{e}e \quad (2.17)$$

Here the coupling constant f and masses m 's are 3×3 matrices, since we have three generations of fermions so far. And the weak interaction Lagrangian for the fermions has the form under the broken or hidden symmetry:

$$\mathcal{L} = -\bar{\psi}_L \gamma^\mu \begin{pmatrix} \frac{1}{2}(Y+1)eA_\mu + \frac{1}{2} \frac{g_2^2 - Y g_1^2}{\sqrt{g_1^2 + g_2^2}} Z_\mu^0 & gW_\mu^+ \\ gW_\mu^- & \frac{1}{2}(Y-1)eA_\nu + \frac{1}{2} \frac{g_2^2 + Y g_1^2}{\sqrt{g_1^2 + g_2^2}} Z_\mu^0 \end{pmatrix} \psi_L \quad (2.18)$$

$$(2.19)$$

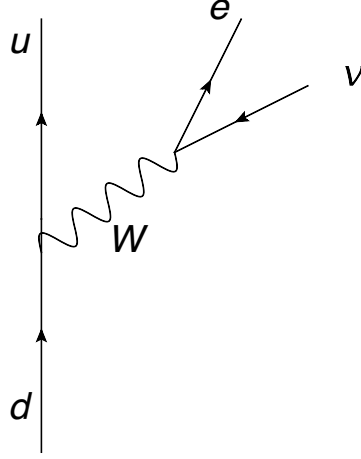


Figure 2.1: Fynmann diagram for β decay.

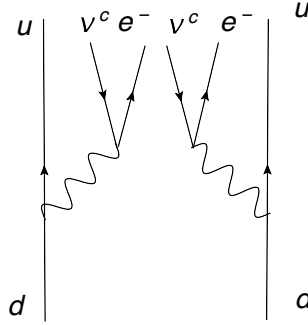


Figure 2.2: Fynmann diagram for $2\nu\beta\beta$ -decay.

From the Lagrangian above we can construct the Feynman diagram for the usual beta-decay which has the form like figure 2.1, a d quark decays into an u quark with emission of an electron and an anti-electron-neutrino through the virtual intermediate charged weak boson W . Because of the heavy mass of the intermediate weak bosons, the weak interaction hence has a much smaller effective interaction strength ($\frac{G_F}{\sqrt{2}} = \frac{g_2^2}{8M_W^2}$) compared with strong and even with electromagnetic interactions. Thus the interaction has a very short range according to the uncertainty principle. This character makes it possible to treat it as an approximate point interaction in nuclear physics. Double beta decay is a rare process which is allowed due to nuclear pairing. It changes the electric charge by 2 units, so there will be two weak interaction vertices. This is then a second order process. This process is nearly the slowest one in nature.

$2\nu\beta\beta$ is the process with the emission of two electrons and two neutrinos, and the Feynman diagram simply has the form of just two beta decays, fig.2.2.

However, $0\nu\beta\beta$ is a process with a change of lepton number, $\Delta L = 2$. So we will look for these

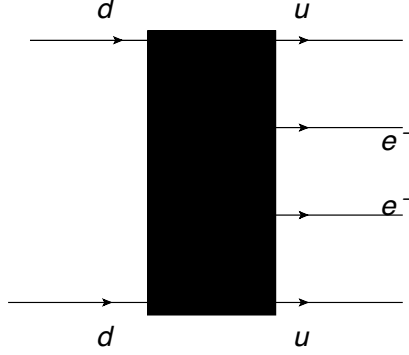


Figure 2.3: Fynmann diagram for $0\nu\beta\beta$ in the fundamental level, here the black box denote the all the possible mechanism.

interactions in new theories beyond the SM which may fulfill this requirement, in other words we look for Lagrangians with lepton number violating terms. First we briefly give some analyses how we can construct the required Feynman diagram from a Lagrangian of new physics. As we know, the products of $0\nu\beta\beta$ are two electrons and a daughter nucleus with two more protons than its parent. On the fundamental level, this is a process of two down quarks transformed to two up quarks with the byproducts of two electrons as illustrated in fig.2.3. The content of the "black box" in fig.2.3 is what we are exploring. The lepton number violation can happen in a vertex or in an inner propagator. So we can search it in both mass or kinetic and interaction terms to find a way to construct the needed diagrams. This is the program we will now follow.

The most economic way should be adding a Majorana mass term for neutrinos as we discussed before which modifies minimally the SM and we just consider the digonalised mass matrix for left-handed neutrinos and ignore its origin since that will not effect the decay width. So we add a term

$$L_{\nu mass} = \sum_i m_{\nu_i} \nu_i^c \nu_i = \sum_{l_1 l_2} M_{l_1 l_2} \nu_{l_1} \nu_{l_2}^c \quad (2.20)$$

with $\nu_l = \sum_i V_{li} \nu_i$, we can see in this term, the lepton number is violated by 2. One scatters a neutrino into an anti-neutrino and *vice versa*. This is what we need for the $0\nu\beta\beta$, and we can easily construct the required process as in fig.2.4. The lepton number violation happens in the neutrino propagator. Thus the virtual neutrino, because of the Majorana nature, can be emitted in the first vertex and be reabsorbed in the second vertex. Comparing to the $2\nu\beta\beta$, where at each weak interaction vertex an electron e^- and an electron anti-neutrino $\bar{\nu}_e$ are emitted, this process has only two emitted electrons.

If the see-saw mechanism is taken into account, then we can have the heavy right-handed neutrinos in the virtual process besides the light left-handed neutrinos. More complicated physics will be involved since we need to add right-handed neutrinos and more Higgs particles, but essentially, this will not change the decay width of the neutrinoless double beta decay drastically. We will discuss this in next chapter.

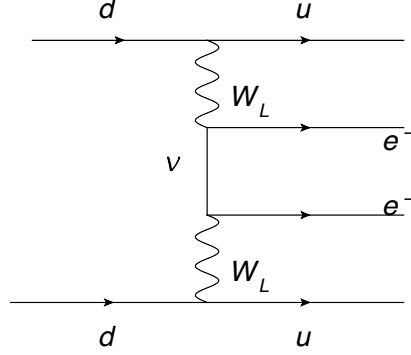


Figure 2.4: Fynmann diagram for $0\nu\beta\beta$ -decays in the case of virtual neutrino.

Majoron Mode

In the previous section we considered the probability that lepton symmetry is an accidental symmetry in the SM, and then it is natural to add the Majorana mass term. But if lepton number symmetry is an exact one, then we should treat it differently and take into account of the possibility of spontaneously breaking of this symmetry[47]. As we know, lepton number symmetry is a global symmetry, it is well known that such broken symmetries are accompanied with a massless Goldstone boson according to the Goldstone theorem [43, 44, 45]. In the case of a broken lepton number symmetry, we call this the Majoron. So besides Higgs bosons, we need to introduce extra scalar bosons. The most general way is as in [46], the introduction of two more Higgs multiplet:

$$\varphi \quad (l = -2)$$

$$h = \begin{pmatrix} h^+/\sqrt{2} & h^{++} \\ h^0 & -h^+/\sqrt{2} \end{pmatrix} (l = -2) \quad (2.21)$$

This is the so-called 1 – 2 – 3 model, that has one singlet φ , one doublet Φ from the SM, one triplet h , all are complex scalar fields. So the total number of field component is 12 and of which 6 are neutral. In this system, the broken pattern is $SU(2)_L \times U(1)_Y \times U(1)_L \rightarrow U(1)_{EM}$ ($U(1)_L$ is the group for the lepton number symmetry). Here we consider only the neutral particles and the Higgs particles should have the real VEV like:

$$\begin{aligned} \langle \varphi \rangle &= \langle \bar{\varphi} \rangle \equiv x \\ \langle \Phi^0 \rangle &= \langle \bar{\Phi}^0 \rangle \equiv \lambda \\ \langle h^0 \rangle &= \langle \bar{h}^0 \rangle \equiv y \end{aligned} \quad (2.22)$$

In this case we split the field into a real and an imaginary part:

$$\begin{aligned} \varphi &= \varphi_r + i\varphi_i \\ \Phi^0 &= \Phi_r^0 + i\Phi_i^0 \\ h^0 &= h_r^0 + ih_i^0 \end{aligned} \quad (2.23)$$

The Goldstone bosons and the absorbed bosons should come from the imaginary part of the neutral field. If the interactions between different Higgs field are allowed, particles such as the Majoron

should be combinations of different neutral fields. And to get these combinations, one can vary the Higgs Potential $V(\varphi, \Phi, h)$ and then can get the correct combination [46], the Majoron has the form $J = [4\lambda^2 y^4 + x^2(\lambda^2 + 4y^2)^2 + y^2\lambda^4]^{-1/2}[-2\lambda y^2\phi_i^0 + x(\lambda^2 + 4y^2)\Phi_i + y\lambda^2 h_i^0]$. Then one can introduce the Yukawa couplings, the details depend on the group structure of the Higgs particles. ϕ is an $SU(2)_L$ singlet and has zero hypercharge and lepton number of -2 . So φ will only interact with right-handed neutrinos. Φ is the Higgs field in the SM, with the right-handed neutrinos there will be a Dirac mass term for neutrinos such as that for down quarks in the quark sector. h has lepton-number -2 , and will only interact with leptons. So in this case the introduction of more Higgs particles will not affect the electroweak interactions of the quark sector. This is the general Yukawa interactions for leptons:

$$\mathcal{L}_{Yl} = if_{LL}L^T C\tau_2 hL + f_{LR}\bar{L}\Phi e_R + f_{RL}\bar{L}\tilde{\Phi}\nu_R + f_{RR}\nu_R^T C\tau_2\nu_R + H.c. \quad (2.24)$$

where τ_2 is the second component of the weak isospin, and $\tilde{\Phi} = \tau_2\Phi^*$ is the complex conjugate of the Higgs field Φ .

After the symmetry breaking, we find that the charged lepton mass is unchanged as in SM, and the neutrino mass is:

$$\mathcal{L}_{\nu mass} = yf_{LL}\nu_L^T C\nu_L + \lambda f_{RL}\bar{\nu}_L\nu_R + x f_{RR}\nu_R^T C\tau_2\nu_R + H.c. \quad (2.25)$$

this is the mass matrix of neutrinos. A careful observation shows that this is similar to the See-Saw mechanism with a hidden lepton symmetry. For convenience, we can redefine the neutrino in terms of the two component Majorana form $\nu_e \equiv \nu_L$ and $N_e \equiv C(\bar{\nu}_R)^T$, then the mass term read:

$$\begin{aligned} \mathcal{L}_{\nu mass} &= M_L\nu_e^T C\nu_e + M_R N_e^T C N_e + 2M_D\nu_e^T C N_e + H.c. \\ &= \begin{pmatrix} \nu_e^T & N_e^T \end{pmatrix} C \begin{pmatrix} M_L & M_D \\ M_D^T & M_R \end{pmatrix} \begin{pmatrix} \nu_e \\ N_e \end{pmatrix} \end{aligned} \quad (2.26)$$

Here $M_L = yf_{LL}$, $M_D = \lambda f_{RL}/2$ and $M_R = -x f_{RR}$. The first and third terms change the lepton number by two caused by the spontaneous lepton symmetry breaking, and by diagonalizing this mass matrix we can find the mass eigenstates light ν and heavy N neutrinos. It is easy to generalize this to three flavors, by replacing ν_e and N_e with the vector $\nu_f^T = (\nu_e^T, \nu_\mu^T, \nu_\tau^T)$ and $N_f^T = (N_e^T, N_\mu^T, N_\tau^T)$, in this case each component in the mass matrix is replaced by a 3×3 matrix, and by diagonalization we can get the mass eigenstates $\nu^T = (\nu_1^T, \nu_2^T, \nu_3^T)$, $N^T = (N_1^T, N_2^T, N_3^T)$ and the transformation matrix \mathcal{U}

$$\begin{pmatrix} \nu_f \\ N_f \end{pmatrix} = \mathcal{U} \begin{pmatrix} \nu \\ N \end{pmatrix} = \begin{pmatrix} V & U \\ U^N & V^N \end{pmatrix} \begin{pmatrix} \nu \\ N \end{pmatrix} \quad (2.27)$$

Hence the Yukawa interaction for neutrino can be written as:

$$\mathcal{L} = \begin{pmatrix} \nu_f^T & N_f^T \end{pmatrix} C \begin{pmatrix} M_L h^0/y & M_D \Phi^0/\lambda \\ M_D^T \Phi^0/\lambda & M_R \phi^*/x \end{pmatrix} \begin{pmatrix} \nu_f \\ N_f \end{pmatrix} \quad (2.28)$$

To make things a bit easier, we can make a simplification of dropping out the Higgs triplet, then we have a model called 1 – 2 model. This may give us a clear scenario on how it can be connected

to the $0\nu\beta\beta$. Without the triplet, the Majoron has the form $J = \varphi_i = Im(\varphi)$, and the mass matrix is now:

$$\mathcal{L} = \begin{pmatrix} \nu_f^T & N_f^T \end{pmatrix} C \begin{pmatrix} 0 & M_D \\ M_D^T & M_R \end{pmatrix} \begin{pmatrix} \nu_f \\ N_f \end{pmatrix} \quad (2.29)$$

As we know the mass scale of left-handed neutrinos is very tiny, so in this case, just as in see-saw models a large M_R is required since $m_\nu \approx M_D^T M_R^{-1} M_D$, this means either a larger x or larger f_{RR} or both, and because the Majoron will not interact with SM particles, we can not predict which one should be dominant. GUT's predict a right-handed neutrino with a mass around GUT scale or below. This makes the right-handed neutrino mediating $0\nu\beta\beta$ a lower order process as we will see in next chapter.

Now considering the $0\nu\beta\beta$, the Majorana mass terms are obviously lepton number violating, similar to the possibility we considered above of a simple Majorana mass term added to the SM. In such a model, the process of fig.2.4 is allowed. Besides this possibility, we have other possible diagrams. The decay energy Q is about several MeV . Thus besides electrons, only particles with tiny masses can be emitted, in $2\nu\beta\beta$ such a particle is the neutrino. In $0\nu\beta\beta$, no neutrinos are emitted, but there may be other particles with a small mass. In this model, a good candidate is Majoron J , it is massless, while emission of other massive particles are not allowed since they have very large masses. Because Majoron has a lepton number of 2, so this process conserves the lepton numbers. As we have shown, Majoron can only interact with heavy neutrinos:

$$\mathcal{L}_{Majoron} = \frac{1}{x} N_f^T C M_R N_f J \quad (2.30)$$

Only the left-handed neutrinos participate in weak interactions, and thus in the $0\nu\beta\beta$, we are only interested in ν_{eL} . So we need the interactions of the Majoron J with left-handed neutrinos, in four-component representation, the interaction can be derived directly from above fundamental interactions as:

$$\mathcal{L}_{Majoron} = \frac{i}{2} g_{eff} \bar{\nu}_{eL} \gamma_5 \nu_e \varphi + H.c. \quad (2.31)$$

Here the effective interaction strength has the value of:

$$g_{eff} = \frac{1}{x} \sum_{f_1 f_2} S_{ef_1} (M_{RR})_{f_1 f_2} S_{f_2 e} \quad (2.32)$$

Here f_1 and f_2 are flavor indices and the transformation matrix S connects the left- and right-handed neutrinos by the mass eigenstates, $S_{fe} = \sum_i U_{fi}^N V_{ei}^* + V_{fi}^N U_{ei}^*$. This is the general Lagrangian although somehow suppressed by the smallness of V^N and U . But there are other effective models which may have a different underlying mechanism which will yield a much larger interaction strength *c.f.* [48].

From the above interactions, we can construct the Feynman diagrams as in fig.2.5: a Majoron is emitted during the propagation of the virtual neutrino, this changes the electron spectrum since the scalar particle will take away the decay energy and the momentum and in next chapter we will calculate the decay rates for this process.

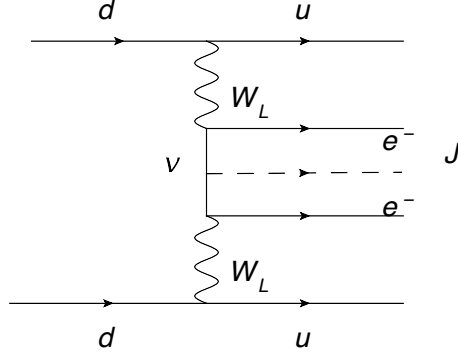


Figure 2.5: Fynmann diagram for $0\nu\beta\beta$ in the case of Majoron emission.

2.2.2 Grand Unification Theory

The success of the unification of the electromagnetic and weak interactions has inspired further attempts of the unifications of all the interactions in our universe, the so-called theory of everything(TOE). We are far from this final aim, but the SM give us some enlightenment, after more than one century ago Maxwell unified the magnetic and electric force into the electromagnetic force, one succeeded to combine the weak and electromagnetic interactions into one electroweak force. So one wonders that if the electroweak and QCD (quantum chromodynamic) can be incorporated into one larger symmetry group as a single force.

Large Gauge Symmetry

The aim of GUT is to embed the SM symmetry to a larger symmetry group. Since $SU_c(3) \times SU_L(2) \times U_Y(1)$ is a product of Lie algebra, this larger symmetry should be a simple or a semi-simple or even a non-simple Lie symmetry group. The advantage of the simple Lie algebra is that a unified coupling constant can be predicted, while this is not the case for products of symmetry groups. The symmetry group of SM has a rank of 4 which requires the underlying symmetry group should have a rank equal or larger than 4. The simplest simple Lie group of this case is the $SU(5)$ proposed by [11].

The general idea of GUT is similar to that of the SM, that all the fermions and bosons lie in some representations of the underlying symmetry group. By choosing suitable VEV(vacuum expectation value)'s of certain Higgs scalars, the symmetry was broken spontaneously to the group structure we need while the gauge bosons of the broken symmetry became massive by absorbing the Higgs particle, altogether with the remaining massive Higgs particles[6]. As an example, for the $SU(5)$ group, for each family, the fermions are assigned the representations of 5^* and 10, the former is the complex fundamental representation and the latter is the antisymmetric product of 2 5 's($(5 \times 5)_A$), these 15 particles include up and down quarks each with three color and their antiparticles altogether 12 quarks, 1 left-handed neutrino and 1 electron with its antiparticle, the positron, so in this case, no right-handed neutrinos is involved and the neutrinos are massless. The gauge bosons in this case reside in the adjoint representation of $SU(5)$, in total 24 particles. From

the SM we know that the SSB pattern should have the form $SU(5) \xrightarrow{M_X} SU_c(3) \times SU(2)_L \times U_Y(1) \xrightarrow{M_W} SU_c(3) \times U_{EM}(1)$, so the simplest Higgs sector should have two multiplets, of which one is consistent with the SM Higgs and the other is responsible for the symmetry breaking at high energies. The former in this case is in the representation 5 and has the VEV at the direction of the $v^T = (0, 0, 0, 0, 1)v_0$ and the latter should be in representation 24 which may have a VEV of the form $diag(a, a, a, b, b)$. Of course more Higgs particles can be added, but this will make the SSB much more complicated especially the Higgs potentials. For the gauge boson sector we see that there will be 12 heavy bosons besides the SM gauge bosons. But this allows proton decay. The half-life of proton is one of the important constraints for the broken scale M_X . The $SU(5)$ GG model is the simplest examples of GUT, the least number of extra particles are introduced. But it has also many drawbacks such as the massless neutrinos, the hierarchy problem *etc.* In the $SU(5)$ model no $0\nu\beta\beta$ is allowed. This is not the GUT we need in our discussion.

Another group which has a larger rank is $SO(10)$, this group is anomaly free as $SU(5)$ and it admits complex representation[49]. The fermions reside in a 16 dimensional complex spinor σ_+ [50], which contains the 15 SM fermions and 1 right-handed neutrino for each family. The adjoint representation is 45 dimensionals, so we have 45 gauge bosons in this case and most of them become very heavy after SSB. For this rank 5 Lie group, there are different SSB patterns which lead to the final SM symmetry group, they are summarized in refs.[51, 12, 52]:

$$\begin{aligned}
 & SO(10) \xrightarrow{M_G} SU(5) \xrightarrow{M} G_s \\
 & SO(10) \xrightarrow{M_G} G' \xrightarrow{M} G_s \\
 & SO(10) \xrightarrow{M_G} SU_c(4) \times SU_L(2) \times U_R(1) \xrightarrow{M_c} SU_C(3) \times SU_L(2) \times U_R(1) \times U'(1) \xrightarrow{M} G_s
 \end{aligned}
 \tag{2.33}$$

Here $G_s \sim SU_c(3) \times SU_L(2) \times U_Y(1)$ the SM symmetry and $G' \sim SU_c(3) \times SU_L(2) \times SU_R(2) \times U(1)$ is the left-right symmetric group. Different SSB pattern correspond to different Higgs sectors and VEV structures. The first is just a trivial extension of the $SU(5)$ GG model and the last is compatible with the Pati-Salam model[53, 54]. Here we are interested in the L-R symmetry since it can give the neutrino mass as we shall see later, it requires less steps of symmetry breaking than others. The breaking from $SO(10)$ to G' can be acquired through a Higgs of representation 54 at the mass scale $M_G \sim 10^{14-15} GeV$ as that of $SU(5)$ GG model. Under G' the 45 gauge bosons have the transformation properties as:

$$45 = (8, 1, 1) + (1, 3, 1) + (1, 1, 3) + (1, 1, 1) + (3^*, 2, 2) + (3, 2, 2) + (3, 1, 1) + (3^*, 1, 1)
 \tag{2.34}$$

The former four types have altogether 15 gauge bosons g , $W_{L(R)}$ and B , which are massless after the first stage of the symmetry breaking while the the latter 4 types have 30 gauge bosons with a heavy mass around M_G . These 30 bosons are decoupled from the late stage breaking. Here we briefly introduced the idea of GUT and in the next section we will discuss intensively how we can get the correct neutrino physics from the L-R symmetric model and the second stage SSB in the $SO(10)$ model.

L-R Symmetry and Heavy Right-handed Gauge Bosons

The $SO(10)$ GUT model is one of the most discussed and applied models till present, although the idea of a large gauge symmetry is no longer popular. This first stage GUT symmetry breaking takes place at some energy scales between the Planck scale and the electroweak symmetry breaking scale, roughly $10^{14} - 10^{15} GeV$. At a lower energy of about 100 GeV, the second stage electroweak symmetry breaking happens successively. So we may have many heavy Higgs and also heavy gauge bosons in this model. In this section we will discuss the possibility of a different electroweak symmetry breaking pattern by introducing right-handed gauge bosons[54]. The smallness of neutrino mass can be explained by the difference between the VEVs of different Higgs scalars and the Majorana nature of the neutrino.

This model is a straightforward extension of the SM with an additional symmetry $SU(2)_R$ included. The overall SSB process can be expressed as $SO(10) \rightarrow SU(2)_L \times SU(2)_R \times U(1)_{B-L} \times SU(3)_c \rightarrow U(1)_{EM} \times SU(3)_c$ with two sequential SSB at different energies. We also introduce the local $B-L$ symmetry which reduces to $U(1)_Y$ in the limit with only the right-handed symmetry breaking. And we will focus on the second stage SSB, and neglect the possible effect from the first SSB with very heavy gauge bosons and Higgs particles.

For the $L-R$ symmetric electroweak model, we should first introduce the right handed gauge bosons which is similar to left-handed bosons in the SM. Now the symmetry group is extended, so we will have also the right-handed gauge bosons W_R^i .

Then the corresponding fermions, with the existence of $SU(2)_R$, the right-handed fermions which used to be singlets in the SM are now doublets which span a fundamental representation of $SU(2)_R$. In this case, we need to introduce the right-handed neutrinos which are not presented in SM. Now we have a relation for the electrical charge Q similar to the Gell-Mann-Nishijima formula[55], $Q = I_{3L} + I_{3R} + \frac{B-L}{2}$. So for the first generation, the fermions can be categorized as:

$$\begin{aligned} q_L &= \begin{pmatrix} u_L \\ d_L \end{pmatrix} \left(\frac{1}{2}, 0, \frac{1}{3} \right) & q_R &= \begin{pmatrix} u_R \\ d_R \end{pmatrix} \left(0, \frac{1}{2}, \frac{1}{3} \right) \\ \psi_L &= \begin{pmatrix} \mu_L \\ e_L \end{pmatrix} \left(\frac{1}{2}, 0, -1 \right) & \psi_R &= \begin{pmatrix} \mu_R \\ e_R \end{pmatrix} \left(0, \frac{1}{2}, -1 \right) \end{aligned} \quad (2.35)$$

in $SU(2)_L \times SU(2)_R \times U(1)_{B-L}$, here in the horizontal brackets $(t_L, t_R, B-L)$, the notations are the isospin of the left- and right-handed multiplets and the baryon number minus the lepton number. For an anomaly free theory, some authors argue that more fermions should be included, but that can only change our related electroweak interaction at loop level. so we omit this in the current thesis.

Finally for the Higgs part which is responsible for the SSB and gives also the masses to fermions. In the SM, we have only one Higgs with quantum number $(1/2, 1)$, which broke the $SU(2)_L \times U(1)_Y$. Now more Higgs particles are needed for a new model with a new symmetry. For the breaking of $U(1)_{B-L}$, the corresponding Higgs particle must have a certain value of $B-L$ so that it can interact with $B-L$ bosons. From previous assignment we see that in order to build the Yukawa interaction, $B-L$ can only have the value 0 (Dirac type Yukawa interaction) or ± 2 (Majorana type Yukawa interaction) (No Majorana type Yukawa interaction for quarks exists because only neutrinos can be Majorana particles). So two types of Higgs are needed, one for fermion mass and

another for breaking of local $B - L$ symmetry. For the first type, we can use a similar technique as used in the SM, but instead of a doublet, now a bidoublet, which is both doublet for $SU(2)_L$ and $SU(2)_R$, and from the argument in [40], the different mass scale for fermions and gauge bosons may imply two different bidoublets, one couples with fermions and another couples with gauge bosons. For the latter type, for the Majorana mass terms, the best choices are the triplets, because of the $L - R$ symmetry, two triplets are needed, one is left handed and another right-handed. From the discussion above we find the Higgs set as:

$$\begin{aligned} \varphi_f & \left(\frac{1}{2}, \frac{1}{2}, 0 \right) & \varphi_W & \left(\frac{1}{2}, \frac{1}{2}, 0 \right) \\ \Delta_L & (1, 0, 2) & \Delta_R & (0, 1, 2) \end{aligned} \quad (2.36)$$

in representations of $SU_L(2) \times SU_R(2) \times U_{B-L}(1)$. Here we have two Higgs particles φ , one responsible for fermion mass and the other for the gauge boson mass. The general SSB pattern should have the form:

$$\begin{aligned} \langle \varphi_f \rangle & = \begin{pmatrix} \kappa_f & 0 \\ 0 & \kappa'_f \end{pmatrix} & \langle \varphi_W \rangle & = \begin{pmatrix} \kappa_W & 0 \\ 0 & \kappa'_W \end{pmatrix} \\ \langle \Delta_L \rangle & = \begin{pmatrix} 0 & 0 \\ v_L & 0 \end{pmatrix} & \langle \Delta_R \rangle & = \begin{pmatrix} 0 & 0 \\ v_R & 0 \end{pmatrix} \end{aligned} \quad (2.37)$$

Here all κ s, κ' s and v s are the VEV's with values to be determined from the experiments. From current knowledge of the SM, we can at first have some constraints on these VEVs. The mass difference from fermion masses and gauge boson masses tell us that $\langle \varphi_f \rangle \ll \langle \varphi_W \rangle$. In order to suppress the $L - R$ mixing which should be small from the results of recent experiments, one must request $\kappa' \ll \kappa$ [40]. The smallness of $\Delta S = 2$ transitions induced by Higgs requires $v_R \gg \kappa$ [40]. Finally the stability condition of the Higgs potential requires $v_L = \gamma(\kappa^2/v_R)$, γ is some ratios of Higgs self-coupling constants with the values around unity [40].

From the above structure of the VEV's, we can construct the mass matrix for fermions and gauge bosons. As we discussed before, Δ_L and Δ_R lead to the lepton number violating terms since it breaks the $B - L$ symmetry spontaneously. So this model allows $0\nu\beta\beta$ process as we shall see.

The Yukawa coupling terms for the fermions are:

$$\begin{aligned} \mathcal{L}_Y & = h_1 \bar{\psi}_L \varphi_f \psi_R + h_2 \bar{\psi}_L \tilde{\varphi}_f \psi_R + h_3 \bar{Q}_L \varphi_f Q_R + h_4 \bar{Q}_L \tilde{\varphi}_f Q_R \\ & \quad + ih_5 (\psi_L^T C \tau_2 \Delta_L \psi_L + \psi_R^T C \tau_2 \Delta_R \psi_R) + H.c. \end{aligned} \quad (2.38)$$

From (2.38) we can easily derive the masses for different fermions for one generation. For charged fermions, the masses emerge as:

$$\begin{aligned} m_e & = h_1 \kappa'_f + h_2 \kappa_f \\ m_u & = h_3 \kappa_f + h_4 \kappa'_f \\ m_d & = h_4 \kappa_f + h_3 \kappa'_f \end{aligned} \quad (2.39)$$

and the mass matrix for neutrinos with the conventions $\nu_e \equiv \nu_L$ and $N_e \equiv C\bar{\nu}_R^T$ are:

$$\begin{aligned}
\mathcal{L}_{mass}^\nu &= (h_1\kappa_f + h_2\kappa'_f)\nu_e^T C N_e + h_5(v_L\nu_e^T C\nu_e - v_R N_e^T C N_e) + H.c. \\
&= \begin{pmatrix} \nu_e^T & N_e^T \end{pmatrix} C \begin{pmatrix} h_5 v_L & \frac{1}{2}(h_1\kappa_f + h_2\kappa'_f) \\ \frac{1}{2}(h_1\kappa_f + h_2\kappa'_f) & -h_5 v_R \end{pmatrix} \begin{pmatrix} \nu_e \\ N_e \end{pmatrix} \\
&= \begin{pmatrix} \nu_e^T & N_e^T \end{pmatrix} C \begin{pmatrix} M_L & M_D \\ M_D & M_R \end{pmatrix} \begin{pmatrix} \nu_e \\ N_e \end{pmatrix}
\end{aligned} \tag{2.40}$$

Therefore the mass eigenstates ν and N for neutrinos are given as:

$$\begin{aligned}
\nu &= \nu_e \cos \xi + N_e \sin \xi \\
N &= -\nu_e \sin \xi + N \cos \xi
\end{aligned} \tag{2.41}$$

with $\tan 2\xi = \frac{2M_D}{M_R - M_L} \approx 2M_D/M_R$. From the above analysis we find that $\tan \xi \ll 1$, so $\xi \approx -\frac{1}{2}h_1\kappa_f/h_5v_R$, this again predicts a tiny mixing between the left- and right-handed neutrinos. So we get the approximate mass $m_\nu \approx M_L - M_D^2/M_R \approx (h_5\gamma + h^2/4h_1)\kappa^2/v_r$, which naturally explains the smallness of neutrino mass, and $M_N \approx M_R$ predicts a very heavy right-handed neutrino. At the limit $v_R \rightarrow \infty$, we get $m_\nu \rightarrow 0$ and $M_N \rightarrow \infty$. The advantage of the choice of the two φ 's is that we needn't adjust M_D to fit the gauge boson masses. The Majorana terms in (2.38) allows the $0\nu\beta\beta$ as these terms change the lepton number by two. This implies a lepton number violation in the intermediate propagator.

Now, we should turn our attentions to the gauge sector, especially the charged weak currents which are responsible for the β decay. At the elementary level, this is a process with a transformation $d \rightarrow u$, it involves also the $e^- \rightarrow \nu$ lepton current. Breaking the gauge symmetry gives the gauge bosons masses. Given the configurations for each Higgs, we have for these particles the general transformation properties under $SU(2)_L$ and $SU(2)_R$ as:

$$\Delta_L \rightarrow U_L \Delta_L U_L^\dagger \quad \Delta_R \rightarrow U_R \Delta_R U_R^\dagger \quad \varphi \rightarrow U_L \varphi U_R^\dagger \tag{2.42}$$

So, the kinetic and covariant terms for all the Higgs particles are given by:

$$\mathcal{L}_K = (D^\nu \varphi_f)^\dagger D_\nu \varphi_f + (D^\nu \varphi_W)^\dagger D_\nu \varphi_W + (D^{L\mu} \Delta_L)^\dagger D_\mu^L \Delta_L + (D^{R\mu} \Delta_R)^\dagger D_\mu^R \Delta_R \tag{2.43}$$

Here $D^\mu = \partial_\mu - i\frac{g}{2}t_L^a W_{L\mu}^a - i\frac{g}{2}t_R^a W_{R\mu}^a$ and $D_\mu^{L(R)} = \partial_\mu - igT_{L(R)}^a W_{L(R)\mu}^a - 2ig'B_\mu$, here t^a and T^a are both generators for different representations for $SU(2)$.

After breaking the symmetry [40] with a suitable choice of the Higgs potential, six out of seven gauge bosons acquire mass with one photon remains massless. For the charged sector, we have:

$$\begin{aligned}
W_1 &= W_L \cos \epsilon + W_R \sin \epsilon \\
W_2 &= -W_L \sin \epsilon + W_R \cos \epsilon
\end{aligned} \tag{2.44}$$

with

$$\begin{aligned}
m_{W_1}^2 &\simeq \frac{1}{2}g^2(\kappa^2 + \kappa'^2 + 2v_L^2) \\
m_{W_2}^2 &\simeq \frac{1}{2}g^2(\kappa^2 + \kappa'^2 + 2v_R^2)
\end{aligned} \tag{2.45}$$

While for the neutral bosons, one has

$$\begin{aligned}
A_\mu &= \sin \theta_W (W_{L\mu}^3 + W_{R\mu}^3 + \sqrt{\cos 2\theta_W} B_\mu) \\
Z_{L\mu} &\simeq \cos \theta_W W_{L\mu}^3 - \sin \theta_W \tan \theta_W W_{R\mu}^3 - \tan \theta_W \sqrt{\cos 2\theta_W} B_\mu \\
Z_{R\mu} &\simeq \frac{\sqrt{\cos 2\theta_W}}{\cos \theta_W} W_{R\mu}^3 - \tan \theta_W B_\mu
\end{aligned} \tag{2.46}$$

where $\tan \theta_W = g'/(g^2 + g'^2)^{1/2}$ and the masses are

$$\begin{aligned}
m_A &= 0 \\
m_{Z_L}^2 &\simeq \frac{g^2}{2} \frac{1}{\cos \theta_W} (\kappa^2 + \kappa'^2 + 4v_L^2) \\
m_{Z_R}^2 &\simeq 2(g^2 + g'^2)v_R^2
\end{aligned} \tag{2.47}$$

In this case the Weinberg angle θ_W is defined similar to that of the SM, so $e^2 = g^2 \sin^2 \theta_W$.

The gauge interactions for fermions are as in the SM:

$$\mathcal{L}_F = \bar{\psi}_i \not{D} \psi_i \tag{2.48}$$

In $0\nu\beta\beta$ we only need the charged weak currents. The charged current interaction from the above Lagrangian is:

$$\begin{aligned}
\mathcal{L}_{CC}^l &= \frac{g}{\sqrt{2}} [(\cos \epsilon \bar{\nu}_L \gamma_\nu e_L + \sin \epsilon \bar{\nu}_R \gamma_\nu e_R) W_1^{-\nu} + (\cos \epsilon \bar{\nu}_R \gamma_\nu e_R - \sin \epsilon \bar{\nu}_L \gamma_\nu e_L) W_2^{-\nu}] \\
&+ H.c. \\
&= \frac{g}{\sqrt{2}} (j_\nu^{(1)} W_1^{-\nu} + j_\nu^{(2)} W_2^{-\nu}) + H.c. \\
\mathcal{L}_{CC}^q &= \frac{g}{\sqrt{2}} [(\cos \epsilon \bar{u}_L \gamma_\nu d_L + \sin \epsilon \bar{u}_R \gamma_\nu d_R) W_1^{-\nu} + (\cos \epsilon \bar{u}_R \gamma_\nu d_R - \sin \epsilon \bar{u}_L \gamma_\nu d_L) W_2^{-\nu}] \\
&+ H.c. \\
&= \frac{g}{\sqrt{2}} (J_\nu^{(1)} W_1^{-\nu} + J_\nu^{(2)} W_2^{-\nu}) + H.c.
\end{aligned} \tag{2.49}$$

In this case we can construct more diagrams similar to fig.2.4, and now many left-handed particles can be replaced by the right-handed ones, but because of the small mixing between the left- and right-handed neutrinos and the gauge bosons and also the different masses of the left- and right-handed gauge bosons, *c.f.* fig.2.6, the leading contributions are those originate from the SM with a Majorana neutrino.

The generalization to three generations is straightforward. For the gauge interaction, the 2nd and 3rd generations have the same interactions as the 1st generation. The change comes from the Yukawa coupling terms. Now the coupling constant h become a 3×3 matrix. The non-diagonal matrix elements indicate the mixing between different flavors. In quark sector, this is the so-called CKM matrix[34, 35] and in lepton sector, the PNMS matrix[33, 36]. In this model, we can not tell where the mixing matrix among the three generations comes from. This needs perhaps the breaking of the family symmetry.

2.2.3 Sterile Kaluza-Klein Neutrinos in Extra Dimensions

The idea of introducing warped Extra Dimensions to particle physics was first proposed by [13], the general idea is the existence of wrapped small dimensions (number of the dimensions is from 1 to

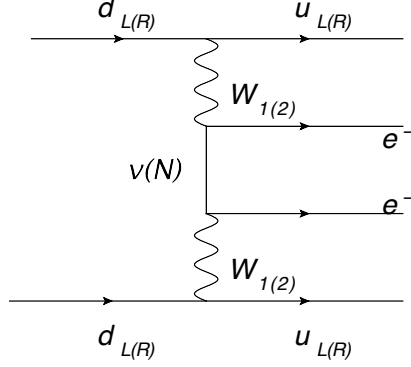


Figure 2.6: Feynman diagram for $0\nu\beta\beta$ with GUT. In this case of both the left- and right-handed currents can be involved.

even more). Our universe is a $3 + 1$ dimensional "brane" stucked to the extra dimensions which are wrapped up. And only gravitons can propagate across the extra dimensions and all SM particles are restricted to the brane. But there is one exception, the right handed neutrino, since it has no SM symmetry charges, it is not bounded to the brane and can propagates in the extra dimensions. The main advantage of extra dimensions is that it can explain the mass scale hierarchy between the electroweak scale (roughly 1 TeV) and the gravitational scale (Planck scale $10^{18} GeV$). In warped space, the gravitational scale is expressed as $M_F \approx M_P^{\frac{2}{2+\delta}} / R^{\frac{\delta}{2+\delta}}$, nearly 1 TeV. This solves the Puzzle of mass Hierarchy naturally, so it can be the best candidate for new physics beyond SM without introductions of complicated structures.

If restricted to $1 + (3 + 1)$ (one extra-dimension) spacetime, the general geometrical setup is the the orbifold (an orbit space) S^1/Z_2 in the warped dimension. In geometry this is a circle with a permutation Z_2 being excluded, the SM particles are restricted to the brane[56]:

$$\begin{aligned} \psi_L(x) &= \begin{pmatrix} \nu_L(x) \\ e_L(x) \end{pmatrix} & e_R(x) \\ q_L(x) &= \begin{pmatrix} u_L(x) \\ d_L(x) \end{pmatrix} & u_R(x) & d_R(x) \end{aligned} \quad (2.51)$$

And one extra (bulk) neutrino singlet which can be written in the form of two two-component spinors in the Weyl basis [57]:

$$N(x, y) = \begin{pmatrix} \xi(x, y) \\ \bar{\eta}(x, y) \end{pmatrix} \quad (2.52)$$

The orbifold of the fifth dimension requires that $N(x, y) = N(x, y + 2\pi R)$, where y is the coordinate of the fifth dimension and R is the radius of fifth compactified dimension. General assumption is that ξ is symmetric and η is antisymmetric under y reflection: $\xi(x, y) = \xi(x, -y)$ and $\eta(x, y) = -\eta(x, -y)$. Next we introduce the γ matrices in five dimensions[58]:

$$\gamma_\mu = \begin{pmatrix} 0 & \sigma_\nu \\ \bar{\sigma}_\mu & 0 \end{pmatrix} \quad \gamma_4 = \begin{pmatrix} -1 & 0 \\ 0 & 1 \end{pmatrix} \quad (2.53)$$

With these spinors and matrices, we can write down the general form Lagrangian in five dimensions [58, 59]:

$$\begin{aligned} \mathcal{L}_{eff}(x) = & \int_0^{2\pi R} dy \{ \bar{N}(x, y) (i\gamma^\nu \partial_\mu + \gamma^4 \partial_y) N(x, y) - \frac{1}{2} (MN^T C^{(5)-1} N + H.c.) \\ & + \delta(y-a) [\frac{h_1^l}{M_F^{\delta/2}} \bar{\psi}_L \tilde{\Phi}^* \xi + \frac{h_2^l}{M_F^{\delta/2}} \bar{\psi}_L \tilde{\Phi}^* \eta + H.c.] + \delta(y-a) \mathcal{L}_{SM} \} \end{aligned} \quad (2.54)$$

The Yukawa coupling constant is a vector: $h_{1(2)}^l{}^T = (h_{1(2)}^e, h_{1(2)}^\mu, h_{1(2)}^\tau)$, as before $\tilde{\Phi} = i\sigma_2 \Phi^*$ is the Hypercharge conjugate, which is also responsible for the mass of the up component of quark sector. The five-dimensional charge conjugate is defined as: $C^{-1} \gamma_\mu C = -\gamma_\mu^T$.

From the periodicity and the reflection symmetry Z_2 , we can expand the five dimensional neutrino field by separating the coordinates as[60]:

$$\begin{aligned} \xi(x, y) &= \frac{1}{\sqrt{2\pi R}} \xi_0(x) + \frac{1}{\sqrt{\pi R}} \sum_{n=0}^{\infty} \xi_n(x) \cos\left(\frac{ny}{R}\right) \\ \eta(x, y) &= \frac{1}{\sqrt{\pi R}} \sum_{n=0}^{\infty} \eta_n(x) \sin\left(\frac{ny}{R}\right) \end{aligned} \quad (2.55)$$

Here $\xi_n(x)$ and $\eta_n(x)$ are called infinite towers of Kaluza-Klein(KK) neutrinos, as shown above, they have different reflection symmetries also different CP as well. So the simultaneous existence of both terms in the interaction with the weak bosons may bring CP violation into weak interactions. After substituting (2.55) into the Lagrangian we may get the effective interactions for an infinite tower of KK modes as:

$$\begin{aligned} \mathcal{L} = & \mathcal{L}_{SM} + \xi_0^\dagger (i\bar{\sigma}^\mu \partial_\mu) \xi_0 + (h_1^{l(0)} \bar{\psi}_L \tilde{\Phi}^* \xi_0 - \frac{1}{2} M \xi_0^T (i\sigma_2) \xi_0 - H.c.) \\ & + \sum_{n=1}^{\infty} [\xi_n^\dagger (i\bar{\sigma}^\mu \partial_\mu) \xi_n + \eta_n^\dagger (i\bar{\sigma}^\mu \partial_\mu) \eta_n + \frac{n}{R} (\xi_n^T (i\sigma_2) \eta_n + \bar{\xi}^T (i\sigma_2) \bar{\eta}) \\ & - \frac{1}{2} M (\xi_n^T (i\sigma_2) \xi_n + \eta_n^T (i\sigma_2) \eta_n + H.c.) \\ & + \sqrt{2} (h_1^{l(n)} \bar{\psi}_L \tilde{\Phi}^* \xi_n + \bar{h}_2^{l(n)} \bar{\psi}_L \tilde{\Phi}^* \eta_n + H.c.)] \end{aligned} \quad (2.56)$$

Here the effective Yukawa coupling constants are

$$\begin{aligned} h_1^{l(n)} &= \frac{h_1^l}{(2\pi M_F R)^{\delta/2}} \cos\left(\frac{na}{R}\right) = \left(\frac{M_F}{M_P}\right)^{\delta/n_g} h_1^l \cos\left(\frac{na}{R}\right) \\ h_2^{l(n)} &= \frac{h_2^l}{(2\pi M_F R)^{\delta/2}} \sin\left(\frac{na}{R}\right) = \left(\frac{M_F}{M_P}\right)^{\delta/n_g} h_2^l \sin\left(\frac{na}{R}\right) \end{aligned} \quad (2.57)$$

The last step of the r.h.s is due to the large Planck mass. The Dirac mass for neutrinos is suppressed due to the large M_P , for $M_F \approx 1TeV$, $M_F/M_P \approx 10^{-15}$. If the brane is located at $y = 0$, there exists only the ξ particles. In this case, the lepton numbers is preserved. So shifting the brane from away the origin is need for lepton number violation.

From non-diagonal mass terms in(2.56), we see it is convenient to define $\chi_{\pm n} = (\xi_n \pm \eta_n)/\sqrt{2}$, after SSB, with the VEV $\langle \Phi^T \rangle = (0, v)$, one gets the mass terms for neutrinos and effective particles. The kinetic term is written as:

$$\mathcal{L}_{kin} = \bar{\chi} i\sigma^{\bar{m}} u \partial_\mu \chi - \left(\frac{1}{2} \chi^T (i\sigma_2) \mathcal{M} \chi + H.c.\right) \quad (2.58)$$

The multiplet is defined as $\chi^T = (\nu_L, \xi_0, \chi_1, \chi_{-1}, \dots, \chi_n, \chi_{-n}, \dots)$, the mass matrix behaves like

$$\mathcal{M} = \begin{pmatrix} 0 & m^{(0)} & m^{(1)} & m^{(-1)} & m^{(2)} & m^{(-2)} & \dots \\ m^{(0)} & M & 0 & 0 & 0 & 0 & \dots \\ m^{(1)} & 0 & M + \frac{1}{R} & 0 & 0 & 0 & \dots \\ m^{(-1)} & 0 & 0 & M - \frac{1}{R} & 0 & 0 & \dots \\ m^{(2)} & 0 & 0 & 0 & M + \frac{2}{R} & 0 & \dots \\ m^{(-2)} & 0 & 0 & 0 & 0 & M + \frac{2}{R} & \dots \\ \dots & \dots & \dots & \dots & \dots & \dots & \dots \end{pmatrix} \quad (2.59)$$

here $m^{(\pm n)} \equiv \frac{v}{\sqrt{2}}(h_1^{l(n)} \cos(\frac{na}{R}) \pm h_2^{l(n)} \sin(\frac{na}{R}))$. We see that this is similar to the see-saw mechanism with zero left handed neutrino Majorana masses and small Dirac masses together with large right handed neutrino Majorana masses. But this model is more complicated because of the infinite number of effective right handed neutrino states. It is useful to define $k_0 \equiv [MR]$ (the symbol $[\]$ get the the integer part of the values inside), $\epsilon \equiv M - k_0/R$ which should be the smallest mass of the KK states. And one can rearrange the Mass Matrix like[60]:

$$\mathcal{M} = \begin{pmatrix} 0 & m^{(0)} & m^{(1)} & m^{(-1)} & m^{(2)} & m^{(-2)} & \dots \\ m^{(0)} & \epsilon & 0 & 0 & 0 & 0 & \dots \\ m^{(1)} & 0 & \epsilon + \frac{1}{R} & 0 & 0 & 0 & \dots \\ m^{(-1)} & 0 & 0 & \epsilon - \frac{1}{R} & 0 & 0 & \dots \\ m^{(2)} & 0 & 0 & 0 & \epsilon + \frac{2}{R} & 0 & \dots \\ m^{(-2)} & 0 & 0 & 0 & 0 & \epsilon + \frac{2}{R} & \dots \\ \dots & \dots & \dots & \dots & \dots & \dots & \dots \end{pmatrix} \quad (2.60)$$

Different from above definition is here $m^{(n)} \equiv v\sqrt{2}(h_1 \cos[\frac{(n-k_0)R}{a}] + h_2 \sin[\frac{(n-k_0)R}{a}]) = m \cos(\frac{n}{R} - \phi_h)$ with $m = v\sqrt{h_1^2 + h_2^2} = v(M_F/M_p)^{\delta/n_g} \sqrt{h_1^2 + h_2^2}$ and $\phi_h = \tan^{-1}(h_1^l/h_2^l) - k_0R/a$. The eigenvalue equation of this matrix can be derived analytically from [60] if $a = \pi R/n$, where n is an integer greater than 2:

$$\lambda = \pi m^2 R \{ \cos^2[\phi_h - a(\lambda - \epsilon)] \cot[\pi R(\lambda - \epsilon)] - \frac{1}{2} \sin[2\phi_h - 2a(\lambda - \epsilon)] \} \quad (2.61)$$

If $|\epsilon| \gg m$, an rough estimation of left handed neutrino mass is[60]:

$$m_\nu = \pi m^2 R \{ \cot(\pi R\epsilon) + \frac{\sin[(\pi - 2a/R)MR]}{\sin(\pi MR)} \} \quad (2.62)$$

The value $m^2 R$ supposed to be tiny for m is highly suppressed, but different from see-saw, the dependence of m_ν on M is not the leading term, the magnitude of the radii for the warped dimensions determines the mass scale of light neutrinos and also the heavy ones as they have the approximated mass $m_{(n)} \approx \frac{n}{R} + \epsilon$ [60].

Although the mass matrix can not be easily diagonalized, we can obtain the approximate transformation after making some truncations on n . As in see-saw, we can expand the left handed neutrinos by their mass eigenstates:

$$|\nu_l \rangle = \sum_{i=1}^3 U_{li} |\nu_i \rangle + \sum_{n=-\infty}^{\infty} U_{ln} |N_n \rangle \quad (2.63)$$

N_n are the mass eigenstates for KK modes. And as shown in the Appendices in [59], this matrix obey the sum rule as:

$$\begin{aligned} \sum_i U_{li} U_{l'i}^* + \sum_n U_{ln} U_{l'n}^* &= \delta_{ll'} \\ \sum_i U_{li} m_i U_{l'i}^* + \sum_n U_{ln} m_{(n)} U_{l'n}^* &= 0 \end{aligned} \quad (2.64)$$

So now the Lagrangian of the charged weak currents can be written as:

$$\begin{aligned} \mathcal{L}_{int}^W &= -\frac{g_W}{\sqrt{2}} W^{-\mu} \sum_{l=e,\mu,\tau} \bar{l}_L \gamma_\mu \nu_{lL} + H.c. \\ &= -\frac{g_W}{\sqrt{2}} W^{-\mu} \sum_{l=e,\mu,\tau} \left(\sum_{i=0}^3 U_{li} \bar{l}_L \gamma_\mu \nu_i + \sum_{n=-\infty}^{\infty} U_{ln} \bar{l}_L \gamma_\mu N_n \right) \end{aligned} \quad (2.65)$$

As N_n and ν_i are Majorana neutrinos, we can construct the Feynman diagram for $0\nu\beta\beta$, just as in the previous section, and the lepton violating process happens in the virtual neutrino propagator section as before, see fig.2.4

2.3 R Parity Violated SuperSymmetry

In this section we will explore another possibility for the $0\nu\beta\beta$, that is the process without virtual intermediate neutrino. In the previous section we saw that the existence of right handed neutrinos and massive Majorana neutrinos give rise to a lepton number 2 violating intermediate process. But in the new theory of SUSY, no neutrinos are involved, this is indeed "neutrinoless".

2.3.1 SuperSymmetry Theories and MSSM

The fermions and bosons have rather different properties such as the commutation relations and the space-time transformation rules. However, the idea of Supersymmetry is that fermions and bosons are in fact correlated by a symmetry which is allowed by the Coleman-Mandula theorem[61] which exclude the possibilities of combinations of space-time and internal symmetries. In the mathematical form, this is different from the normal Lie algebra. one needs the graded Lie algebra[62] which introduces the anti-commuting besides normal commuting generators.

The infinitesimal supersymmetric transformations for scalars and spinors have the form:

$$\begin{aligned} \delta\phi &= \xi\psi, & \delta\phi^* &= \xi^\dagger\psi^\dagger \\ \delta\psi_\alpha &= i(\sigma^\mu\xi^\dagger)_\alpha\partial_\mu\phi, & \delta\psi^\dagger_{\dot{\alpha}} &= -i(\xi\sigma^\mu)_{\dot{\alpha}}\partial_\mu\phi^* \end{aligned} \quad (2.66)$$

Here ξ is the infinitesimal transformation parameters. This transformation will leave the free fermion and scalar field unchanged.

From above supersymmetric transformations, one can introduce the spinor supercharge for SUSY in the form 4-component Dirac spinor as [63]:

$$Q^a = \begin{pmatrix} Q_\alpha^a \\ \bar{Q}^{a\dot{\alpha}} \end{pmatrix} \quad (2.67)$$

Here Q_α^a ($\alpha = 1, 2$) is a left-handed Weyl spinor and $\bar{Q}^{a\dot{\alpha}} = (Q_\alpha^a)^\dagger$ a right-handed Weyl spinor, both of which are in the representation of $SO(1, 3)$ of the space-time. $a = 1, \dots, \mathcal{N}$, \mathcal{N} is the number of the independent supersymmetries of the algebra. If the graviton is the particle with the largest spin, then the maximum value of \mathcal{N} can be 8. Q^a transforms between the fermions and bosons and the commutation relations is defined as:

$$\begin{aligned} \{Q_\alpha^a, \bar{Q}_\beta^b\} &= 2\delta^{ab}\sigma_{\alpha\beta}^\mu P_\mu \\ \{Q_\alpha^a, Q_\beta^b\} &= 2\epsilon_{\alpha\beta}Z^{ab} \end{aligned} \quad (2.68)$$

Here Z^{ab} is the central charge which is anti-symmetric in the indices of a and b , For $\mathcal{N} = 1$ this obviously gives that $Z^{ab} = 0$. And the supercharge Q^1 itself commute with translations.

With the supercharge operator we can construct the supersymmetry multiplets, as the fermionic operator Q generates the transformations as:

$$Q^1|Boson\rangle = |Fermion\rangle \quad Q^1|Fermion\rangle = |Boson\rangle \quad (2.69)$$

From the commutation relations we may draw the conclusion that the Bosonic and Fermionic degrees of freedom are equal[15] in SUSY (supersymmetry). In the SM we have different fermions and bosons but it is obvious that they cannot be particles in the same SUSY multiplets. For the simplest case we take $\mathcal{N} = 1$, in this case we can have the chiral fermions and parity violations. The simplest possibility for a supermultiplet is then a single Weyl spinor and two real scalars(or a complex scalar), $n_B = n_F = 2$, this is called a chiral or matter of scalar supermultiplet. If we include a massless spin-1 vector boson in a supermultiplet, which has a degree of freedom $n_B = 2$, this then may correspond to a superpartner of a massless Weyl spinor. So for $\mathcal{N} = 1$, we have these two type of multiplets which should be enough for the SM.

The Minimal Supersymmetric SM(MSSM) is the minimal extension of the SM. Now all the particles in the SM may have their superpartners, for fermions, they are named by adding a 's' in front and for bosons by adding a suffix 'ino'. In the superfield formalism, the SM multiplets can be expressed in the forms of the chiral superfields for Higgs and fermions while the gauge vector superfields for gauge bosons. This is listed in table 1.1 and 1.2 in Ref.[63]. We have the left-handed chiral superfield Q^i for the quarks and L^i for the leptons for the i th generation, H_u and H_d for Higgs particles, while U^i and D^i for right-handed quarks and E^i for right-handed leptons, again i is the indices for the generations. The reason for the requirement of two Higgs superfield is that in supersymmetry, the complex conjugation of the superfield is not supersymmetric invariant, to give mass to right handed chiral superfields, we need one more Higgs chiral superfield. For the gauge part, we should have gauge superfields V_g^α , V_W^i and V_B for $SU_c(3)$, $SU_L(2)$ and $U(1)_Y$ respectively. With above field contents, we can construct the supersymmetric Lagrangian using the superfield formalism introduced in Appedix A. The superpotential for MSSM is:

$$W_{MSSM} = \bar{U}^i y_u^{ij} Q^j H_u - \bar{D}^i y_d^{ij} Q^j H_d - \bar{E}^i y_e^{ij} L^j H_d + \mu H_u H_d \quad (2.70)$$

Here the y 's are 3×3 Yukawa coupling matrices.

Since we have only observed the SM particles but not their superpartners, so if SUSY exists, it must be broken. In SUSY, as for other symmetries, the breaking comes from a finite VEV. This can be

obtained by the non-zero constant F or D terms such as the "Fayet-Iliopoulos term" $L_{F.I.} = \xi D$ [64] or the "O'Raifeartaigh term" [65]. These terms may originate from the gravitational interactions at the Planck scale or from gauge interactions with a "Messenger" chiral superfield[66, 67, 68, 69]. For MSSM, the soft supersymmetry breaking terms can be written as[63]:

$$\begin{aligned} \mathcal{L}_{soft}^{MSSM} = & -\frac{1}{2}(M_3\tilde{g}\tilde{g} + M_2\tilde{W}\tilde{W} + M_1\tilde{B}\tilde{B} + c.c.) \\ & -(\tilde{u}_R^i a_u^{ij} \tilde{Q}^j H_u - \tilde{d}_R^i a_d^{ij} \tilde{Q}^j H_d - \tilde{e}_R^i a_e^{ij} \tilde{L}^j H_d + c.c.) \\ & -\tilde{Q}^{i\dagger} m_Q^{ij} \tilde{Q}^j - \tilde{L}^{i\dagger} m_L^{ij} \tilde{L}^j - \tilde{u}_R^{i\dagger} m_u^{ij} \tilde{u}_R^j - \tilde{d}_R^{i\dagger} m_d^{ij} \tilde{d}_R^j \\ & -m_{H_u}^2 H_u^* H_u - m_{H_d}^2 H_d^* H_d - (bH_u H_d + c.c.) \end{aligned} \quad (2.71)$$

Here M_1, M_2, M_3 are the bino, wino and gluino mass terms, each a is a 3×3 mass matrix with dimension $[M]$, each m^2 is also 3×3 matrix for scalar particles. And it is expected all these quantities have similar mass at the tree level, that is:

$$M_1, M_2, M_3, a_u, q_d, a_e \sim m_0 \quad m_Q^2, m_L^2, m_U^2, m_D^2, m_E^2, m_{H_u}^2, m_{H_d}^2, b \sim m_0^2 \quad (2.72)$$

But at the TeV level the mass may be different due to the renormalization effects and from the renormalization group (RG) equations we can expect the sfermions for the first generation to have the mass as[63]:

$$\begin{aligned} m_Q^2 &= m_0^2 + K_3 + K_2 + \frac{1}{36}K_1 \\ m_U^2 &= m_0^2 + K_3 + \frac{4}{9}K_1 \\ m_D^2 &= m_0^2 + K_3 + \frac{1}{9}K_1 \\ m_L^2 &= m_0^2 + K_2 + \frac{1}{4}K_1 \\ m_E^2 &= m_0^2 + K_1 \end{aligned} \quad (2.73)$$

Here K 's are contributions from the renormalizations of different gauge interactions, and it is found at one loop level to be:

$$K_a(Q) = \left\{ \begin{array}{c} 3/5 \\ 3/4 \\ 4/3 \end{array} \right\} \times \frac{1}{2\pi^2} \int_{\ln Q}^{\ln Q_0} dt g_a^2(t) |M_a(t)|^2 \quad (a = 1, 2, 3) \quad (2.74)$$

g_a is the running gauge coupling constant for three different interactions and $M_a(t)$ the running mass of gauginos. Q^0 is the input scales for RG.

Higgs particles get an extra mass contributions from the SUSY symmetry breaking. We have the two Higgs potential as (if we set $H_u^+ = H_d^- = 0$):

$$\begin{aligned} V &= (|\mu|^2 + m_{H_u}^2)|H_u^0|^2 + (|\mu|^2 + m_{H_d}^2)|H_d^0|^2 - (bH_u^0 H_d^0 + c.c.) \\ &+ \frac{1}{8}(g^2 + g'^2)(|H_u^0|^2 - |H_d^0|^2)^2 \end{aligned} \quad (2.75)$$

This potential will give the non-zero VEV's for H_u and H_d (v_a and v_b respectively), these VEV's are responsible for the SM fermion masses as in the SM.

After gauge SSB, a mixture between the neutral SUSY partners of gauge bosons and Higgs bosons is induced. The mass matrix for the neutral particles $\tilde{N}^T = (\tilde{B}, \tilde{W}^0, \tilde{H}_d^0, \tilde{H}_u^0)$ is:

$$M_{\tilde{N}} = \begin{pmatrix} M_1 & 0 & -g'v_d/\sqrt{2} & g'v_u/\sqrt{2} \\ 0 & M_2 & gv_d/\sqrt{2} & -gv_u/\sqrt{2} \\ -g'v_d/\sqrt{2} & gv_d/\sqrt{2} & 0 & -\mu \\ g'v_u/\sqrt{2} & -gv_u/\sqrt{2} & -\mu & 0 \end{pmatrix} \quad (2.76)$$

Here M_1 and M_2 come directly from soft SUSY breaking of MSSM as in (2.71) while $-\mu$ comes from the Higgsino mass from superpotential (2.70). The g and g' terms comes from the Higgs-Higgsino-gaugino coupling from the "Kähler Potential" in Appedix A, with the Higgs VEV's from the broken symmetry. After diagonalization, we can get the mass eigenstates χ_i the so-called neutrinos:

$$\tilde{\chi}_i = \mathcal{N}_{ij} N_j \quad (2.77)$$

which gives the diagonalized matrix elements

$$M_{\chi} = N^* M_{\tilde{N}} N^{-1} = \begin{pmatrix} M_{\chi_1} & 0 & 0 & 0 \\ 0 & M_{\chi_2} & 0 & 0 \\ 0 & 0 & M_{\chi_3} & 0 \\ 0 & 0 & 0 & M_{\chi_4} \end{pmatrix} \quad (2.78)$$

If the condition $m_Z \gg |\mu \pm M_1|, |\mu \pm M_2|$ is imposed we can get the mass eigenstates very close to superpartner states, with $\chi_1 \approx \tilde{B}_0$, $\chi_2 \approx \tilde{W}_0$ and $\chi_3, \chi_4 \approx (\tilde{H}_u^0 \pm \tilde{H}_d^0)/\sqrt{2}$ with mass eigenvalue:

$$\begin{aligned} m_{\chi_1} &= M_1 - \frac{m_Z^2 \sin^2 \theta_W (M_1 + \mu \sin 2\beta)}{\mu^2 - M_1^2} + \dots \\ m_{\chi_2} &= M_2 - \frac{m_Z^2 (M_2 + \mu \sin 2\beta)}{\mu^2 - M_2^2} + \dots \\ m_{\chi_3} &= |\mu| + \frac{m_Z^2 (I - \sin 2\beta) (\mu + M_1 \cos^2 \theta_W + M_2 \sin^2 \theta_W)}{2(\mu + M_1)(\mu + M_2)} \\ m_{\chi_4} &= |\mu| + \frac{m_Z^2 (I + \sin 2\beta) (\mu - M_1 \cos^2 \theta_W - M_2 \sin^2 \theta_W)}{2(\mu - M_1)(\mu - M_2)} \end{aligned} \quad (2.79)$$

Here θ_W is the Weinberg angle and $\beta = \tan^{-1}(v_u/v_d)$ and I can be ± 1 .

Above we briefly introduced the MSSM, which is the minimal extension of SM under SUSY. Here, we haven't found terms which can lead to $0\nu\beta\beta$, this will be discussed immediately as we introduce the R -Parity which is important for the decays of LSP(Lightest SUSY particle).

2.3.2 R Parity and Lepton Number Conservation

As we did show in last section, by replacing the SM particles by corresponding superfields, we can construct the SUSY Lagragian as in the SM. However, we can find some extra terms which are SUSY invariant but do not originate from the SM:

$$f = \bar{U} \bar{D} \bar{D} + Q \bar{D} L + L \bar{E} L + L H \quad (2.80)$$

These terms will introduce some extra interactions which may lead to instability of LSP and also the decay of the proton. So one new discrete symmetry called R-parity(or matter parity) is introduced[70, 71], the most convenient definition is:

$$M \rightarrow -M \quad V \rightarrow V, \theta \rightarrow -\theta \quad X \rightarrow X, \bar{\theta} \rightarrow -\bar{\theta} \quad (2.81)$$

Here M are matter superfields, V vector superfield and X denote other chiral superfields (*e.g.* Higgs superfield). As we can see, SUSY partners are R-parity odd (empirical definitions: $R_p = (-1)^{3B+L+2S}$, B for baryon number, L for lepton number and S for spin). This prevents the spontaneous decay of the LSP's, since it is the lightest R-parity odd particle. This also makes LSP the best candidate for Dark Matter. Also in this case, above superpotential (2.80) is R-parity violating and cannot be presented in the MSSM.

However, the Supersymmetry breaking may also accompanied with the R_p violation[72]. Current experiments have strong constraints on this violation and make R_p nearly an exact discrete symmetry. In this occasion, $0\nu\beta\beta$ is allowed but should be suppressed. So the $0\nu\beta\beta$ can be a good indicator for this violation of R-parity if this mechanism dominates the process. We now discuss this possibility.

In the MSSM model, with three generations of leptons and quarks, the R-parity violating terms can be written as:

$$f_{\mathcal{R}_p} = \lambda_{ijk} L_i L_j \bar{E}_k + \lambda'_{ijk} L_i Q_j \bar{D}_k + \lambda''_{ijk} \bar{U}_i \bar{D}_j \bar{D}_k \quad (2.82)$$

Here i, j, k are indices of the generations and the Last term in (2.80) has been rotated away by the redefinition of superfield L [73], the coupling constants $\lambda(\lambda')$ are antisymmetric in the first(last) two indices. As pointed out before, the simultaneous existence of these three terms will lead to the proton decay since B and L are violated together, this makes the λ s extremely small from current experiments. But if we, instead of R_p , impose another discrete symmetry which is compatible with GUT theories[73, 74]:

$$(Q, \bar{U}, \bar{D}) \rightarrow -(Q, \bar{U}, \bar{D}), (L, \bar{E}, H_{1,2}) \rightarrow (L, \bar{E}, H_{1,2}) \quad (2.83)$$

Then the third term in (2.82) is excluded out ($\lambda'' = 0$), in this case the Baryon number is conserved while the lepton number is violated, this prevents the proton decay. For the $0\nu\beta\beta$, only the first generation of the fermions (u, d, e) are concerned and we are interested in the lepton number violations. Thus we can write down the Lagrangians which are involved in this decay as following, first the lepton number violating terms in the R_p violating superpotential:

$$\begin{aligned} \mathcal{L}_{\mathcal{R}_p} &= \lambda'_{111} \left[\begin{pmatrix} \bar{u}_L & \bar{d}_L \end{pmatrix} \begin{pmatrix} e_R^C \\ -\nu_R^C \end{pmatrix} \right] \tilde{d}_R + \begin{pmatrix} \bar{e}_L & \bar{\nu}_L \end{pmatrix} \bar{d}_R \begin{pmatrix} \tilde{u}_L^* \\ -\tilde{d}_L^* \end{pmatrix} \\ &+ \begin{pmatrix} \bar{u}_L & \bar{d}_L \end{pmatrix} \bar{d}_R \begin{pmatrix} \tilde{e}_L^* \\ -\tilde{\nu}_L^* \end{pmatrix} + H.c. \end{aligned} \quad (2.84)$$

Then the interactions for gluino(for colored particles) and neutralino with the SM fermions and

their superpartners:

$$\mathcal{L}_{\tilde{g}} = -\sqrt{2}g_3 \frac{\lambda_{\alpha\beta}^{(a)}}{2} (\bar{q}_L^\alpha \tilde{g}^a \tilde{q}_L^\beta - \bar{q}_R^\alpha \tilde{g}^a \tilde{q}_R^\beta) + H.c. \quad (2.85)$$

$$\mathcal{L}_\chi = \sqrt{2}g_2 \sum_{i=1}^4 [\epsilon_{Li}(\psi_i) \bar{\psi}_L \chi_i \tilde{\psi}_L + \epsilon_{Ri}(\psi_i) \bar{\psi}_R \chi_i \tilde{\psi}_R] + H.c. \quad (2.86)$$

Here α and β are color indices and λ 's are the $SU(3)_c$ generators (the Gell-Mann Matrices). Neutrino χ 's are the mass eigenstates of the electrical neutral superpartners mentioned above, the coupling constants ϵ 's are defined as [75]:

$$\begin{aligned} \epsilon_{Li}(\psi) &= -T_3(\psi) \mathcal{N}_{i2} + \tan \theta_W [T_3(\psi) - Q(\psi)] \mathcal{N}_{i1} \\ \epsilon_{Ri}(\psi) &= Q(\psi) \tan \theta_W \mathcal{N}_{i1} \end{aligned} \quad (2.87)$$

$Q(\psi)$ and $T_3(\psi)$ are the electrical charge and third component of weak isospin for fermions respectively. And \mathcal{N}_{ij} comes from the diagonalizations of the mass matrix $\chi_i = \mathcal{N}_{i1} \tilde{B} + \mathcal{N}_{i2} \tilde{W}^3 + \mathcal{N}_{i3} \tilde{H}_1^0 + \mathcal{N}_{i4} \tilde{H}_2^0$ expressed in the previous section, θ_W is the Weinberg angle. The mass terms are included in the SUSY soft-breaking Lagrangians we mentioned above.

With these interactions in hand, we can begin to construct the required $0\nu\beta\beta$ Feynmann diagrams. As we have mentioned before, the basic $0\nu\beta\beta$ process at the quark level is a process with two incoming d quarks, two outgoing u quarks and two outgoing electrons, fig.2.3. For the moment we consider only tree level diagrams, so from the topological point of view, to connect six fermion lines, from above Lagrangians with only 3-particle interactions (Fermion-scalar-fermion interactions), one needs four vertices and three intermediate propagators. Among these three propagators, one should be fermionic due to the continuation of fermion lines in Feynman diagram (This is because fermion has a mass dimension of 3/2, and the overall mass dimensions for any interactions must be integers). So first we chose from the above Lagrangian the required vertices, which contains only terms of $\bar{u}(u^C)$, $\bar{e}(e^C)$ and $d(\bar{d}^c)$ for the possible external lines. This gives (together with the illustrated graph, fig.2.7):

$$\begin{aligned} i \quad & a). \quad \lambda'_{111} \bar{u}_L e_R^c \tilde{d}_R \quad b). \quad \lambda'_{111} \bar{e}_L d_R \tilde{u}_L^* \quad c). \quad \bar{u}_L d_R \tilde{e}_L^* \\ ii \quad & a). \quad -\frac{g_3 \lambda_{\alpha\beta}^{(a)}}{\sqrt{2}} \bar{d}_L^\alpha \tilde{g}^a \tilde{d}_L^\beta \quad b). \quad \frac{g_3 \lambda_{\alpha\beta}^{(a)}}{\sqrt{2}} \bar{d}_R^\alpha \tilde{g}^a \tilde{d}_R^\beta \quad c). \quad -\frac{g_3 \lambda_{\alpha\beta}^{(a)}}{\sqrt{2}} \bar{u}_L^\alpha \tilde{g}^a \tilde{u}_L^\beta \quad d). \quad \frac{g_3 \lambda_{\alpha\beta}^{(a)}}{\sqrt{2}} \bar{u}_R^\alpha \tilde{g}^a \tilde{u}_R^\beta \\ iii \quad & a). \quad \sqrt{2}g_2 \sum_{i=1}^4 \epsilon_{L(R)i}(u) \bar{u}_{L(R)} \chi_i \tilde{u}_{L(R)} \quad b). \quad \sqrt{2}g_2 \sum_{i=1}^4 \epsilon_{L(R)i}(d) \bar{d}_{L(R)} \chi_i \tilde{d}_{L(R)} \\ & c). \quad \sqrt{2}g_2 \sum_{i=1}^4 \epsilon_{L(R)i}(e) \bar{e}_{L(R)} \chi_i \tilde{e}_{L(R)} \end{aligned} \quad (2.88)$$

We find that the \hat{R}_p interactions correspond to the vertices of two SM fermions with one SUSY partner scalars while the gluino and neutrino interactions correspond to vertices of one SM fermion, one SUSY scalar and one SUSY fermion. From the above analysis we can see, that the diagrams should contain two vertices of the \hat{R}_p type and the other two vertices of the gluino or neutrino types. Then we can choose the required vertices which contain required out and in particles. *E.g.* first choose two vertices of \hat{R}_p types containing two fermions, then choose two vertices from gluino or neutrino terms which contain the two SM fermions not included in the two previous vertices,

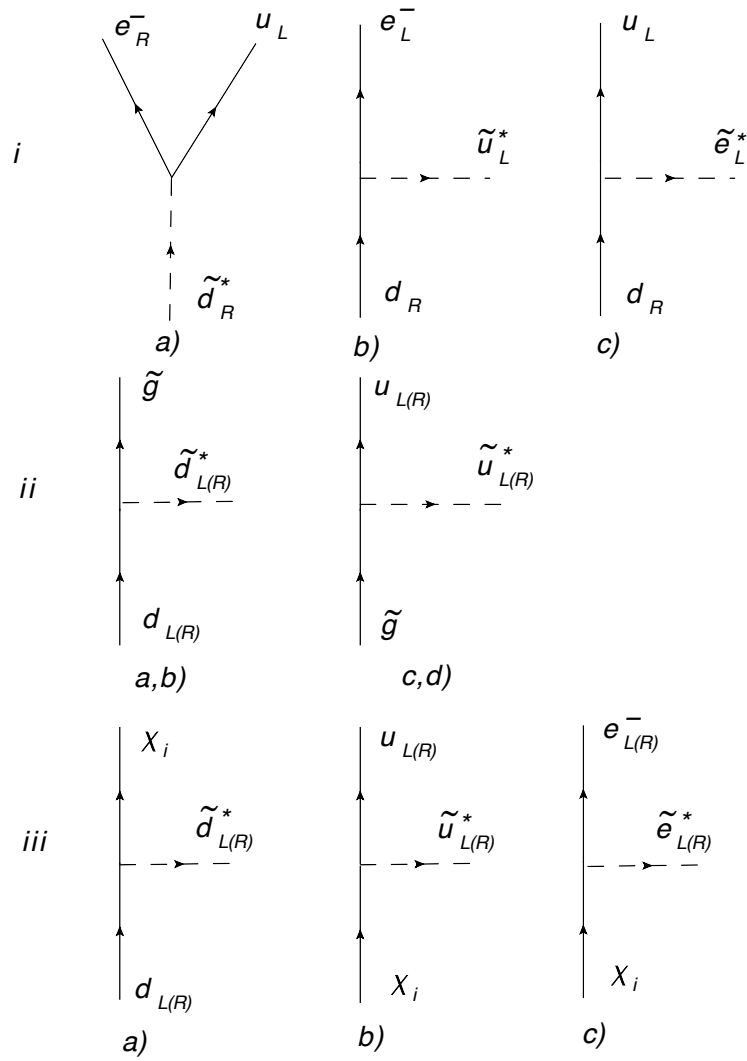


Figure 2.7: The interaction vertices which are involved in $0\nu\beta\beta$, the corresponding Lagrangian refer to (2.88).

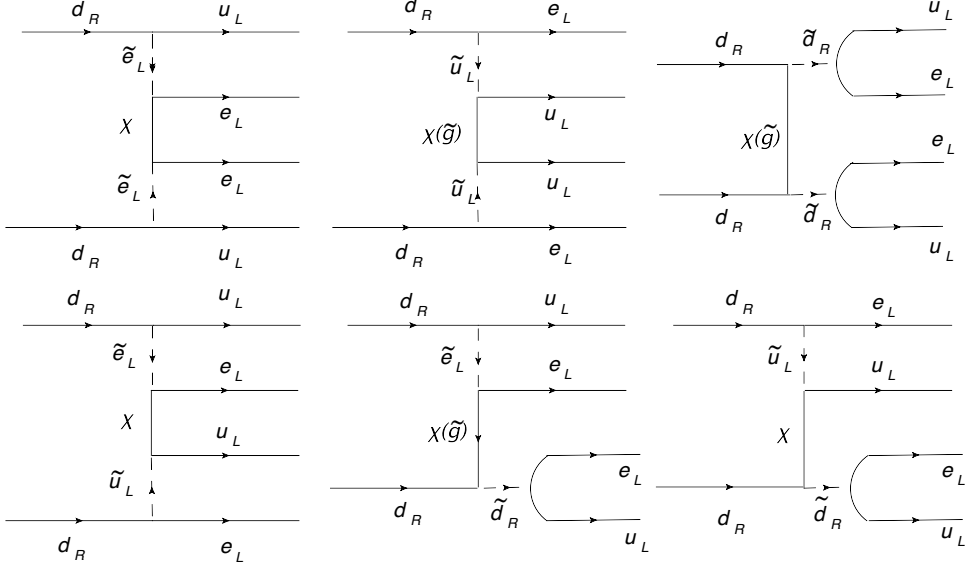


Figure 2.8: In this graph, we list all the possible diagrams for $0\nu\beta\beta$ under the \mathcal{R}_p .

these vertices should be connected by proper propagators. And we give an illustrated example of these procedures:

- i) choose the vertex $\bar{u}_L e_R^C \tilde{d}_R^*$, then we have two incoming d quarks, one outgoing u quarks and one outgoing e^- remained;
- ii) choose a vertex $\bar{u}_L d_R \tilde{e}_L^*$, now only one incoming d quark and one outgoing e^- left;
- iii) Now we should find the two vertices from the gluino or neutrino terms which contain \tilde{d}_R and \tilde{e}_L , besides, they can be connected by a fermion propagator, these can be easily found: $\bar{\chi} d_R \tilde{d}_R^*$ and $\bar{\chi} e_L \tilde{e}_L^*$, then we have an internal fermionic propagator of χ .

Following this procedure, we construct all the possible diagrams as in 2.8. We see here that one can divide these diagrams into two different types called 'Diagonal' and 'non-diagonal' ones. The former is graphically symmetric under the reflex around the axis of the intermediate heavy fermions propagators, the latter is somehow without this symmetry.

This is the most direct way to get the Feynman diagrams. However, using the effective field theories, one can get the same results, the advantages of this method are that no diagrams will be missed or repeated and the interaction strengths can be well calculated in the mean time.

The effective Lagrangian according to [73] can be defined from:

$$\begin{aligned}
 \mathcal{R}_{0\nu\beta\beta} &= \langle (A, Z + 2 | T \exp(i \int d^4x \mathcal{L}_{int}(x)) | (A, Z) \rangle \\
 &\approx i \int d^4x \langle (A, Z + 2 | \mathcal{L}_{eff}^{\Delta L_e=2}(x) | (A, Z) \rangle
 \end{aligned} \tag{2.89}$$

With $\mathcal{L}_{int} = \mathcal{L}_{\mathcal{R}_p} + \mathcal{L}_{\tilde{g}} + \mathcal{L}_{\chi}$. In principle the expansion of the exponent include all the possible diagrams for tree levels and loops. For simplicity, one considers only the leading order – the tree level diagrams, the loop diagrams can be neglected at this stage due to the heavy mass of the intermediate propagators. Because of the definite initial and final states, the expansions of the

effective actions which don't include the in and out particles in the $0\nu\beta\beta$ will be excluded out automatically. The effective Lagrangian were derived by integrating out the heavy particles. The propagators for fermions and scalar bosons can be written as:

$$\begin{aligned}\langle 0|T(\psi_i(x)\bar{\psi}_j(y))|0\rangle &= S_F(x-y) \approx -\delta^4(x-y)\frac{i}{m_i}\delta_{ij} \quad (m_i \gg p_F) \\ \langle 0|T(\phi_i(x)\phi_j^*(y))|0\rangle &= D_F(x-y) \approx -\delta^4(x-y)\frac{i}{m_i^2}\delta_{ij} \quad (m_i \gg p_F)\end{aligned}\quad (2.90)$$

In this model, heavy fermions are \tilde{g} and χ , heavy bosons are the SUSY partners of the SM fermions. Because of their heavy mass, the interactions behave like point-interactions similar to Fermi's four-fermion point interaction. We will discuss how to realize these point-like interactions at the hadron level in next chapter. For color charged particles, we should make sure their combinations are colorless in the final expression due to the color confinement. We add the color summation to those color independent Lagrangian $\mathcal{L}_{\tilde{g}_p}$ and \mathcal{L}_χ , e.g. $\mathcal{L} = \sqrt{2}/3g_2\epsilon_{Li}(\psi)\bar{d}_L^\alpha\chi_i\tilde{d}_L^\alpha$. After integrating out the heavy particles we should get the general form for the effective Lagrangian as:

$$\mathcal{L}_{eff}^{\Delta L_e=2} = \sum_{\alpha,\beta,\gamma,\delta} \mathcal{C}_{\alpha,\beta,\gamma,\delta}^{\sigma,\omega} \bar{u}^\alpha d^\beta \cdot \bar{u}^\gamma d^\delta \cdot \bar{e}_\sigma e_\omega^c \quad (2.91)$$

The coefficient \mathcal{C} is color dependent and this has the general form as point-like current-current interactions for the quark and electron currents.

Using the properties of the Gell-Mann matrices, it is easy to get:

$$\lambda_{\alpha\beta}^k \cdot \lambda_{\gamma\delta}^k = \frac{16}{9}\delta_{\alpha\delta}\delta_{\gamma\beta} - \frac{1}{3}\lambda_{\alpha\delta}^k \cdot \lambda_{\gamma\beta}^k \quad (2.92)$$

The second term is the color octet, it will not contribute to the final expressions because of the color confinement. So with these δ 's, one gets overall colorless effective actions. By using Fierz rearrangement, one can get the effective Lagrangian as[73]:

$$\begin{aligned}\mathcal{L}_{eff}^{\Delta L_e=2}(x) &= 8\pi\alpha_2\lambda'_{111} \sum_{i=1}^4 \frac{1}{m_{\chi_i}} \left[\frac{\epsilon_{Li}^2(e)}{m_{\tilde{e}_L}^4} (\bar{u}_L^\alpha d_{R\alpha}) (\bar{u}_L^\beta d_R^\beta) (\bar{e}_L e_R^c) \right. \\ &+ \frac{\epsilon_{Li}^2(u)}{m_{\tilde{u}_L}^4} (\bar{u}_L^\alpha u_{R\beta}^c) (\bar{e}_L d_{R\alpha}) (\bar{e}_L d_R^\beta) + \frac{\epsilon_{Ri}^2(d)}{m_{\tilde{d}_R}^4} (\bar{u}_L^\alpha e_R^c) (\bar{u}_L^\beta e_R^c) (\bar{d}^c_{L\alpha} d_{R\beta}) \\ &+ \left(\frac{\epsilon_{Li}(u)\epsilon_{Ri}(d)}{m_{\tilde{u}_L}^2 m_{\tilde{d}_R}^2} + \frac{\epsilon_{Li}(u)\epsilon_{Li}(e)}{m_{\tilde{u}_L}^2 m_{\tilde{e}_L}^2} + \frac{\epsilon_{Li}(e)\epsilon_{Ri}(d)}{m_{\tilde{e}_L}^2 m_{\tilde{d}_R}^2} \right) (\bar{u}_L^\alpha d_R^\beta) (\bar{u}_{L\beta} e_R^c) (\bar{e}_L d_{R\alpha}) \\ &+ \lambda'_{111} \frac{8\pi\alpha_s}{m_{\tilde{g}}} \frac{\lambda_{\alpha\beta}^a}{2} \frac{\lambda_{\gamma\delta}^a}{2} \left[\frac{1}{m_{\tilde{u}_L}^4} (\bar{u}_L^\alpha u_R^{c\gamma}) (\bar{e}_L d_R^\beta) (\bar{e}_L d_R^\delta) + \frac{1}{m_{\tilde{d}_R}^4} (\bar{u}_L^\alpha e_R^{c\gamma}) (\bar{u}_L^\gamma e_R^c) (\bar{d}^c_{L\alpha} d_R^\delta) \right. \\ &\left. - \frac{1}{m_{\tilde{d}_R}^2 m_{\tilde{u}_L}^2} (\bar{u}_L^\alpha d_R^\delta) (\bar{u}_L^\gamma e_R^c) (\bar{e}_L d_R^\beta) \right]\end{aligned}\quad (2.93)$$

This formula has a one to one correspondence to the Feynman diagrams in fig.2.8. The gauge coupling constants are defined as $\alpha_2 = g_2^2/(4\pi)$ and $\alpha_s = g_3^2/(4\pi)$, and it is highly dependent on the energy scale due to the renormalization. The usual treatment is to take the Z boson pole[76]: $\alpha_s(M_Z) = 0.127$ and $\alpha_2(M_Z) = 0.0337$. These Dirac bilinears are not colorless, but as a whole, the interactions are colorless, by suitable arrangement we can make the these bilinears colorless as we shall see.

As we have seen in fig.2.8, there are different currents for different diagrams such as electrical charged and neutral quark currents and also quark-lepton currents. These currents make the calculations of $0\nu\beta\beta$ in this model rather complicated, but since the mediating particles are extremely heavy (heavier than W boson), so these interactions are point-like four- or six-fermion interaction. It is convenient to rearrange the orders of the fermion in these fermion pairs by Fierz transformations. These are deduced by [73]:

$$\mathcal{L}_{eff}^{\Delta L_e=2}(x) = \frac{G_F^2}{2m_P} [(\eta_{\tilde{g}} + \eta_\chi)(J_{PS}J_{PS} - \frac{1}{4}J_T^{\mu\nu}J_{T\mu\nu}) + (\eta_{\chi\tilde{e}} + \eta'_{\tilde{g}} - \eta_{\chi\tilde{f}})J_{PS}J_{PS}][\bar{e}(1 + \gamma_5)e^c] \quad (2.94)$$

The currents J are defined as:

$$\begin{aligned} J_{PS} &= \bar{u}^\alpha(1 + \gamma_5)d_\alpha \\ J_T^{\mu\nu} &= \bar{u}^\alpha\sigma^{\mu\nu}(1 + \gamma_5)d_\alpha, \quad \sigma^{\mu\nu} = \frac{i}{2}[\gamma^\mu, \gamma^\nu] \end{aligned} \quad (2.95)$$

These are different from the weak currents which are with a $V - A$ type. In SUSY theory, one has then the pseudoscalar and tensor currents. And all the violating parameters η are defined as:

$$\begin{aligned} \eta_{\tilde{g}} &= \frac{2\pi\alpha_s}{9} \frac{\lambda_{111}^2}{G_F^2 m_{\tilde{d}_R}^4} \frac{m_p}{m_{\tilde{g}}} [1 + (\frac{m_{\tilde{d}_R}}{m_{\tilde{u}_L}})^4] \\ \eta_\chi &= \frac{\pi\alpha_2}{6} \frac{\lambda_{111}^2}{G_F^2 m_{\tilde{d}_R}^4} \sum_{i=1}^4 \frac{m_p}{m_\chi} [\epsilon_{Ri}^2(d) + \epsilon_{Li}^2(u) (\frac{m_{\tilde{d}_R}}{m_{\tilde{u}_L}})^4] \\ \eta'_{\tilde{g}} &= \frac{4\pi\alpha_s}{9} \frac{\lambda_{111}^2}{G_F^2 m_{\tilde{d}_R}^4} \frac{m_p}{m_{\tilde{g}}} (\frac{m_{\tilde{d}_R}}{m_{\tilde{u}_L}})^2 \\ \eta_{\chi\tilde{e}} &= 2\pi\alpha_2 \frac{\lambda_{111}^2}{G_F^2 m_{\tilde{d}_R}^4} (\frac{m_{\tilde{d}_R}}{m_{\tilde{e}_L}})^2 \sum_{i=1}^4 \frac{m_p}{m_\chi} \epsilon_{Li}^2(e) \\ \eta_{\chi\tilde{f}} &= \pi\alpha_2 3 \frac{\lambda_{111}^2}{G_F^2 m_{\tilde{d}_R}^4} (\frac{m_{\tilde{d}_R}}{m_{\tilde{e}_L}})^2 \sum_{i=1}^4 \frac{m_p}{m_\chi} [\epsilon_{Ri}(d)\epsilon_{Li}(e) + \epsilon_{Li}(u)\epsilon_{Ri}(e) (\frac{m_{\tilde{d}_R}}{m_{\tilde{u}_L}})^2] \end{aligned} \quad (2.96)$$

We see that in these effective Lagrangians, we divided the quark currents from the lepton currents, and this eases the final calculations of the NME. Here we have many parameters such as the masses and the coupling constants from MSSM which are supposed to be derived from the renormalization group techniques, as it was supposed that above the SUSY broken scale, these masses should have similar origin and values. With the running behaviors of the coupling constants in RG method, one can get their values at the low energies, and these results are illustrated in the last section.

Chapter 3

Decay Width and Nuclear Matrix Element for Double Beta Decay

The $0\nu\beta\beta$ has not been observed yet, though there're some highly contesting speculations[7]. With its observation, one can then get the half-lives, and also other measurables such as the electron spectrum. In this sense, a precise calculation of the half-lives is very important. A comparisons between the theoretical and experimental results can give us information on the underlying physics of this process.

$0\nu\beta\beta$ is a weak process with the emissions of two electrons: at the nucleon level, two neutrons transform into two protons $n + n \rightarrow p + p + e^- + e^-$, at the level of nuclei, a parent nucleus transform into a daughter nucleus: $(A, Z) \rightarrow (A, Z + 2) + e^- + e^-$. In the previous chapter, we discussed the possible underlying physics behind this process, which describes this process at the quark level: $d + d \rightarrow u + u + e^- + e^-$. At this level we have Quantum Field Theory as a tool to describe this process, so everything can be deduced analytically. But this is not enough for the descriptions of the actual process, since the decay takes place in the complicated nuclear system (due to the nuclear pairing this process can happen). But until now we can't find a perfect way to describe the properties of this system, despite the fact that it has been studied for nearly one century. This is due to the limitations of our knowledge on the few- and many- body theories. And also because of the complicated forces between the nucleons. These nucleons are governed by the strong interaction. This interaction is the strongest interaction, it can be well described by Quantum Chromodynamics (QCD) which was developed at 70s of the last century. However, due to strong interaction strength at low energies, it cannot be treated by normal perturbative methods. And a lack of treatment for the non-pertubative theory makes it really hard to deduce the details of the nucleon-nucleon forces from QCD. So one usually builds some empirical models to describe these interactions. Because of the difficulties mentioned above, it is nearly impossible to perform exact calculations for these nuclear processes. What we can do now is to use the nuclear models and reduce all uncertainties as far as possible from these models. Then one gets optimized values hopefully close to the experimental values. At the hadron level, if we compare the processes to those at at the quark level, one finds that the u and d quarks are replaced by the protons and neutrons. We now consider the interactions on the lepton and hadron level. Normally, these

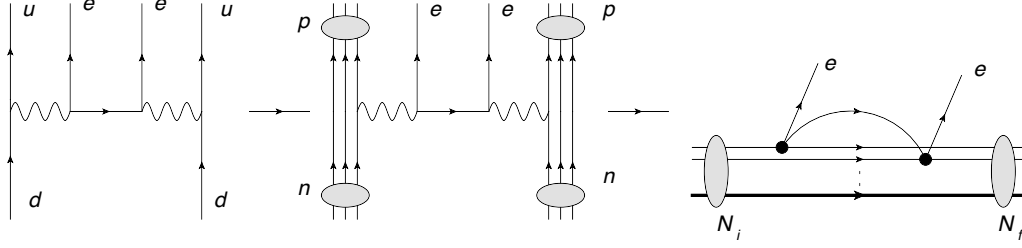


Figure 3.1: The sketch for how we simulate the nuclear process step by step from the underlying mechanism

hadrons in our case refer to nucleons. But as there are mesons inside the nuclei, in this case one can also replace the quark-antiquark pairs in the Feynman Diagrams with the mesons (the lightest mesons are the pions). Besides, there exists also the possibility that the quarks are replaced by exotic nucleons such as N^* [89] in the nuclei.

3.1 General Results of Decay Widths

The Half-life is the most important observable for $\beta\beta$ decay. From quantum theories we know that it is related with the decay width Γ given by the transition probability, $t_{1/2} = 1/\Gamma$. We treat the nucleons and the nuclear many body problem non-relativistically. But neutrinos and electrons need a fully relativistic descriptions. Our treatment for the $\beta\beta$ decay is a combination of QM and QFT methods. For relativistic particles as electrons we use the QFT. By making some assumptions, we can separate Γ into two parts: first the integrations over the momenta of the electrons and for the $2\nu\beta\beta$ also of the neutrinos yielding a phase space factor and second the nuclear matrix element (NME).

3.1.1 Decay width for $2\nu\beta\beta$

First, we give the expression of NMEs for the $2\nu\beta\beta$. This process has been observed and the half-lives for different nuclei are tabulated in table.1.1. The reason we calculate the decay widths for $2\nu\beta\beta$ first is that we use the same methods for calculating the nuclear matrix elements (NME's) for both $0\nu\beta\beta$ and $2\nu\beta\beta$. In our calculations, the NME for $2\nu\beta\beta$ is important for the determination of the parameters in our model. Values of the NME's in other nuclear models are good crosschecks for their respective quality.

The differential decay width for $2\nu\beta\beta$ decay is giving in [95, 96]:

$$d\Gamma^{2\nu} = \prod_i \frac{d^3 p_i}{(2\pi)^3 p_i^0} \sum_{jk} |\mathcal{M}_{jk}|^2 \quad (3.1)$$

Here p_i are momenta for two electrons p_1, p_2 and two neutrinos k_1, k_2 respectively. j, k are indices for the neutrino mass eigenstates. In the nuclear Coulomb field, the electron has the form of a plane wave e^{-ipx} multiplied by the square-root of the Fermi factor $F(Z, p) = (p^0/|\vec{p}|)2\pi\alpha Z[1 -$

$\exp(-2\pi\alpha Z)]^{-1}$ with Z the electric charge of the nucleus and α the fine-structure constant. Then we get the amplitude \mathcal{M} as:

$$\begin{aligned} \mathcal{M}_{jk} &= \frac{\epsilon_{jk}}{\sqrt{2}} \left(\frac{G_F}{\sqrt{2}}\right)^2 V_{ei} V_{ej} \int d^4x \int d^4y [F(Z+2, p_1^0) F(Z+2, p_2^0)]^{\frac{1}{2}} \{e^{i(p_1+k_1)x} e^{i(p_2+k_2)y} \\ &\times \bar{u}_e(p_1) \gamma_\mu (1-\gamma_5) v_{\nu_i}(k_1) \bar{u}_e(p_2) \gamma_\nu (1-\gamma_5) v_{\nu_j}(k_2) \\ &\times \langle N_f | \sum_n T(e^{-iH_0 x_0} J^\mu(\vec{x}) | N_n) \langle N_n | J^\nu(\vec{y}) e^{-iH_0 y_0} | N_i \rangle - (p_1 \leftrightarrow p_2) \} \end{aligned} \quad (3.2)$$

V is the neutrino mass matrix element in Eq.2.2. The statistical factor ϵ_{jk} comes from the exchange between two neutrinos, $\epsilon_{jk} = 1$ for $j \neq k$ and $\epsilon_{jk} = 1/\sqrt{2}$ for $j = k$. The weak currents J^μ has the form:

$$J_L^\mu(\vec{x}) = \sum_{n=1}^A \tau_n^+ [g^{\mu 0} g_V(q^2) + g^{\mu j} g_A(q^2) \sigma_j] \delta(\vec{x} - \vec{r}_n), \quad j = 1, 2, 3 \quad (3.3)$$

from the non-relativistic impulse approximations. Because the momenta of the outgoing particles are small, we can neglect here the form factors of the lepton-nucleon interaction.

The decay from the initial nucleus to the final nucleus into the ground state is a transition without changes of the angular momentum and parity. In this case we should choose the $J = 0$ operators such as $1 \cdot 1$ for 0^+ and $\vec{\sigma} \cdot \vec{\sigma}$ for 1^+ intermediate states from (3.2). By making the assumption that each electron-neutrino pair shares half of the Q value, one arrives at the expression of the decay width for the $2\nu\beta\beta$ as [88, 90]:

$$\Gamma^{2\nu}(0^+ \rightarrow 0^+) = G^{2\nu} |M^{2\nu}|^2 = a_{2\nu} m_e^2 F_0(T) g_A^4 \left(\frac{g_V}{g_A}\right)^2 |M_F^{2\nu} - M_{GT}^{2\nu}|^2 \quad (3.4)$$

Here the nuclear matrix element M is defined as[81]:

$$\begin{aligned} M_F^{2\nu} &= \sum_{M,n,m} \frac{\langle 0_f^+ | \tau_n^+ | 0_M^+ \rangle \langle 0_M^+ | \tau_m^+ | 0_i^+ \rangle}{E_M - (E_i - E_f)/2} \\ M_{GT}^{2\nu} &= \sum_{M,n,m} \frac{\langle 0_f^+ | \tau_n^+ \vec{\sigma} | 1_M^+ \rangle \cdot \langle 1_M^+ | \tau_m^+ \vec{\sigma} | 0_i^+ \rangle}{E_M - (E_i - E_f)/2} \end{aligned} \quad (3.5)$$

E_i and E_f are just the masses of the initial and final nuclei. And the quantities $a_{2\nu}$ and $F_0(T)$ in the phase space factor $G^{2\nu}$ have the form [88, 91]:

$$\begin{aligned} a_{2\nu} &= \frac{1}{4} \frac{G_F^4 m_e^9}{2\pi^7} \left[\frac{2\pi\alpha(Z+2)}{1 - \exp(-2\pi\alpha(Z+2))} \right] \\ F_0(T) &= \frac{2^4 m_e^{11}}{11!} T^7 (T^4 + 22T^3 + 220T^2 + 990T + 1980) \end{aligned} \quad (3.6)$$

Here $T = (M_i - M_f - 2m_e)/m_e$ is the total kinetic energy in units of the electron mass for all the out going particles. And the electron-neutrino phase space integrations are separated from the nuclear transition part, the NME. We get the phase space factors analytically. From the half-lives, one can then get the NME as listed in table 1.1.

3.1.2 Half-lives for the $0\nu\beta\beta$

The general Feynman diagrams for the $0\nu\beta\beta$ at the different levels are shown in fig. 3.1.

Light Majorana neutrino mechanism

For the simplest case, we have the intermediate Majorana neutrinos. We consider the light ones, that is $m_i \sim 0$. In this case the calculations are close to that of the $2\nu\beta\beta$, but now the neutrinos are virtual, carrying the internal momenta. So the outgoing particles are two electrons only. Then, the differential decay widths can be written as [88]:

$$d\Gamma^{0\nu} = \prod_{i=1}^2 \frac{d^3 p_i}{(2\pi)^3 p_i^0} |\mathcal{M}|^2 \quad (3.7)$$

The amplitude \mathcal{M} is given by [88, 91]:

$$\begin{aligned} \mathcal{M} &= \int d^4 x d^4 y \int \frac{d^4 q}{(2\pi)^4} \frac{1}{(p_1 + q)^2 - M_W^2} \frac{1}{(p_2 + q)^2 - M_W^2} \\ &\times \frac{1}{\sqrt{2}} (1 - P_{12}) \sum_{i=1}^3 U_{ei}^2 [F(Z + 2, p_1^0) F(Z + 2, p_2^0)]^{\frac{1}{2}} e^{i(p_1 x + p_2 y)} e^{iq(x-y)} \\ &\times [\bar{u}(p_2) \gamma^\mu (1 - \gamma_5) \frac{\not{q} + m_i}{q^2 - m_i^2} \gamma^\nu (1 + \gamma_5) v(p_1)] \\ &\times \sum_M e^{-i(E_M - E_i)y_0} e^{-i(E_M - E_f)x_0} \langle f | J_\mu(\vec{x}) | M \rangle \langle M | J_\nu(\vec{y}) | i \rangle \end{aligned} \quad (3.8)$$

Using the γ matrices technique, one gets $\bar{u}(p_2) \gamma^\mu (1 - \gamma_5) (\not{q} + m_i) \gamma^\nu (1 + \gamma_5) v(p_1) = \bar{u}(p_2) \gamma^\mu (1 - \gamma_5) m_i \gamma^\nu v(p_1)$, one finds that for the light Majorana neutrino mechanism with the SM symmetry, the neutrino propagator is suppressed by the helicity.

Using the non-relativistic impulse reductions, we get the current J^μ in the form

$$\begin{aligned} J^\mu(\vec{x}) &= \sum_{n=1}^A \tau_n^+ [g^{\mu 0} J_n^0(\vec{q}^2) + g^{\mu k} J_n^k(\vec{q}^2)] \delta(\vec{x} - \vec{r}_n), \quad k = 1, 2, 3 \\ J^0(\vec{q}^2) &= g_V(\vec{q}^2) \\ \vec{J}_n(\vec{q}^2) &= g_M(\vec{q}^2) i \frac{\vec{\sigma}_n \times \vec{q}}{2m_p} + g_A(\vec{q}^2) \vec{\sigma} - g_P(\vec{q}^2) \frac{\vec{q} \vec{\sigma} \cdot \vec{q}}{2m_p} \end{aligned}$$

We have for the $0\nu\beta\beta$ larger momentum transfer inside the loop in fig.3.1 than for $2\nu\beta\beta$ because the neutrino is virtual. For the size the nucleus, the uncertainty principle gives the average momentum of neutrino as about $|\vec{q}| \approx 20 MeV$. For such an exchange momentum, we must consider the form factors of the nucleons. We adopt the form factors in our numerical calculation from [81]: $g_V(\vec{q}^2) = g_V / (1 + \vec{q}^2 / \Lambda_V^2)^2$, $g_M(\vec{q}^2) = (\mu_p - \mu_n) g_V(\vec{q}^2)$, $g_A(\vec{q}^2) = g_A / (1 + \vec{q}^2 / \Lambda_A^2)^2$. From PCAC, one obtains $g_P(\vec{q}^2) = 2m_p g_A(\vec{q}^2) (1 - m_\pi^2 / \Lambda_A^2) / (\vec{q}^2 + m_\pi^2)$. Here, $g_V = 1$ and $g_A \approx 1.25$, $(\mu_p - \mu_n) = 3.70$. We choose different cutoffs for different interactions $\Lambda_V^2 = 0.71(GeV)^2$ and $\Lambda_A = 1.09 GeV$ [81].

We focus on the $0^+ \rightarrow 0^+$ case. For this case, the final result is given as in [91] by integrations over the momenta of the electrons:

$$\begin{aligned} \Gamma^{0\nu} &= G_{01}^{0\nu} |m_{ee}|^2 |g_V^2 M_F - g_A^2 (M_{GT} - M_T)|^2 \\ &= g_A^4 a_{0\nu} F_{01}(T) |m_{ee}|^2 \left(\frac{g_V}{g_A} \right)^2 |M_F - (M_{GT} - M_T)|^2 \end{aligned} \quad (3.9)$$

with $F_{01}(T) = \frac{1}{15} T(T^4 + 10T^3 + 40T^2 + 60T + 30)$, T is the same as defined before for ground state decay of $2\nu\beta\beta$ as total kinetic energy of the two emitted electrons. Here we see that the

dependence on the Q value $Q = M_i - M_f$ is for $2\nu\beta\beta$ approximately Q^{11} and for $0\nu\beta\beta$ Q^5 . This is the final expression of ground state decay width for $0\nu\beta\beta$, and this is also considered to be the leading contributions for the decay width (much larger than that of decay to the excitation state). Here, m_{ee} is the effective neutrino mass defined as:

$$m_{ee} = \sum_j V_{ej}^2 m_j \quad (3.10)$$

with V_{ej} the neutrino mass matrix elements defined in Eq.2.2.

The coefficients $a_{0\nu}$ and the Nuclear matrix elements have the form:

$$\begin{aligned} a_{0\nu} &= \frac{G_F^4 m_e^7}{2(2\pi)^5} \left[\frac{2\pi\alpha(Z+2)}{1 - \exp(-2\pi\alpha(Z+2))} \right]^2 \\ M_F &= \langle N_f | \sum_{n,m=1}^A \tau_n^+ \tau_m^+ H_F(r_{nm}) | N_i \rangle / g_V^2 \\ M_{GT} &= \langle N_f | \sum_{n,m=1}^A \tau_n^+ \tau_m^+ H_{GT}(r_{nm}) \sigma_{nm} | N_i \rangle / g_A^2 \\ M_T &= \langle N_f | \sum_{n,m=1}^A \tau_n^+ \tau_m^+ H_T(r_{nm}) S_{nm} | N_i \rangle / g_A^2 \end{aligned} \quad (3.11)$$

with

$$\begin{aligned} H_F(r_{mn}) &= \int \frac{d^3q}{(2\pi)^3} \frac{g_V^2(\vec{q}^2) e^{i\vec{q}\cdot\vec{r}_{mn}}}{q^0(q^0 + E_n - (E_f - E_i)/2)} \\ H_{GT}(r_{mn}) &= \int \frac{d^3q}{(2\pi)^3} \frac{[g_A(\vec{q}^2) + \frac{1}{3} \frac{\vec{q}^2}{4m_p^2} (2g_M(\vec{q}^2) - \vec{q}^2 g_P^2(\vec{q}^2) + 4m_p g_P(\vec{q}^2) g_A(\vec{q}^2))] e^{i\vec{q}\cdot\vec{r}_{mn}}}{q^0(q^0 + E_n - (E_f - E_i)/2)} \\ H_T(r_{mn}) &= \int \frac{d^3q}{(2\pi)^3} \frac{\frac{1}{3} \frac{\vec{q}^2}{4m_p^2} (g_M(\vec{q}^2) + \vec{q}^2 g_P^2(\vec{q}^2) - 4m_p g_P(\vec{q}^2) g_A(\vec{q}^2)) e^{i\vec{q}\cdot\vec{r}_{mn}}}{q^0(q^0 + E_n - (E_f - E_i)/2)} \end{aligned} \quad (3.12)$$

With $\vec{r}_{nm} = \vec{r}_n - \vec{r}_m$, $\sigma_{nm} = \vec{\sigma}_n \cdot \vec{\sigma}_m$, while $S_{nm} = 3(\vec{\sigma}_n \cdot \vec{q} \vec{\sigma}_m \cdot \vec{q}) - \sigma_{nm}$. The functions H 's are usually called the neutrino potentials, and if the nucleons are point-like, then this integration may give us the value $H \sim 1/r$, this is the leading order term in these expressions. So for $0\nu\beta\beta$ at the leading order, we have the Coulomb like neutrino potentials because of the smallness of the neutrino masses.

We have to add one more correction to this final result. As we are dealing with the problems in the nuclear system, the strong repulsive nature of the nuclear forces may prevent the two nucleons to get closer. So, the $0\nu\beta\beta$ potentials are changed at the short range. In our calculation, one adds the Short-Range-Correlation (SRC) to the neutrino potential to account this effect, the expression now looks like $M_i = \langle N_f | \sum_{n,m=1}^A \mathcal{O}(n, m) f(r_{nm}) H_F(r_{nm}) f(r_{nm}) | N_i \rangle$. The simplest form of this correction is of the Jastrow type [92]:

$$f(r) = 1 - e^{-ar^2} (1 - br^2) \quad (3.13)$$

with $a \approx 1, 1 fm^{-2}$ and $b \approx 0.68 fm^{-2}$.

This is the complete expression for $0\nu\beta\beta$ with the light Majorana neutrino mechanism and in the present thesis we mainly focus on this mechanism with numerical calculations for several nuclei.

Other mechanisms

In the previous chapter, we discussed different emission mechanisms for the $0\nu\beta\beta$. Different mechanisms will probably give different half-lives of the $0\nu\beta\beta$ decay.

For the see-saw mechanism, one has the right-handed neutrino besides the left-handed one. The right-handed neutrino is very heavy, with a scale from TeV to even the GUT energy scale. So their contribution will be suppressed by their heavy mass. The detailed expression of the half-lives are given in [107]. Calculations of $0\nu\beta\beta$ with sterile neutrinos in a model of extra dimensions are performed in [59, 60].

With the L-R (Left-Right) symmetrical model, one can have more complicated mechanisms for the half-lives of the $0\nu\beta\beta$. A full expression is given in [94]. And a simplified result neglecting the mixing between the left- and right-handed gauge bosons is derived by [91].

For \hat{R}_p SUSY, the result was derived in [73]. But one finds extra contributions from the intermediate pions in [78, 79, 80].

As we don't have enough experimental evidence, it is hard to say which mechanism will contribute the most to the $0\nu\beta\beta$. One would think that the light Majorana neutrino mechanism dominates, as a light neutrino has a long range which is not suppressed by SRC. So in this thesis we focus on this mechanism and all the following numerical calculations are with this one.

3.2 Nuclear Matrix Element For $0\nu\beta\beta$

In this section, we briefly represent the form of the NME for the $0\nu\beta\beta$, and in next chapter, we will give detailed expressions for different methods. As we have seen in the previous sections, the NME's can be viewed as the two-body contributions. The general form of NME from above discussions looks like:

$$M_I = \langle N_i | \sum_{n,m}^A \tau_n^+ \tau_m^+ H_I(r_{nm}) \mathcal{O}_I | N_f \rangle \quad (3.14)$$

$H_I(r_{nm})$ is the neutrino potential, which we derived in the proceeding sections. If we abandon the closure approximation by introduction of virtual intermediate states, the expressions may become slightly different as we will show in next chapter. From this point of view, we need to construct the initial and final ground states and sometimes the intermediate states. The details of these technique are the tasks of the next chapter.

Chapter 4

Many Body Approaches for Calculation of NME

In previous chapter, we derived the expression for $0\nu\beta\beta$ decay widths (or the half-lives) for different mechanisms. They can be divided in two parts: the phase space factor G which can be calculated analytically and the NME. The latter is important because it allows to determine the lepton-violation scales for different new physics models. For calculations of NME, we need nuclear structure theories which can simulate the microscopic nuclear transitions. Till present, there is no final theory which could perfectly describe the nucleus since this is a complicated many-body system. Many nuclear structure models have been proposed. The mean field theory is a starting point of them. An average mean field is calculated from the two and three body interactions by the so-called Hatree-Fock method which is also widely applied for other many-body systems such as atoms. From these mean fields, physicists usually construct the nucleus ground state, and then the excited states can be calculated.

As we have shown, $0\nu\beta\beta$ decay is governed by a two-body operator transforming two initial neutrons into two final protons in the nucleus environment. This is a charge changing process and its two-body transition matrix elements can be calculated by using the methods of many-body theory. In this section we will introduce how the NME for $0\nu\beta\beta$ decay can be calculated by different methods. The first method we are using is the pn-QRPA (proton-neutron quasiparticle random phase approximation), then we consider another important method: the Nuclear Shell Model. We will also mention other methods.

4.1 Quasi-particle RPA

The QRPA formalism is one of the widely used approaches for calculations of $0\nu\beta\beta$ decay[104]. It is developed in the Random Phase Approximation(RPA)[99] which has its origin from the TDA[98] method. So at first, we briefly introduce the RPA formalism following Ref.[101]. In the RPA formalism, we can define the excitation phonon operators as:

$$Q_m^\dagger = \sum_{l>F, i<F} [X_{li}^m c_l^\dagger c_i - Y_{li}^m c_i^\dagger c_l] \quad (4.1)$$

Here F is the Fermi energy, X and Y are the forward and backward amplitudes respectively, and c and c^\dagger are the single particle annihilation and creation operators. Then the ground state, namely the RPA vacuum, is defined by the relation $Q|RPA\rangle = 0$. The excitation states are defined as: $|m\rangle = Q_m^\dagger|RPA\rangle$ for the m th states.

To get the forward and backward amplitudes, we need first to get the RPA equations. With the variational methods: $\delta\langle m|H|m\rangle = 0$, one can get [101]:

$$\langle RPA|[\delta Q_m, [H, Q_m^\dagger]]|RPA\rangle = (E_m - E_0)\langle RPA|[\delta Q_m, Q_m^\dagger]|RPA\rangle \quad (4.2)$$

We then get the RPA equations from $\delta\langle m|H|m\rangle/\delta X(Y) = 0$,

$$\begin{aligned} \langle RPA|[c_i^\dagger c_l, [H, Q_m^\dagger]]|RPA\rangle &= \omega_m \langle RPA|[c_i^\dagger c_l, Q_m^\dagger]|RPA\rangle \\ \langle RPA|[c_l^\dagger c_i, [H, Q_m^\dagger]]|RPA\rangle &= \omega_m \langle RPA|[c_l^\dagger c_i, Q_m^\dagger]|RPA\rangle \end{aligned} \quad (4.3)$$

where the excitation energies are defined as $\omega_m \equiv E_m - E_0$ for the states $|m\rangle$'s. To derive the final form of these equations, we adopt the following approximation, by replacing the RPA ground state with the HF ground state. Then, we have, $c_i^\dagger|RPA\rangle = 0 (i < F)$ and $c_l|RPA\rangle = 0 (i > F)$. This gives the commutation relation:

$$\begin{aligned} \langle RPA|[c_i^\dagger c_l, c_n^\dagger c_j]|RPA\rangle &= \delta_{ij}\delta_{ln} - \delta_{ln}\langle RPA|c_j c_i^\dagger|RPA\rangle - \delta_{ij}\langle RPA|c_n^\dagger c_l|RPA\rangle \\ &= \delta_{ij}\delta_{ln} \end{aligned} \quad (4.4)$$

This commutation relation treats the product of two single-particle operators as a single boson operator, so this approximation is sometimes called Quasi-Boson Approximation(QBA). But in the QBA the Pauli Exclusion principle(PEP) is somehow violated, this will bring out some problems as we shall see later.

With the approximation of QBA, one then arrives to the the final form of the RPA equations from(4.3):

$$\begin{pmatrix} \mathcal{A} & \mathcal{B} \\ \mathcal{B}^* & \mathcal{A}^* \end{pmatrix} \begin{pmatrix} X^m \\ Y^m \end{pmatrix} = \omega_m \begin{pmatrix} 1 & 0 \\ 0 & -1 \end{pmatrix} \begin{pmatrix} X^m \\ Y^m \end{pmatrix} \quad (4.5)$$

The vectors $(X^m)_{ij} = X_{ij}^m$ and $(Y^m)_{ij} = Y_{ij}^m$ are forward and backward amplitudes for the excitation states $|m\rangle$ and ω_m are the energies of these excitation states. The matrices \mathcal{A} and \mathcal{B} have the form:

$$\begin{aligned} \mathcal{A}_{linj} &= \langle RPA|[c_i^\dagger c_l, [H, c_n^\dagger c_j]]|RPA\rangle = (\epsilon_l - \epsilon_i)\delta_{ln}\delta_{ij} + \bar{V}_{ljin} \\ \mathcal{B}_{linj} &= \langle RPA|[c_i^\dagger c_l, [H, c_j^\dagger c_n]]|RPA\rangle = \bar{V}_{lnij} \end{aligned} \quad (4.6)$$

Here the Hamiltonian has the form: $H = H_0 + H_i = \epsilon_i c_i^\dagger c_i + (1/4)\bar{V}_{ijkl}c_i^\dagger c_j^\dagger c_l c_k$, with ϵ the single particle energy and V the residual interaction, $\bar{V}_{ii'jj'} = V_{ii'jj'} - V_{ii'j'j}$ for convenience. By diagonalizing these RPA equations, one can get the excitation energy and the forward and backward amplitudes X and Y.

As we have mentioned earlier, nuclear pairing is important in the nuclei, and the quasi-particle RPA(QRPA) approach[100]takes into account this important phenomenon. So for a introduction of QRPA method, we first introduce the usual treatment of nuclear pairing, within the BCS

formalism. In this formalism, nucleons near the Fermi surface are paired with each other by the residual interactions, and calculations show that the pairs with total angular momentum $J = 0$ are energetically favorite, so the ground state, namely the BCS vacuum, should be with only $J = 0$ pairs. These pairs are formed by nucleons with the same angular momentum and opposite projections. So the BCS vacuum is defined as[105]:

$$|BCS\rangle = \prod_{k>0} (u_k + v_k c_k^\dagger c_{\tilde{k}}^\dagger) |0\rangle \quad (4.7)$$

Here $k > 0$ refer to all states with positive angular momentum projections J_z , and \tilde{k} are the time-reversed states which have an opposite J_z , so the states (k, \tilde{k}) run out the whole space, u_k and v_k are the BCS coefficients, and v_k^2 is the occupation probability of states (k, \tilde{k}) . In our thesis, we consider only the proton-proton and the neutron-neutron pairing. Because in even-even nuclei, all protons and neutrons can be paired, so this brings out the existence of the $0\nu\beta\beta$ decay. And, one can see that the BCS formalism is suitable to describe the ground states of these even-even nuclei, and all the $0\nu\beta\beta$ emitters are even-even nuclei. To get the BCS coefficients, we must first derive the BCS equations and solve it. The Halmitonian include the pairing interactions reads:

$$H = \sum_{k>0} \epsilon_k + \sum_{k, k'>0} v_{k\tilde{k}k'\tilde{k}'} c_k^\dagger c_{\tilde{k}}^\dagger c_{\tilde{k}'} c_{k'} \quad (4.8)$$

we can get the BCS equations by variational methods: $\langle BCS | \hat{H} - \lambda \hat{N} | BCS \rangle$:

$$2\tilde{\epsilon}_k u_k v_k + \Delta_k (v_k^2 - u_k^2) = 0, \quad k > 0 \quad (4.9)$$

with

$$\begin{aligned} \tilde{\epsilon}_k &= 1/2(\epsilon_k + \epsilon_{\tilde{k}}) - \lambda \\ \Delta_k &= - \sum_{k'>0} \bar{v}_{k\tilde{k}k'\tilde{k}'} u_{k'} v_{k'} \end{aligned}$$

And then one can get the solution for u_k and v_k as:

$$\begin{aligned} v_k^2 &= \frac{1}{2} \left[1 - \frac{\tilde{\epsilon}_k}{\sqrt{\tilde{\epsilon}_k^2 + \Delta_k^2}} \right] \\ u_k^2 &= \frac{1}{2} \left[1 + \frac{\tilde{\epsilon}_k}{\sqrt{\tilde{\epsilon}_k^2 + \Delta_k^2}} \right] \end{aligned} \quad (4.10)$$

In BCS formalism, with the the BCS coefficients, one can introduce a new kind of annihilation and creation operators, the so-called Bogoliubov quasi-particle operators, defined as:

$$\alpha_i^\dagger = u_i c_i^\dagger - v_i c_{\tilde{i}}^\dagger = u_i c_i^\dagger + v_i c_i$$

Under this formalism, the BCS vacuum can then be written in a much simpler form:

$$|BCS\rangle \propto \prod_i \alpha_i |0\rangle \quad (4.11)$$

The QRPA formalism, as a generalization of RPA, uses the quasi-particle operators to replace the single particle operators. So in the QRPA, the phonon creation operators are now defined as[106]:

$$Q_m^\dagger = \sum_{ii'} [X_{ii'}^m \alpha_i^\dagger \alpha_{i'}^\dagger - Y_{ii'}^m \alpha_i \alpha_{i'}] \quad (4.12)$$

QRPA ground states are defined in the same manner: $Q_m|QRPA\rangle = 0$. And the QRPA ground states is replaced by the BCS vacuum by using the QBA. Using the same Hamiltonian as in the case of RPA, one can derive the QRPA equations [101]:

$$\begin{aligned}
\mathcal{A}_{ii'jj'} &= \langle QRPA|[\alpha_{i'}\alpha_i, [H, \alpha_j^\dagger\alpha_{j'}^\dagger]]|QRPA\rangle \\
&= (E_i + E_{i'})\delta_{ij}\delta_{i'j'} + \bar{V}_{ii'jj'}(u_i u_{i'} u_j u_{j'} + v_i v_{i'} v_j v_{j'}) \\
&\quad + \bar{V}_{ij\bar{i}j'}(u_i v_{i'} u_j v_{j'} + v_i u_{i'} v_j u_{j'}) - \bar{V}_{i\bar{j}\bar{i}'j'}(u_i v_{i'} v_j u_{j'} + v_i u_{i'} u_j v_{j'}) \\
\mathcal{B}_{ii'jj'} &= -\langle QRPA|[\alpha_{i'}\alpha_i, [H, \alpha_j\alpha_{j'}]]|QRPA\rangle \\
&= \bar{V}_{ii'jj'}(u_i u_{i'} v_j v_{j'} + v_i v_{i'} u_j u_{j'}) \\
&\quad + \bar{V}_{ij\bar{i}j'}(u_i v_{i'} u_j v_{j'} + v_i u_{i'} v_j u_{j'}) - \bar{V}_{i\bar{j}\bar{i}'j'}(u_i v_{i'} v_j u_{j'} + v_i u_{i'} u_j v_{j'}) \quad (4.13)
\end{aligned}$$

$E_i = \sqrt{\tilde{\epsilon}_i^2 + \delta_i^2}$ is the quasiparticle energy. To get the forward and backward amplitudes in QRPA, one need to diagonalize the matrices \mathcal{A} and \mathcal{B} . The obtained eigenvalues are the excitation energies.

4.1.1 Introduction of the pn-QRPA

The $0\nu\beta\beta$ decay changes the electrical charge of the nucleus by 2. Two neutrons in the initial even-even nucleus transform into two protons in the final even-even nuclei. An intermediate odd-odd nucleus is virtually excited in this process. To describe the states of this intermediate odd-odd nucleus, we use the pn-QRPA (proton-neutron QRPA) approach. In pn-QRPA formalism, these virtual states of the odd-odd nucleus are described as the excitations from the ground states of the even-even nuclei. Hence, these excitations involve the transitions from proton (neutron) to neutron (proton). So now we can introduce the two-quasiparticle creation operators in pn-QRPA, which have a general form as $A_{pn}^\dagger = \alpha_p^\dagger\alpha_n^\dagger$. In different system they may have different forms, *e.g.*, for spherical system, they have a form where two quasiparticles are coupled to specific angular momentums[81]. In subsequent section, we discuss mainly the deformed pn-QRPA. This method is introduced to deal with the heavily deformed nuclei such as ^{150}Nd . Later on, we will introduce some modifications to the pn-QRPA formalism.

4.1.2 pn-QRPA for deformed Nuclei

In the deformed system, the angular momentum is no longer a good quantum number, so one cannot couple the quasiparticles to a specific angular momentum. From now on we work in the intrinsic frame. In this case only the projections K are good quantum numbers, one can then define the phonon operators for the excitations as $Q_{K\pi}^{m\dagger} = \sum_{pn} X_{pn,K\pi}^m A_{pn,K\pi}^\dagger + Y_{pn,K\pi}^m \bar{A}_{pn,K\pi}$. The two quasiparticle creation and annihilation operators are defined as $A_{pn,K\pi}^\dagger = \alpha_p^\dagger\alpha_n^\dagger$ and $\bar{A}_{pn,K\pi} = \alpha_{\bar{p}}\alpha_{\bar{n}}$ with the selection rule $\Omega_p - \Omega_n = K$ and $\pi_p\pi_n = \pi$. The definition of the quasiparticle is as before $\alpha_{\bar{p}}^\dagger = u_{\bar{p}}c_{\bar{p}}^\dagger - v_{\bar{p}}c_{\bar{p}}$, c^\dagger is creation operator for single particle states, and the tilde denotes the time-reversed states. In the following part we will introduce the pn-QRPA approach in the deformed systems.

In the deformed basis, many quantities are derived by the decompositions over the spherical basis since we have these quantities expressed in that basis already, so we have first to derive the decomposition coefficients. The single particle deformed basis decompositions over the spherical

one are presented in Appendix B. For the particle-hole or particle-particle pairs(ph or pp), they can be expressed as the superpositions of the of quasiparticle pairs in spherical basis:

$$\begin{aligned} |\tau\bar{\tau}'\rangle &= \sum_{\eta_\tau\eta_{\tau'}J} F_{\tau\eta_\tau\tau'\eta_{\tau'}}^{JK} |\eta_\tau\eta_{\tau'}, JK\rangle \\ |\tau\tau'\rangle &= \sum_{\eta_\tau\eta_{\tau'}J} F_{\tau\eta_\tau\tau'\eta_{\tau'}}^{JK} |\eta_\tau\eta_{\tau'}, JK\rangle \end{aligned} \quad (4.14)$$

Here τ and τ' refer to neutron or proton. The coupled quasiparticle pairs in spherical basis have the form:

$$|\eta_\tau\eta_{\tau'}, JK\rangle = \sum_{\Omega_\tau\Omega_{\tau'}} C_{j_\tau\Omega_\tau j_{\tau'}\Omega_{\tau'}}^{JK} |\eta_\tau\Omega_\tau\rangle |\eta_{\tau'}\Omega_{\tau'}\rangle \quad (4.15)$$

The decomposition coefficients are:

$$F_{\tau\eta_\tau\tau'\eta_{\tau'}}^{JK} = B_{\eta_\tau}^\tau B_{\eta_{\tau'}}^{\tau'} (-1)^{j_{\tau'}-\Omega_{\tau'}} C_{j_\tau\Omega_\tau j_{\tau'}-\Omega_{\tau'}}^{JK} \quad (4.16)$$

Here $B_{\eta_\tau}^\tau$ is the single particle decomposition coefficients derived in Appendix B.

The BCS coefficients can be derived from the BCS equations. In the deformed case, using the realistic forces as pairing interactions, one can get the gaps in the form[29]:

$$\Delta_\tau = - \sum_J \sum_{\tau>0} F_{\tau\eta_\tau\bar{\tau}\eta_\tau}^{J0} F_{\tau'\eta_{\tau'}\bar{\tau}'\eta_{\tau'}}^{J0} G(\eta_\tau\eta_{\bar{\tau}}\eta_{\tau'}\eta_{\bar{\tau}'}, J) u_\tau v_{\tau'} \quad (4.17)$$

Here τ, τ' are proton or neutron levels. G is the G-matrix of realistic forces in the spherical harmonic oscillator basis. With these gaps, one can solve the BCS equations and get the BCS coefficients. With the BCS coefficients, one can define the two-quasiparticle operators and the QRPA phonon operators.

The pn-QRPA equations are similar to the QRPA equations. To get the matrices \mathcal{A} and \mathcal{B} , we have to derive the correct forms of the residual interactions in the deformed systems. These interactions can be express as the form of G-matrix. These matrix elements in the deformed basis can be decompositions over that in the spherical harmonic oscillator basis. With the above decomposition coefficients, we get:

$$V_{p\bar{n},p'\bar{n}'} = -2 \sum_J \sum_{\eta_p\eta_n} \sum_{\eta_{p'}\eta_{n'}} F_{p\eta_p n\eta_n}^{JK} F_{p'\eta_{p'} n'\eta_{n'}}^{JK} G(\eta_p\eta_n\eta_{p'}\eta_{n'}, JK) \quad (4.18)$$

$$V_{pn,p'n'} = 2 \sum_J \sum_{\eta_p\eta_n} \sum_{\eta_{p'}\eta_{n'}} F_{p\eta_p \bar{n}\eta_n}^{JK'} F_{p'\eta_{p'} \bar{n}'\eta_{n'}}^{JK'} G(\eta_p\eta_n\eta_{p'}\eta_{n'}, JK') \quad (4.19)$$

Here $K' = \Omega_p + \Omega_n$. We include two types of interactions, one for ph and one for pp because these two types of interactions are presented in the \mathcal{A} and \mathcal{B} matrices in (4.13). With the two-quasi particle operators and the residual interactions, we get the pn-QRPA equations in the deformed basis with the form:

$$\begin{pmatrix} \mathcal{A}(K^\pi) & \mathcal{B}(K^\pi) \\ -\mathcal{B}(K^\pi) & -\mathcal{A}(K^\pi) \end{pmatrix} \begin{pmatrix} X_{K^\pi}^m \\ Y_{K^\pi}^m \end{pmatrix} = \omega_{K^\pi, m} \begin{pmatrix} X_{K^\pi}^m \\ Y_{K^\pi}^m \end{pmatrix} \quad (4.20)$$

The matrices \mathcal{A} and \mathcal{B} have the form:

$$\begin{aligned}
\mathcal{A}_{pn,p'n'}(K^\pi) &= \delta_{pn,p'n'}(E_p + E_n) + g_{pp}(u_p u_n u_{p'} u_{n'} + v_p v_n v_{p'} v_{n'}) V_{p\bar{n}p'\bar{n}'} \\
&\quad - g_{ph}(u_p v_n u_{p'} v_{n'} + v_p u_n v_{p'} u_{n'}) V_{pn'p'n} \\
\mathcal{B}_{pn,p'n'}(K^\pi) &= -g_{pp}(u_p u_n v_{p'} v_{n'} + v_p v_n u_{p'} u_{n'}) V_{p\bar{n}p'\bar{n}'} \\
&\quad - g_{ph}(u_p v_n v_{p'} v_{n'} + v_p u_n u_{p'} v_{n'}) V_{pn'p'n}
\end{aligned} \tag{4.21}$$

Here we have introduced two new parameters: g_{ph} (the renormalization parameter for ph interactions) and g_{pp} (the renormalization parameter for pp interactions). We need to determine these two parameters to solve the QRPA equation, this will be presented later.

The details of the diagonalizations of these matrices can be found in [29], after the diagonalizations, one can get the solutions for the eigenvalues and the eigenvectors. And with the solution, we can construct the virtual states of odd-odd nuclei. In our calculations, we use two sets of intermediate states. They are excitations from either the initial or the final states:

$$|K^\pi, m_{i(f)}\rangle = Q_{K^\pi}^{m_{i(f)\dagger}} |RPA\rangle \tag{4.22}$$

This is the representation of the states in the intrinsic system. One usually needs these states in the laboratory systems under the angular momentum representations. In the laboratory frame, the states of angular momentum J with projection M can be represented as superpositions of the wave functions in the intrinsic frame:

$$\begin{aligned}
|JM(K), m\rangle &= \sqrt{\frac{3}{16\pi^2}} [\mathcal{D}_{MK}^J(\phi, \theta, \psi) Q_{m,K}^\dagger \\
&\quad + (-1)^{J+K} \mathcal{D}_{M-K}^J(\phi, \theta, \psi) Q_{m,-K}^\dagger] |0_{g.s.}^+\rangle \quad (K \neq 0) \\
|JM(K), m\rangle &= \sqrt{\frac{3}{8\pi^2}} [\mathcal{D}_{MK}^J(\phi, \theta, \psi) Q_{m,K}^\dagger |0_{g.s.}^+\rangle] \quad (K = 0)
\end{aligned} \tag{4.23}$$

Here \mathcal{D} are the rotation matrices which connect the lab system with the intrinsic system. In this case we neglect the effect of the Coriolis force which may mix states with different K . And one can prove that the calculations in these two different frames are equivalent [29], so later on we consider only calculations in the intrinsic frame.

4.1.3 Final Expression for NME

With the solutions for the QRPA equations, we can proceed to the calculations of the NME's. The NME's for $\beta\beta$ decays are expressed in the preceding chapter in a general form, in this section we will introduce the detailed forms of these expressions in the QRPA formalism.

As we have seen, the operators or the states may be transformed from one frame to another under the rotations of the axes. But the rotational symmetry will prompt the invariance of measured quantities such as the decay rates in different frames, so different choices of these frame will not change the final results of the NME's. For calculations of the deformed nuclei, it is convenient to work in the intrinsic frame.

For $2\nu\beta\beta$ decay, one finds contributions from both the Fermi and GT transition operators (3.5), but one can safely neglect the contributions from the Fermi operator as it arises from isospin mixing

effect[94]. So for $2\nu\beta\beta$, only contributions from GT operator present. So only intermediate states $K \leq 1$ and $\pi = +1$ are included from the selection rules. We then have nuclear matrix elements for $2\nu\beta\beta$ with the form:

$$M_{GT}^{2\nu} = \sum_{K=0,\pm 1} \sum_{m_i, m_f} (-1)^K \frac{\langle 0_f^+ | \beta_{-K}^- | K^+, m_f \rangle \langle K^+, m_f | K^+, m_i \rangle \langle K^+, m_i | \beta_K^- | 0_i^+ \rangle}{\bar{\omega}_{K, m_i m_f}} \quad (4.24)$$

Here $\beta_K^- = \sum_{pn} \langle p | \tau^+ \sigma_K | n \rangle c_p^\dagger c_{\bar{n}}$, this operator is derived directly from (3.5). In (3.5), the energy denominator is defined as $E_M - (E_i + E_f)/2 \rightarrow (E_{m_i} + E_{m_f})/2 - (E_i + E_f)/2 = (\omega_{m_i} + \omega_{m_f})/2$, this is the usual definition in QRPA calculations. Now we made some modifications[29] in order to fit the first experimental 1^+ energy of the intermediate nucleus. This then gives the energy denominator the form as $\bar{\omega}_{K, m_i m_f} = (\omega_{K, m_f} - \omega_{K, 1_f} + \omega_{K, m_i} - \omega_{K, 1_f})/2 + \bar{\omega}_{1^+}$, here $\bar{\omega}_{1^+}$ is the experimental energy of 1^+ state defined as $M(A, Z+1) - (M(A, Z) + M(A, Z+2))/2 + E_{1^+}$, M are the masses of these nuclei and E_{1^+} the energy of the first 1^+ excited states for the odd-odd intermediate nucleus, if the ground states of the odd-odd nuclei is 1^+ , then $E_{1^+} = 0$. The two sets of the intermediate states, the initial one and the final one expand on the same Hilbert space, the overlap factors have been calculated [106, 29]:

$$\langle K^\pi, m_f | K^\pi, m_i \rangle = \sum_{l_i l_f} [X_{l_f, K^\pi}^{m_f} X_{l_i, K^\pi}^{m_i} - Y_{l_f, K^\pi}^{m_f} Y_{l_i, K^\pi}^{m_i}] \mathcal{R}_{l_f l_i} \langle BCS_f | BCS_i \rangle \quad (4.25)$$

The factors $\mathcal{R}_{l_f l_i}$ which include overlaps of single particle wave functions of the initial and final nuclei are given by:

$$\mathcal{R}_{ll'} = \langle p \rho_p | p' \rho_{p'} \rangle (u_p^{(i)} u_{p'}^{(f)} + v_p^{(i)} v_{p'}^{(f)}) \langle n \rho_n | n' \rho_{n'} \rangle (u_n^{(i)} u_{n'}^{(f)} + v_n^{(i)} v_{n'}^{(f)}) \quad (4.26)$$

And the last term $\langle BCS_f | BCS_i \rangle$ is the overlap factor of the initial and final BCS vacua, It was given in [106].

And now we come to the calculations of $0\nu\beta\beta$. In $0\nu\beta\beta$, more intermediate states are involved. As we have seen in (3.11), the NME is in fact the matrix elements of two-body operators. In QRPA calculation we restore the intermediate states which are set to be unity matrix under the closure approximations. In this case, the NME's have the form:

$$M_I = \sum_{K^\pi} \sum_{pn, p'n'} \langle p'n' | \mathcal{O}_I | pn \rangle \langle 0_f | \widetilde{c_p^\dagger c_{\bar{n}}} | K^\pi, m_f \rangle \langle K^\pi, m_f | K^\pi, m_i \rangle \langle K^\pi, m_i | c_p^\dagger c_{\bar{n}} | 0_i \rangle \quad (4.27)$$

The overlap factors between the initial and final intermediate states are the same as that for $2\nu\beta\beta$. The initial(final) leg of the transitions between the initial(final) nucleus to the intermediate nucleus can be written as:

$$\begin{aligned} \langle 0_f | \widetilde{c_p^\dagger c_{\bar{n}}} | K^\pi, m_f \rangle &= v_p u_n X_{pn, K^\pi}^{m_f} + u_p v_n Y_{pn, K^\pi}^{m_f} \\ \langle K^\pi, m_i | c_p^\dagger c_{\bar{n}} | 0_i \rangle &= u_p v_n X_{pn, K^\pi}^{m_i} + v_p u_n Y_{pn, K^\pi}^{m_i} \end{aligned} \quad (4.28)$$

The most important part is the neutrino potential. It behaves as a two-body operator here in this formula. It is an integration over the momentum space and can be calculated numerically. In the deformed basis, it can be expressed as decompositions over the spherical ones :

$$\langle p'n' | \mathcal{O}_I | pn \rangle = \sum_J \sum_{\eta_p \eta_n \eta_{p'} \eta_{n'}} F_{p\eta_p n \eta_n}^{JK} F_{p'\eta_{p'} n \eta_{n'}}^{JK} S_{\eta_p \eta_{p'} \eta_n \eta_{n'}}^{sph}(J) \quad (4.29)$$

Here $s_{\eta_p \eta_{p'} \eta_n \eta_{n'}}^{sph}(J)$ has the form[81]:

$$s_{\eta_p \eta_{p'} \eta_n \eta_{n'}}^{sph}(J) = \sum_{\mathcal{J}} (-1)^{j_n + j_{p'} + J + \mathcal{J}} \hat{\mathcal{J}} \left\{ \begin{array}{ccc} j_p & j_n & J \\ j_{p'} & j_{n'} & \mathcal{J} \end{array} \right\} \langle \eta_{p'} \eta_{n'}, \mathcal{J} \| \mathcal{O}_I \| \eta_p \eta_n, \mathcal{J} \rangle \quad (4.30)$$

Where $\hat{\mathcal{J}} = \sqrt{2\mathcal{J} + 1}$ The operator forms of these neutrino potentials have been derived in the previous chapter. For example, the light Majorana neutrino mediating potentials are given as:

$$\mathcal{O}_F = H_F(r_{12}) \mathcal{O}_{GT} = \vec{\sigma} \cdot \vec{\sigma} H_{GT}(r_{12}) \mathcal{O}_T = S_{12} H_T(r_{12})$$

The detailed form of $H_I(r_{12})$ is expressed in the previous chapter as a result of the integration on the transferred momentum, and r_{12} the interval between the two nucleons. The total NME is expressed in (3.11).

In the expression of $H_I(r_{12})$, we see that the dependence on the excitation energies of the intermediate states may make the numerical calculation too difficult to perform, so we make the approximations by replacing the energy denominator by some closure energies as in [81].

The derivations of the NMEs for other mechanisms are similar, only the neutrino potential and the two-body transition operators are changed, the detailed expressions of these NME's are given in[80, 107].

4.1.4 Modification and Improvement for QRPA

The pn-QRPA formalism with the QBA approximations can solve a lot of many-body problems in nuclear physics, but it has also drawbacks, the most serious one is that the solution of the QRPA equations will collapse for large g_{pp} , this is due to the overestimation of the ground states correlations. In order to overcome these drawbacks, some modifications of this approach have been proposed. The first attempt is the Renormalized QRPA(RQRPA)[21, 22, 108, 109], it partially restores the PEP in (4.4) by changing the QBA approximation, But this method brings a new problem of the violation of the Ikeda sum rule (ISR). So a further improvement of this method has been brought out, the Fully-Renormalized QRPA(FRQRPA), it includes scattering terms[24, 110] in the two-quasiparticle operator, then the ISR violated in RQRPA is restored.

The main change of RQRPA formalism from the QRPA is the modification of the QBA approximation as it violated the PEP, we now adopt the true QRPA vacuum as the ground state, now the commutation relation in pn-QRPA has the form[109]:

$$\begin{aligned} \langle RPA | [A_{pn}, A_{p'n'}^\dagger] | RPA \rangle &= \delta_{pp'} \delta_{nn'} - \delta_{pp'} \langle RPA | \alpha_n^\dagger \alpha_n | RPA \rangle - \delta_{nn'} \langle RPA | \alpha_p^\dagger \alpha_{p'} | RPA \rangle \\ &= \delta_{pp'} \delta_{nn'} \mathcal{D}_{pp'nn'} \end{aligned} \quad (4.31)$$

If we set $|RPA\rangle = |BCS\rangle$, then this expression reduces to the QBA form $\mathcal{D}_{pp'nn'} = 1$ as in QRPA. Under this new RQBA approximation, the QRPA equation has a form as:

$$\begin{pmatrix} \mathcal{A}(K^\pi) & \mathcal{B}(K^\pi) \\ -\mathcal{B}(K^\pi) & -\mathcal{A}(K^\pi) \end{pmatrix} \begin{pmatrix} X_{K^\pi}^m \\ Y_{K^\pi}^m \end{pmatrix} = \omega_{K^\pi, m} \mathcal{D} \begin{pmatrix} X_{K^\pi}^m \\ Y_{K^\pi}^m \end{pmatrix} \quad (4.32)$$

Here \mathcal{A} and \mathcal{B} have the same definitions as before, and we now have new definitions: $\bar{\mathcal{A}} = \mathcal{D}^{-1/2} \mathcal{A} \mathcal{D}^{-1/2}$, $\bar{\mathcal{B}} = \mathcal{D}^{-1/2} \mathcal{B} \mathcal{D}^{-1/2}$ and $\bar{X} = \mathcal{D}^{1/2} X$, $\bar{Y} = \mathcal{D}^{1/2} Y$, these new definitions make

the QRPA equations the same form as before[109]:

$$\begin{pmatrix} \bar{A}(K^\pi) & \bar{B}(K^\pi) \\ -\bar{B}(K^\pi) & -\bar{A}(K^\pi) \end{pmatrix} \begin{pmatrix} \bar{X}_{K^\pi}^m \\ \bar{Y}_{K^\pi}^m \end{pmatrix} = \omega_{K^\pi, m} \begin{pmatrix} \bar{X}_{K^\pi}^m \\ \bar{Y}_{K^\pi}^m \end{pmatrix} \quad (4.33)$$

Now the normalization relations read:

$$\begin{aligned} \sum_{pn} \bar{X}_{pn, K^\pi}^m \bar{X}_{pn, K^\pi}^k - \bar{Y}_{pn, K^\pi}^m \bar{Y}_{pn, K^\pi}^k &= \delta_{km} \\ \sum_m \bar{X}_{pn, K^\pi}^m \bar{X}_{p'n', K^\pi}^m - \bar{Y}_{pn, K^\pi}^m \bar{Y}_{p'n', K^\pi}^m &= \delta_{pp'} \delta_{nn'} \\ \sum_m \bar{X}_{pn, K^\pi}^m \bar{Y}_{p'n', K^\pi}^m - \bar{Y}_{pn, K^\pi}^m \bar{X}_{p'n', K^\pi}^m &= 0 \end{aligned} \quad (4.34)$$

If we follow the mappings of the quasiboson operator in [109]:

$$\begin{aligned} \alpha_p^\dagger \alpha_{p'} &= \sum_n A_{pn}^\dagger A_{p'n} \\ \alpha_n^\dagger \alpha_{n'} &= \sum_p A_{pn}^\dagger A_{pn'} \end{aligned}$$

we have the self-sistent equation for \mathcal{D} :

$$\mathcal{D}_{pnp'n'} = \delta_{pp'} \delta_{nn'} - \delta_{pp'} \sum_{p''} \mathcal{D}_{p''np''n'} \sum_m \bar{Y}_{p''n', K^\pi}^{m*} \bar{Y}_{p''n, K^\pi}^m - \delta_{nn'} \sum_{n''} \mathcal{D}_{pnp''n''} \sum_m \bar{Y}_{pn'', K^\pi}^{m*} \bar{Y}_{p'n'', K^\pi}^m \quad (4.35)$$

As we can see, the renormalization matrix \mathcal{D} also depends on the RQRPA solutions, so we can use the numerical iterative methods to solve the RQRPA equations.

The RQRPA partially preserves the PEP, reduces the correlations in the ground states, but it also brings a serve problem, that is the violation of the ISR[104]. To solve this problem, some modifications were proposed[24] by introducing the Fully-renormalized QRPA(FRQRPA). In this modified formalism, they checked the differences between the RPA and QRPA phonon operators, and found that, from RPA to QRPA, there may be some terms missing in the phonon operators. Starting from the RPA formalism, one can then have phonon in the form: $Q^{m\dagger} = \sum_{pn} [x_{pn}^m C_{pn}^\dagger - y_{pn}^m \tilde{C}_{pn}]$ with $C_{pn}^\dagger = c_p^\dagger c_n$. Rewrite this operator in the quasiparticle form, we get[24] $Q^{m\dagger} = \sum_{pn} [X_{pn}^m \bar{A}_{pn}^\dagger - Y_{pn}^m \tilde{\bar{A}}_{pn}]$, and here the two quasiparticle operators have a different form from that in QRPA: $\bar{A}_{pn}^\dagger = A^\dagger + (u_n v_n B^\dagger - u_p v_p \tilde{B}) / (v_n^2 - v_p^2)$ with B^\dagger defined as $B^\dagger = \alpha_p^\dagger \alpha_n$ being the quasiparticle scattering term. Unlike two-quasiparticles in QRPA, because these operators originate from the particle creation and annihilation operators, they commute with the number operator \hat{N} . So now one can simulate the RQRPA by replace the two-quasiparticle operator with the new one, the QRPA equations become:

$$\begin{pmatrix} A(K^\pi) & B(K^\pi) \\ -B(K^\pi) & -A(K^\pi) \end{pmatrix} \begin{pmatrix} X_{K^\pi}^m \\ Y_{K^\pi}^m \end{pmatrix} = \omega_{K^\pi, m} \mathcal{U} \begin{pmatrix} X_{K^\pi}^m \\ Y_{K^\pi}^m \end{pmatrix} \quad (4.36)$$

A and B defined as before but with new two-quasiparticle operators. And now the new renormal-

ization matrix \mathcal{U} has the form:

$$\begin{aligned} \mathcal{U}_{pp'nn'} &= \langle RPA | [\bar{A}_{pn}, \bar{A}_{p'n'}^\dagger] | RPA \rangle \\ &= \delta_{pp'} \delta_{nn'} \mathcal{R}_{pn} \\ \mathcal{R}_{pn} &= 1 + ((u_n^2 - v_n^2) \mathcal{N}_n - (u_p^2 - v_p^2) \mathcal{N}_p) / (v_n^2 - v_p^2) \end{aligned} \quad (4.37)$$

Here $\mathcal{N}_\tau = \langle RPA | \alpha_\tau^\dagger \alpha_\tau | RPA \rangle$ is the relative quasiparticle occupation number for level τ in RQRPA vacuum calculated by [109]. With the notations

$$\begin{aligned} \bar{\mathcal{A}} &= \mathcal{U}^{-1/2} \mathcal{A} \mathcal{U}^{-1/2} \\ \bar{\mathcal{B}} &= \mathcal{U}^{-1/2} \mathcal{B} \mathcal{U}^{-1/2} \\ \bar{X} &= \mathcal{U}^{1/2} X, \bar{Y} = \mathcal{U}^{1/2} Y \end{aligned} \quad (4.38)$$

We come to the final form of FRQRPA equations:

$$\begin{pmatrix} \bar{\mathcal{A}}(K^\pi) & \bar{\mathcal{B}}(K^\pi) \\ -\bar{\mathcal{B}}(K^\pi) & -\bar{\mathcal{A}}(K^\pi) \end{pmatrix} \begin{pmatrix} \bar{X}_{K^\pi}^m \\ \bar{Y}_{K^\pi}^m \end{pmatrix} = \omega_{K^\pi, m} \begin{pmatrix} \bar{X}_{K^\pi}^m \\ \bar{Y}_{K^\pi}^m \end{pmatrix} \quad (4.39)$$

These equations are similar to those of RQRPA, as one can see, FRQRPA has nearly the same form as RQRPA, except the inclusions of the scattering terms, this new formalism gives us the fulfillment of ISR[24].

Under RQRPA and FRQRPA formalism, the expression for NME may change a bit. For $2\nu\beta\beta$, these new formalisms may change expressions for the two decay branches from the initial and final nucleus to the intermediate nucleus, and the overlap factors in (4.24) but keep the general forms for the NME's[24], for RQRPA:

$$\begin{aligned} \langle K^\pi m_i | \beta^- | 0_i^+ \rangle &= \sum_{pp'nn'} \langle p | \sigma | n \rangle (\mathcal{D}_{pp'nn'}^i)^{1/2} [\bar{X}_{p'n'}^i u_{p'}^i v_{n'}^i + \bar{Y}_{p'n'}^i v_{p'}^i u_{n'}^i] \\ \langle 0_f^+ | \beta^+ | K^\pi m_f \rangle &= \sum_{pp'nn'} \langle p | \sigma | n \rangle (\mathcal{D}_{pp'nn'}^i)^{1/2} [\bar{X}_{p'n'}^i v_{p'}^i u_{n'}^i + \bar{Y}_{p'n'}^i u_{p'}^i v_{n'}^i] \\ \langle K^\pi, m_f | K^\pi, m_i \rangle &= \sum_{l_i l_f} [\bar{X}_{l_f, K^\pi}^{m_f} \bar{X}_{l_i, K^\pi}^{m_i} - \bar{Y}_{l_f, K^\pi}^{m_f} \bar{Y}_{l_i, K^\pi}^{m_i}] \mathcal{R}_{l_f l_i} \langle BCS_f | BCS_i \rangle \end{aligned} \quad (4.40)$$

For FRQRPA the renormalization matrix \mathcal{U} replace \mathcal{D} in RQRPA .

For $0\nu\beta\beta$, the situation is similar, the forward- and backward- amplitudes are replaced by the renormalized one with the multiplication of $\sqrt{\mathcal{D}}$ in RQRPA or $\sqrt{\mathcal{U}}$ in FRQRPA.

The RQRPA and FRQRPA formalisms have been used for the calculations of double beta decay for spherical nuclei[109, 110] and did solve the problems of the collapse of the QRPA solutions. But an extension to the deformed nuclei are somehow difficult. This is due to the fact the iterative calculations of the renormalization matrices \mathcal{D} or \mathcal{U} are very time consuming and are out of the reach of current computational capacities.

4.2 Nuclear Shell Model

Another approach which is widely used in double beta decay calculations is the Nuclear Shell Model method[112, 113, 19]. In this method, the ground states are constructed in a way different

from the QRPA. And for $0\nu\beta\beta$ decay, they usually use the complete closure approximation in their calculations, no intermediate states are involved. For this approach, the ground states of the initial and final nuclei are not derived directly from the mean field. These states are calculated by suitable effective interactions and basis space, they can correctly reproduce many spectroscopic data of the nuclei. There are many shell model codes dealing with these calculations. A review of these codes can be found in[114], these codes all use the Lanczos algorithm. With this algorithm, one get the Hamiltonian in the form of a tridiagonal H matrix, which is a bit simpler to diagonalize. Due to the blowing up of the dimensions of the configurations with the increase of the levels, truncations are always needed, the truncated single-particle space is called the valence space.

The basis can be written in two forms, the m-scheme and the coupled scheme.

In the case of the m-scheme, the states of basis are the Slater Determinants(SD) of A particles distributed in k single-particle orbits $|nljm\tau\rangle$

$$\Phi_{a_1\dots a_A}(1, \dots, A) = \det\{\phi_{a_k}(r(k))\} = \prod_k a_{a_k}^\dagger |0\rangle \quad (4.41)$$

As in this case only (J_z, T_z) are good quantum number, the degeneracy of the (J, T) are not considered, so the dimensions of the configurations should be maximal. To reduce the dimension, we can have the second possibilities.

In the case of the coupled scheme (J or JT), the basis is defined as following: first for n particles in a given j shell, $|\gamma_i\rangle = |(j_i)_{i}^n v_i J_i x_i\rangle$ (here v_i is the seniority); the next step is to couple the states of different shells successively $[[[|\gamma_1\rangle|\gamma_2\rangle]^{\Gamma_2}|\gamma_3\rangle]^{\Gamma_3} \dots |\gamma_k\rangle]^{\Gamma_k}$, these are the basis state of the coupled scheme. Comparing to the m-scheme, the dimensions are largely reduced, but the calculations of matrix elements are much more complicated. And if we calculate the deformed nuclei, where J and T is no longer good quantum number, this scheme is not available.

Using the Lanczos diagonalization methods[115], first one needs to choose a good pivot state. By acting on the state by the Hamiltonian successively, one gets more states which are orthogonal to each other. Then we can get a tridiagonal H matrices in the basis space, the diagonalizations of these matrices will give us the eigenvalues and eigenstates. The states with the lowest energy should be ground states, and with these ground states we can carry on the calculations. For $2\nu\beta\beta$, the next step is to build the door-way states $\vec{\sigma}t_-|0_i^+\rangle$ and $\vec{\sigma}t_+|J_f^+\rangle$, using the Lanczos strength function, for one of these states at the iterations N , one can produce N 1^+ excitation states with excitation energy E_m , increasing the number of the iterations until it reaches the full converge, then we can overlap these different states with another doorway state, adding the N contributions together with the approximate energy to get $M_{GT}^{2\nu}$. For $0\nu\beta\beta$, the closure approximation is used since the the momenta of the neutrinos are much larger than the excitation energies. In this way, the expression of $M^{0\nu}$ is the two-body matrix elements between the ground states of the initial and final nuclei, without summations over the intermediate states. All the intermediate energies which appear in the calculations of the NME's are now replaced by a constant value, this is similar to our deformed QRPA calculations. But in the QRPA, we have the transitions from the initial and final nucleus to the intermediate nucleus.

As compared with the QRPA, the SM method has only one disadvantage: smaller s.p. basis that can be included due to the blowing up of the dimension of the basis space. It can essentially calculate any spectroscopic observable. This is in contrast to the QRPA, in which only two-

quasiparticle excitation of the ground states are considered. However, for the medium and heavy nuclei, a realistic NSM calculation becomes impossible due to the drastic increase of the shell model basis dimension, especially for levels beyond the pf -shell. To perform such calculations, severe truncations are needed, and this makes the results less reliable.

4.3 Other Methods

Except the approaches mentioned above, there are also some other methods. These methods are somehow not so intensively used, most of them are simplifications of the NSM method, use similar calculation techniques as that of NSM, but with different choices of the model spaces, or effective interactions, to reduce the complexity of NSM calculations.

To make the simplifications of the shell model, many methods use a much simpler basis space, such as the pseudo- $SU(3)$ [25] approach. In this method, there exists such approximated symmetries which exclude many configurations and also the $\beta\beta$ operators are divided into different representations of the pseudo- $SU(3)$ group. This largely reduces the dimension of the states space, simplifies the diagonalizations of the Hamiltonian, make the calculations for the deformed nuclei much easier. In this method the closure approximation is used since no intermediate states are included. But there is also doubt about these symmetries, whether it can describe the nuclear system well and whether these simplifications really work. As in [25], a prediction was made that for certain nuclei such as ^{160}Gd , $\beta\beta$ decays are suppressed by the pseudo symmetry, despite of the fact $Q_{\beta\beta} > 2m_e$. So this could be a good test for this model, especially for ^{160}Gd which has a decent phase space and could be a good candidate for $0\nu\beta\beta$ in addition to ^{150}Nd in the heavy mass region.

The projected-HFB (Hartree-Fock-Bogoliubov) methods[26] can be viewed as a simplified version of the QRPA, using the HFB meanfield together with the projections of the angular momentum in the deformed nuclei to construct the ground states. But in contrast to the QRPA, they have no intermediate states involved in the calculations. The closure approximations are also used as one did in pseudo $SU(3)$ model and the derivations of the NME's are similar.

The IBM (interacting boson model) has been applied to $\beta\beta$ decay recently[27]. This method constructs the ground states with different proton (neutron) pairs, and uses the SDI (surface delta interaction) as the effective interaction to diagonalize the Hamiltonians. And then, with the closure approximation and the ground states, one can calculate the NME's for $\beta\beta$ decay.

We give a very short introductions on these models, and we see that they are more or less similar to the NSM, but in the process of making some approximations, there may be some inaccuracies brought in, and one just know little about how large these inaccuracies can be since a full NSM calculations are not allowed for most of the nuclei in $\beta\beta$ decay. But these methods can be a good test of the calculations of the NME's for $\beta\beta$ decay.

Chapter 5

Results and Outlook

In this chapter we will describe the calculation results. We start from constructions of the single particle wave functions for the ground states for both the initial (parent) and final (daughter) nuclei, with nuclear pairing. The next step is the solution of the QRPA equations, that is needed for the calculations of nuclear matrix elements. In our calculation, we have two free parameter in the QRPA equations, the particle-hole interaction strength g_{ph} and particle-particle strength g_{pp} for the residual interaction. These parameters renormalize the Brückner G matrix elements derived from the realistic Bonn CD NN force. These parameters should be fixed for our final calculation and can be determined from our calculations of the Gamow-Teller strength distributions and the NME for $2\nu\beta\beta$ decay [29]. After that, we can proceed to the final calculation of the NME for the $0\nu\beta\beta$ decay.

In our work, we concentrate on two nuclei, ^{76}Ge and ^{150}Nd . The former is typical medium-mass nucleus, which is well studied in different nuclear models and whose $2\nu\beta\beta$ decay was observed by different experiments. While the latter is a typical heavy nucleus, which is strongly deformed. ^{150}Nd is thought to be the best candidate for $0\nu\beta\beta$ experiments because of its large phase space (due to a large Q value and a large Z which increases the overlap of the electrons with the nucleus). As ^{76}Ge has fewer protons and neutrons, thus a smaller model space is needed. This makes ^{76}Ge easier to calculate and one could find out how different approximations can affect the calculation result. These studies may give us a rough assessment on our calculations for the decay of heavier ^{150}Nd .

This chapter is arranged as following. First we will give the parameter sets derived either from the experiments or from theoretical estimations. We then use them for the calculations of both the ground and the excited states. Then we give some results of the pn-QRPA solutions and make an evaluation of how well our solutions can reproduce the experimental results, such as $2\nu\beta\beta$ decay or GT transitions. The final part is dedicated to a detailed analysis of the $0\nu\beta\beta$ -NME, with a special emphasis on how different parameterizations and approximations affect the results.

5.1 Choice of Model Parameters

As we know, the nucleus is a very complicated many-body system, in which there isn't a simple central potential such as the Coulomb potential in atomic physics for electrons. Instead, we use the mean-field together with the spin-orbit term, obtained in the so-called Hartree-Fock approximation, and get the single particle states with their shell structures. This choice can reproduce the "Magic number"s of the nuclei. In this case, the choice of the mean-field potential in a suitable parameterization is needed. For the spherical nuclei, it is not a good choice to use the harmonic oscillator potential having the form $V(r) \sim \omega r^2$ (and for the deformed nuclei, the deformed Harmonic Oscillator potential). We adopt the deformed Woods-Saxon potential as an improvement, which allows to reproduce well single-particle level schemes. The general form of this potential is given in the Appendix B. Here we introduce the parameterizations from [117] to determine the deformed basis:

$$\begin{aligned}
 V_0 &= -\frac{1}{2}(v_1 + v_2) - T_z(v_1 - v_2)\left(\frac{N - Z}{A}\right), \\
 V_{s.o.} &= 0.263\left(1 + 2\frac{N - Z}{A}\right)V_0 \\
 r_0 &= r_{s.o.} = r_c = 1.24fm, \\
 a_0 &= a_{s.o.} = a_c = 0.63fm
 \end{aligned} \tag{5.1}$$

Here $v_1 = 19.7MeV$, $v_2 = 87.0MeV$, and $T_z = 1/2$ for protons and $T_z = -1/2$ for neutrons is the third component of isospin operator. For the meaning of different symbols, one can look into Appendix B of this work or [101]. Here, in contrast to the previous work [29], we changed the parameterizations of [118] for superheavy nuclei to the one previously used for spherical nuclei [117]. This is due to the following: First, the former parameterization can not reproduce the GT position at a realistic value of the parameter g_{ph} without changing the spin-orbit interaction strength[29], an extra factor of 1.2 is needed. The second reason is that a too large value of $\langle r^2 \rangle$ for neutrons is obtained with parameterization in [118] and this gives a too thick neutron skin. Because of these arguments, we find that the parameterizations in [118] is not suitable for our treatment of $\beta\beta$ -decay and charge-exchanging multipole transitions in the QRPA. The parameters of [117], however, have been proved to be more suitable for the QRPA calculations[119, 120] and can avoid these problems.

With this parameterization, the calculated single-particle energy levels are shown in figures 5.1 and 5.2 for the nuclei to which we focus on in this work, ^{76}Ge and ^{150}Nd (initial nuclei) and ^{76}Se and ^{150}Sm (the $\beta\beta$ -decay products). Deformation splits the degenerated states which have in spherical system the same single particle angular momentum. Although the single-particle angular momentum is not conserved in deformed nuclei, time reversal symmetry is conserved (the Hamiltonian is invariant under the time-reversal). Now a new set of quantum numbers to define different single particle states is used, $(N, n_z, \Lambda, \Omega)$ (here N is the principal quantum number $N = n_z + |\Lambda| + 2n_\rho$, and n_z is the number of quanta in the z -direction, Λ and Ω are the projections on the z -axis of the orbital and total angular momenta) instead of that used previously in the spherical system where the angular momentum j is a good quantum number as well as the principal N and the magnetic Ω quantum numbers. This new basis makes the realistic calculations more difficult since without the j -degeneracy, more states are now involved in the calculation and the numbers

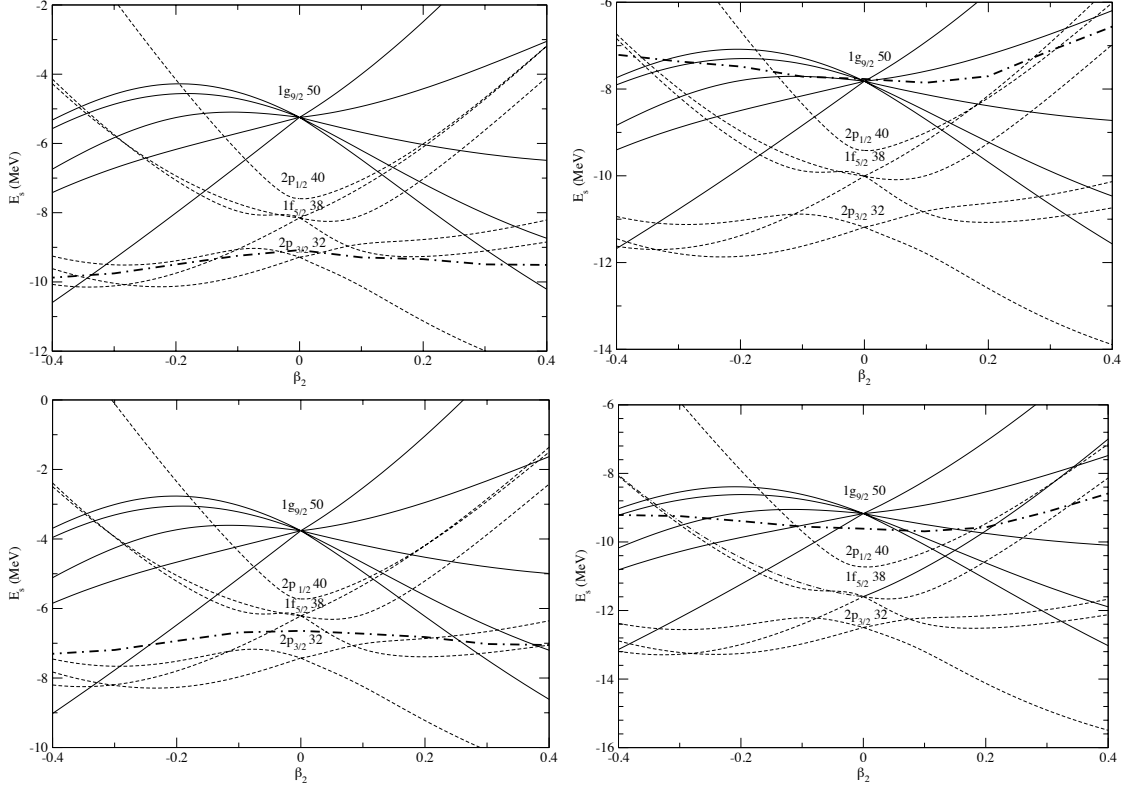


Figure 5.1: Proton and neutron energy levels around the Fermi surface for ^{76}Ge and ^{76}Se as functions of deformations. The bold dash-point line is the Fermi surface, and the y axis is the energies of the levels. The upper panels are for ^{76}Ge , with the left panel for protons and the right panel for neutrons. The lower panels are the corresponding graphs for ^{76}Se . Here β_2 is the input of our Wood-Saxon mean field, and it should be distinguished from the experimental quadrupole deformation β .

of non-degenerate levels increase drastically. This then means increase of computation time in the calculations of $\beta\beta$ decay. For the prolate deformations ($\beta_2 > 0$), the states with larger Ω are shifted to higher energies while for oblate deformations ($\beta_2 < 0$), they are shifted down. The permanent deformations tends to change the behaviors of the single particles, with more particles with low Ω below the Fermi levels for the oblate shapes, and more high Ω states below the Fermi level in the prolate shapes. On the other hand, the Fermi energies are also changed by the deformations.

Our levels have all the characteristics demonstrated in[101]:

- i) the shells which are determined by the single particle angular momentum j at zero deformation, split up into $(2j + 1)/2$ levels for $\beta_2 \neq 0$.
- ii) the quadrupole field r^2Y_{20} causes the levels with lower Ω values to be shifted downwards for positive deformations (prolate shapes) and shifted upwards for negative deformations (oblate shapes).
- iii) For larger deformations, it can happen that the curves of the levels change their slope, *etc.*

The shell structure gets now completely destroyed for large deformations, the level schemes become totally different, not only the energies of different levels, but also the order of each level has been changed. So the spherical shell model is no longer suitable to deal with deformed nuclei. To deal with the $\beta\beta$ decays, the QRPA seems a more appropriate method. As we can see, when

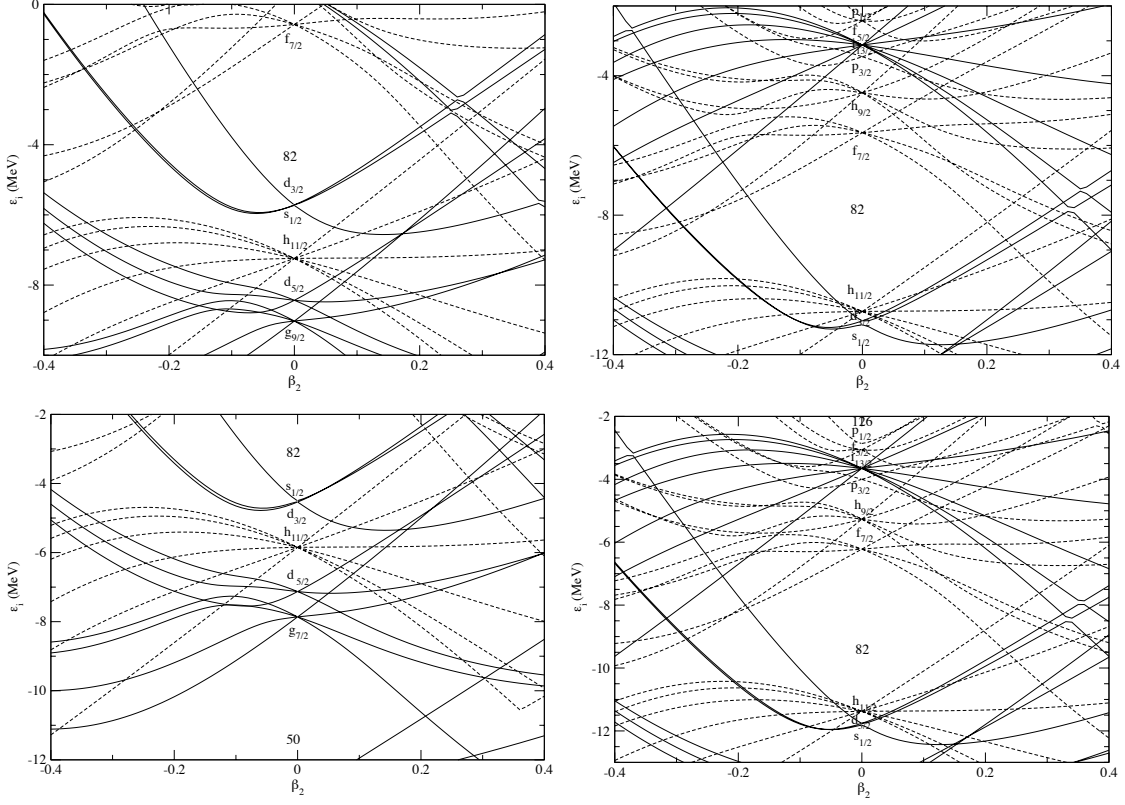


Figure 5.2: Energy levels of ^{150}Nd and ^{150}Sm , upper panels for ^{150}Nd and lower panels for ^{150}Sm , left ones for protons and right ones for neutrons.

deformations are small, although the structures inside the shells are destroyed, but different shells may still be well separated. This gives us the freedom to truncate the level space approximately by the corresponding shell structures in spherical systems. But this kind of truncations may bring us a problem for very large deformations. Since in that case, the shell structures become rather different, many levels with large principle number N may go below the Fermi surface. And the truncations will drop many such levels near the Fermi surface out if we just truncate the level space by just the major shells with the same quantum number N . So by making truncations, one must be aware of this change in the level schemes.

Our Woods-Saxon single-particle wave-functions are expanded in the basis of deformed harmonic oscillator introduced in Appendix B. To make the coefficients converge faster, we use a somewhat different definition of the harmonic oscillator basis than the conventional one. Usually, deformation of the basis is described geometrically, with the oscillator lengths b_z , b_\perp represent through the spherical one b_0 : $b_z = b_0[(1 - \sqrt{5/16\pi}\beta_2)/(1 + 2\sqrt{5/16\pi}\beta_2)]^{1/3}$ and $b_\perp = \sqrt{b_0^3/b_z}$ to keep the volume conservation. We use here $b_z = b_0[(1 - \sqrt{5/16\pi}\beta_2)/(1 + 2\sqrt{5/16\pi}\beta_2)]^{1/6}$, and also the volume conservation condition is imposed. This is the optimal choices in our calculations[121].

The mass differences between the odd-odd and even-even nuclei remind us the existence of the nuclear pairings originating from the residual interactions beyond the mean field approximations. In this work, neutron-neutron and proton-proton pairings have been taken into consideration, and for the possible neutron-proton pairing which have been studied for the $\beta\beta$ -decay in [107] is

neglected. With the five-term formula from [123], one can extract the phenomenological pairing gaps from the experimental mass differences. By renormalizing the G-matrix with the strengths g_{pair}^p and g_{pair}^n , one can reproduce these pairing gaps, calculate the BCS pairing gaps and get the Bogoliubov coefficients u and v , Eq.(4.10). The relations between renormalized strengths g_{pair} 's and the deformation parameters were studied in [111]. The Brückner G-matrix elements are obtained by solving the Bethe-Goldstone equation with a realistic NN potentials (in our case the Charge Dependent Bonn one boson exchange potential [122], other potentials lead to similar results). With the pairing gaps, after solving the BCS equations, one can get the Fermi energy(or chemical potential) λ (Eq.(4.10)) and also the occupation probabilities v^2 (Eq.eq4.10), here we use the level-dependent gaps instead of the constant one. The results for the Fermi levels in ^{76}Ge and ^{76}Se are shown in figures 5.1 for both neutrons and protons. From fig.5.1 one finds that deformations change the chemical potential for both the protons and the neutrons. For neutrons, λ is shifted up with the deformation while for protons the opposite is true. For neutrons, the deformation will change the depth of the potential well and hence the Fermi energies increase; due to the change of the Coulomb potentials, for protons, the behavior is different.

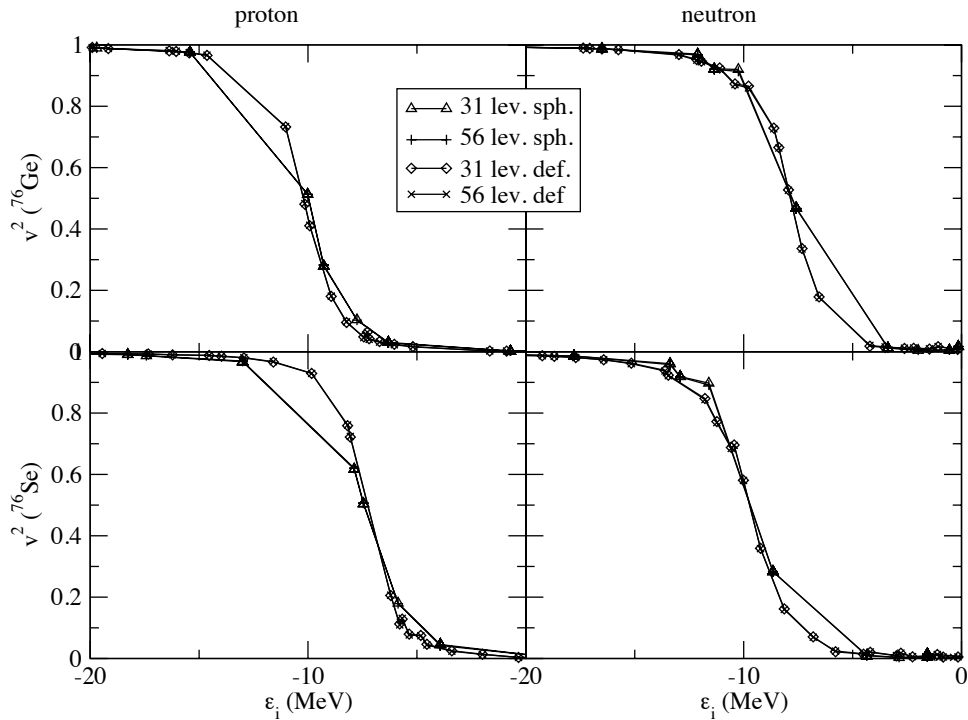


Figure 5.3: The occupation probabilities for ^{76}Ge and ^{76}Se in the spherical and deformed cases, different symbols are illustrated in the graph, 56 lev. corresponds to a level space from 0 to $5\hbar\omega$ while 31 lev. corresponds to a truncated level space from 2 to $4\hbar\omega$. The deformation parameters β_2 are listed in table??.

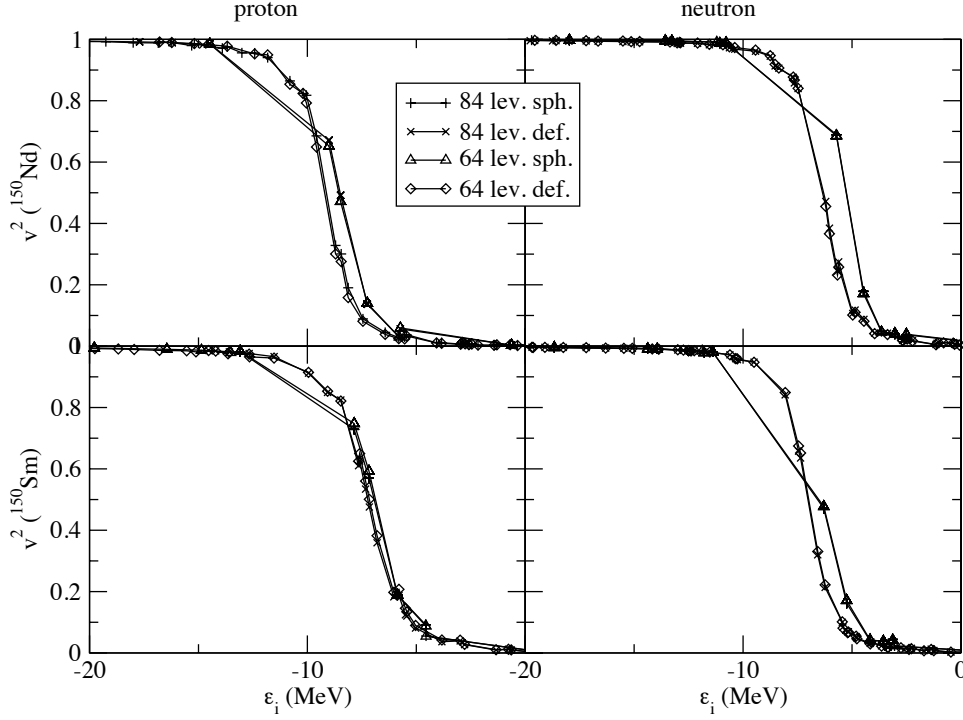


Figure 5.4: The occupation probabilities for ^{150}Nd and ^{150}Sm , different symbols are illustrated in the graph, 84 lev. means a level space from 0 to $6\hbar\omega$ while 64 lev. means a truncated level space from 4 to $6\hbar\omega$.

The solutions of the BCS equations for realistic residual interaction is similar to previous calculations with constant gaps in various references ([101] and references therein), only small changes for certain levels are observed, see figs. 5.3 and 5.4. We see again that around the Fermi surface, the occupation probabilities are smooth functions instead of a step function for the non-pairing case, and most of the levels far away from the Fermi level are either nearly fully occupied or empty. So, the pairing interaction mainly changes the behavior of the single particle levels near the Fermi levels. The effects of the deformations on the solutions were studied in [29], and the authors showed that the deformations make the behavior of the occupation probabilities of single particle levels become much smoother, and our calculations agree well with this. We have also evaluated here how the truncations may affect the calculations. Here we truncate the model space, by the principal number N , $N = 2 - 4$ for ^{76}Ge and $N = 4 - 6$ for ^{150}Nd , this means fewer nucleons are involved in the pairing. The results show that these truncations basically have no effects on the occupation probabilities of different levels since the levels excluded in our calculations are one major shell away from the central active shell (where the Fermi energy lies in). This is also an important check for the QRPA calculations since the strengths of the transitions are strongly dependent on the occupation probabilities of quasi-particles.

Table 5.1: BCS solutions for Fermi energies λ in several nuclei. Here FS (Full space) denotes a model space include all the major shells $0 - 5\hbar\omega$ and TS (Truncated space) a truncated space with major shells $2 - 4\hbar\omega$.

nuclei	β_2	λ_p (MeV)		λ_n (MeV)	
		FS	TS	FS	TS
^{76}Ge	0.0	-9.98	-9.97	-7.69	-7.69
	0.1	-10.20	-10.21	-7.86	-7.86
^{76}Se	0	-7.43	-7.44	-9.40	-9.40
	0.16	-7.27	-7.28	-9.73	-9.73
^{150}Nd	0	-8.49	-8.54	-5.32	-5.32
	0.24	-9.13	-9.22	-6.28	-6.31
^{150}Sm	0	-6.90	-6.97	-6.35	-6.36
	0.153	-7.15	-7.23	-7.00	-7.03

Table 5.2: Experimental and theoretical quadrupole deformation parameters β from different references for the nuclei in question. The first column contains the data obtain from the Coulomb reorientation experiments, the second column contains data from the exp. B(E2) transition probabilities. The third and fourth columns contain theoretical results: obtained from the realistic mean field calculations (column 3) and from the HF mean field calculations (column 4).

nucleus	experimental		theory	
	Ref.[124]	Ref.[125]	Ref.[126]	Ref.[127]
^{76}Ge	+0.095(30)	0.2623(39)	0.157	0.143
^{76}Se	+0.163(33)	0.3090(37)	-0.244	-0.241
^{150}Nd	+0.367(86)	0.2853(21)	0.221	0.243
^{150}Sm	+0.230(30)	0.19312(22)	0.176	0.206

The experiment data indicates that ^{76}Ge and ^{76}Se may be slightly deformed, while ^{150}Nd and ^{150}Sm are undoubtedly strongly deformed. To determine the deformations (in this work only the quadrupole deformation β_2 are taken into account, and other deformations such as the hexadecapole one are not expected to change the results much and are neglected), various methods, theoretical or experimental, are applied. In table ??, values of β obtained from different methods such as that derived from experimental B(E2) strengths or the Coulomb reorientation method, or from the minimum of the binding energies in HF calculations theoretically are presented. To extract the values of β from different experimental datas, the conventional way is to use the formula

$$\beta = \sqrt{\frac{\pi}{5}} \frac{Q_p}{Zr_c^2} \quad (5.2)$$

from the measured quadrupole moments Q_p in intrinsic frame, and r_c is the charge radius. The values of the first column in table?? are derived in this way; and the values of the second column

comes from the formula

$$\beta = (4\pi/3ZR_0^2)[B(E2)(0^+ \rightarrow 2^+)/e^2]^{1/2} \quad (5.3)$$

from the measured $B(E2)(0^+ \rightarrow 2^+)$ (the reduced E2 transition probability from the ground states to the final 2^+ states), Z is the proton number, e is the charge of the proton and $R_0 = 1.24A^{1/3} fm$. Hereafter, β denotes the quadrupole deformation parameter derived from above formulas and β_2 is actual quadrupole deformation parameter we adopt as an input for the Woods-Saxon mean field. One finds that for ^{76}Ge and ^{76}Se , the values in the first and second rows seem reasonable despite the theoretical predictions of a negative β in the third and fourth columns for ^{76}Se . But for ^{150}Nd and ^{150}Sm , the values in the first column have too large errors. So, we prefer the values from the B(E2) transitions, and instead of taking the deformation parameters β directly from above formulas, we adopt a consistent approach which fits the measured β . We first calculate the Quadrupole moment microscopically for the input β_2 and then using above formula connecting Q and β to get the value β^{fit} , then we compare this β^{fit} to the measured one, we repeat these process until we find the correct β_2 input of WS mean field.

Table 5.3: Theoretical and experimental β values from different references for ^{150}Nd and ^{150}Sm . We fit in our calculations the quadrupole moments extracted from the $B(E2)$ values, comparing with the experimental values from the Coulomb orientation methods (first column) and from the B(E2) (second column). Here β_2 is the quadrupole deformation input for our calculations. Q_2 is the quadrupole moment measured in the laboratory system.

nucleus	$Q_2(\text{Exp.})[124]$	$Q_2(\text{Exp.})[125]$	$\beta(\text{Exp.})[125]$	β_2	β^{fit}	Q_2^{fit}
^{150}Nd	-2.00(51)	-1.50(1)	0.2853(21)	0.240	0.285	-1.46
^{150}Sm	-1.32(19)	-1.05(1)	0.1932(21)	0.153	0.193	-1.03

The microscopic quadrupole moment can be expressed as $Q_p = \sum_i \langle i | Q^{20} | i \rangle v_i^2$, here the $|i\rangle$'s are single particle wave-functions which are introduced in Appendix B, which depend on the deformation parameters β_2 . By adjusting the input β_2 , we can correctly reproduce Q_p and sequentially β together with the mean charge radius $\langle r_c \rangle = \sqrt{\sum_i \langle r^2 \rangle v_i^2}$. The results are listed in the table??, one finds the ratio β^{exp}/β_2 is about 1.2, and the quadrupole moments predicted by the B(E2) experiments[125] are somewhat smaller than those determined from the Coulomb Reorientation experiments[124] for ^{150}Nd and ^{150}Sm . And in this work, we adopt as the β input for the wave functions for ^{76}Ge and ^{76}Se the values from the first column in table??, and for ^{150}Nd and ^{150}Sm the fitted values in table??.

From the determined parameters of the mean field potential we then get the s.p. energies and wave functions for both the initial and final nuclei in $\beta\beta$ decay as described in previous chapter and form the s.p. bases for the QRPA descriptions of the intermediate states for the unstable odd-odd nuclei. The intermediate states are constructed in the QRPA from the ground states by quasiparticle $p - n$ pair excitations.

The initial and final ground states are generally not the same, and it is discovered in [110] that the BCS overlaps between these two ground states may introduce suppressions to the NME,

as described in the previous chapter. These overlaps come from the differences between the initial and final BCS vacua, ${}_f\langle BCS|BCS\rangle_i$. The results tell us that a suppression can happen even for the spherical initial and final nuclei, and the analyses show that the differences of the deformations between the initial and final nuclei may give a further reduction [29].

5.2 Illustration of the Results for $M^{2\nu}$ and $M^{0\nu}$

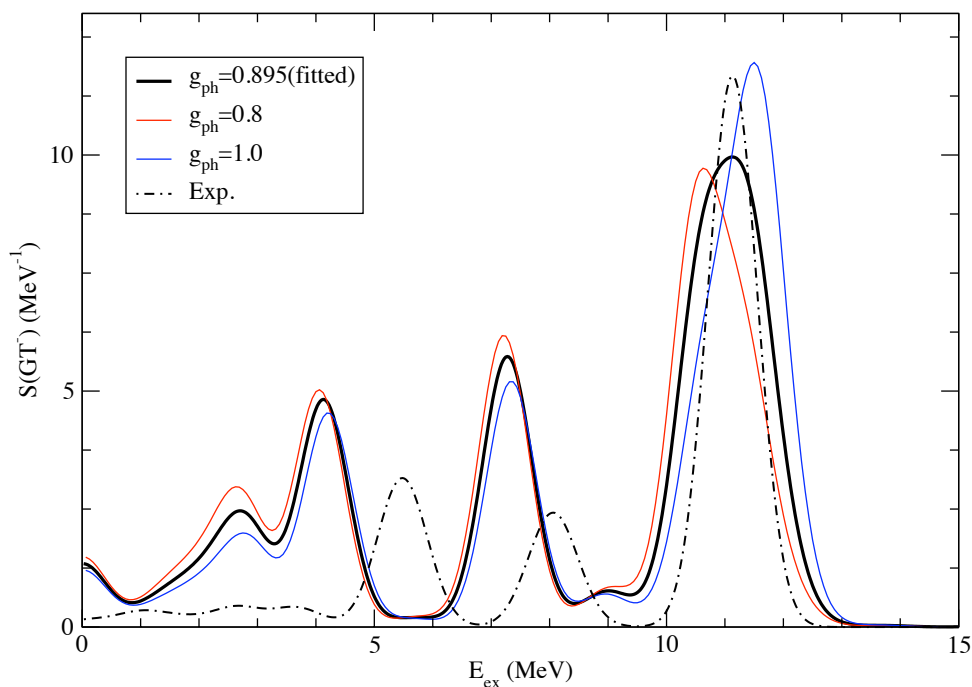


Figure 5.5: In this graph the GT strength distributions for ${}^{76}\text{Ge}$ with different values of g_{ph} are plotted. By comparing with the experiment one (the dot-dashed line) we can determine the values of g_{ph} for the pn-QRPA calculation. The best fit is $g_{ph} = 0.895$ (the bold solid line), that reproduce the experimental GT resonance energy.

In the preceding section we studied some properties of the ground states of the initial and final nuclei. These ground states are the initial and final states for the $\beta\beta$ decay. But as we see in the previous chapter, in our QRPA calculation, we need also the intermediate states for the intermediate nucleus. This then gives us more accurate results beyond the closure approximations. We renormalize the particle-particle and particle-hole channels of G-matrix of the nuclear Hamiltonian by introducing the parameters g_{pp} and g_{ph} (Eq.(4.21)). We fit the g_{ph} values by reproducing the position of the giant Gamow-Teller resonance (GTR). The particle-particle strength parameter g_{pp} is fixed to reproduce the experimental $2\nu\beta\beta$ decay half-lives. With these G-matrix elements,

one can obtain the \mathcal{A} and \mathcal{B} matrices in Eq.(4.21) and solve the QRPA equations to get the forward and backward amplitudes X and Y . These amplitudes together with the BCS solutions and the neutrino potentials can give us the final result of $M^{0\nu}$ from Eq.(4.27).

5.2.1 Multipole Transition Strength from pn-QRPA

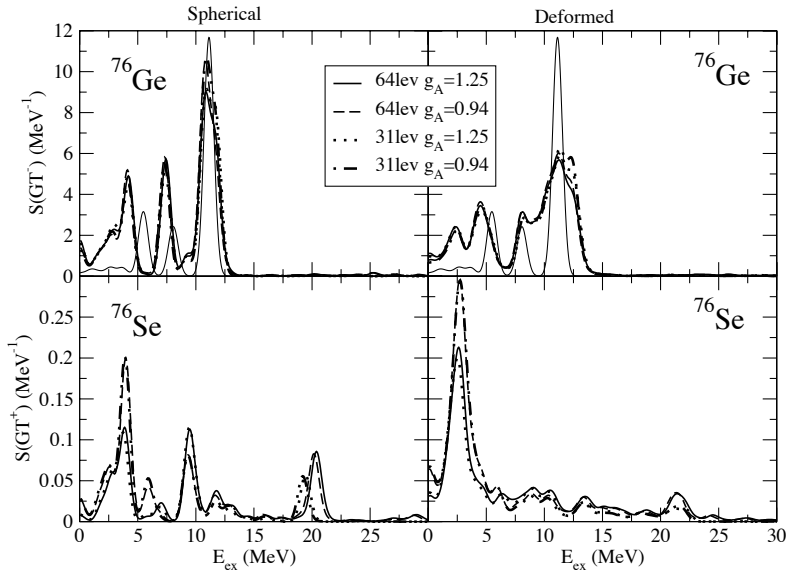


Figure 5.6: GT strength distributions calculated for ^{76}Ge and ^{76}Se for spherical and deformed nuclei by pn-QRPA. The thin solid line is the experimental data. The definitions of the different lines are give in the graphs. Here as before, the 31 lev. or 56 lev. corresponds to different model spaces, and different g_A with the corresponding fitted g_{ph} are as in table??.

The adjustment of g_{ph} has been done as illustrated in fig.5.6. The experimental position of GT resonance (GTR) is around the excitation energy of 11MeV in ^{76}Ge . Here, the relative calculated excitation energies of the intermediate nuclei, discussed in [29], are defined as $E_{ex}^{K,i} = E_{QRPA}^{K,i} - E_{QRPA}^{K,1}$, with $E_{QRPA}^{K,1}$ the first eigenvalue of the K^π states (Here after K denotes the projection of angular momentum on z -axis and J the asymptotic total angular momentum). In fig.5.5, we plot the GT strength distributions for different g_{ph} for ^{76}Ge . It can be seen from the figure that an increase of g_{ph} shifts the position of the GT resonance to higher excitation energy. But the general distribution style of GT strength remains unchanged, one can see that the three peaks have one-to-one correspondence to that of the charge-exchange scattering experiments. As in the case of the GTR, the other two peaks are also shifted to higher excitation energy by the increase of g_{ph} , but the change of their positions is not so significant as that of the GTR. As can be seen this graph, the best fitted value for g_{ph} is about 0.895, somewhat smaller than the previous result in [29]. They had a value of about 1.15[29]. The difference in g_{ph} is due to the different choice of the parameterizations of the WS mean field. This fitted value of g_{ph} is then applied to the

QRPA calculation of ^{150}Nd , since as argued in [29], g_{ph} should have an universal value for most $\beta\beta$ emitters.

The adjustment of g_{pp} is related to the $2\nu\beta\beta$ NME, we will discuss this later in the next section. Here we use in advance the fixed value from table.?? for our analyses on the multipole transitions. The GT transition is used to determine g_{ph} , but it can also be served as a test for the pn-QRPA approach. For this purpose, we have calculated other multipole transitions as well. For different multipole transitions, we choose the same values of the renormalized interaction strengths g_{ph} and g_{pp} . It is believed that in the same nuclei, for the same interaction, one should apply the same parameters for all channels. This is not the case for the separable force: These phenomenological forces need different parameterizations for different channels, one needs to fit these interaction strengths by hand with the experiments. This is why one choose the realistic interactions for the $0\nu\beta\beta$ decay calculation.

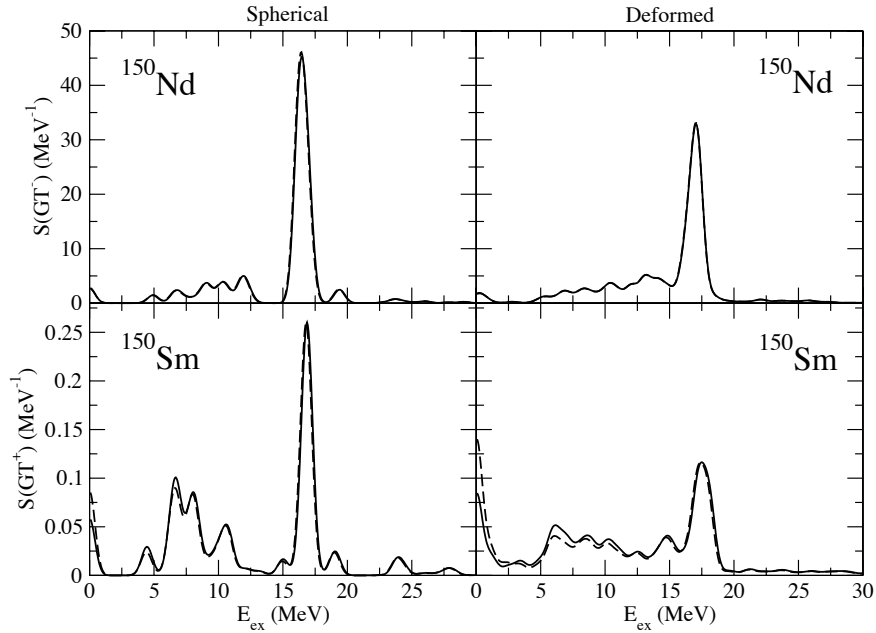


Figure 5.7: The same as in fig.5.6 but for the case of $^{150}\text{Nd} \rightarrow ^{150}\text{Sm}$ (only theoretical results are shown).

First, we study the GT transition as it is well studied by charge-exchange reaction experiments for ^{76}Ge . The GT strengths are important for $2\nu\beta\beta$ decay, as β^- transition for the initial and β^+ transition for the final nuclei are just the initial and final legs of the $2\nu\beta\beta$ -NME. We study only the relevant strength distributions, that is β^+ transition for the final nuclei and β^- for the initial nuclei. The transition probabilities can be derived from the charge exchanging scatterings for certain nuclei experimentally, as the thin solid line in fig.5.6 for ^{76}Ge . We plotted the GT strength distributions as functions of the excitation energy of the intermediate nucleus in fig.5.6 for ^{76}Ge and ^{76}Se and fig.5.7 for ^{150}Nd and ^{150}Sm for both the spherical limits and deformations with the values of β_2 we adopt in this work. The distributions of the GT strength have been folded with Gaussian functions of 1MeV width. So that the original discrete spectrum is transformed

into a continuous profile. In fig.5.6, we plot the results for different model spaces and different g_{pp} values corresponding to the $2\nu\beta\beta$ NME obtained with different axial vector coupling constants g_A . And in fig.5.7, we plot different results for ^{150}Nd and ^{150}Sm for different g_{pp} values obtained in the same way for ^{150}Nd .

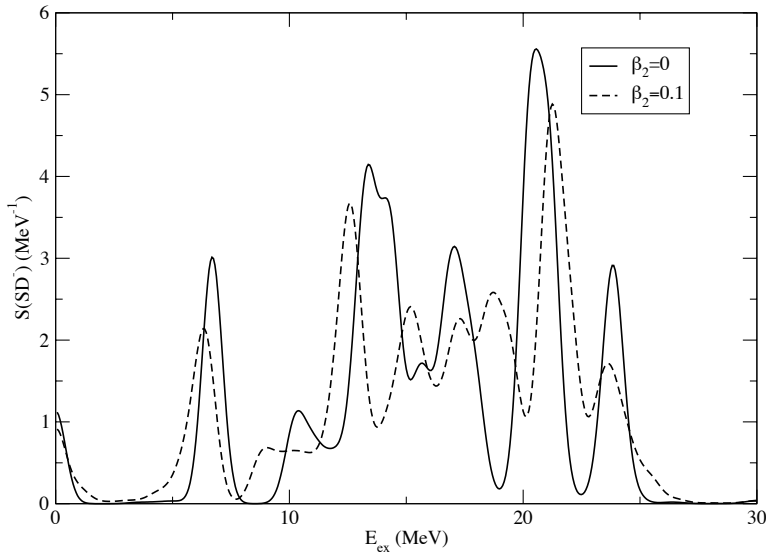


Figure 5.8: Theoretical spin-dipole strength distributions for ^{76}Ge for both the spherical and deformed cases, with the g_{pp} values corresponding to the bare $g_A = 1.25$, see table.??.

From the graphs we see that for β^- strength for the initial nucleus ^{76}Ge , we have clearly the 1^+ excitation states as well as the GT resonance. The GTR has a one-to-one correspondence to the experimental data. When the deformation of ^{76}Ge is taken into account, the peaks become much more fragmented. This is due to the violation of spherical symmetry, the QRPA energies split for the different projection states K which are degenerate in the spherical case. This modifies the strength distributions by increasing the widths and reducing the height of the peaks. For final nucleus, the β^+ has a different scale than that of β^- , about one order of magnitude lower. This is the consequence of Pauli blocking. While the occupation probability amplitudes favor β^- strength, they are very small factors in the β^+ strengths when connecting similar proton and neutron states. Now the distributions of β^+ for the spherical and deformed nuclei are rather different. The reason is the same as that for β^- . The peak structure changes a lot when deformation is taken into account.

For heavier nuclei such as ^{150}Nd , we have similar GT strength distributions for β^- especially for the GT resonance. For ^{150}Nd the total β^- strength is much larger, this comes from the Ikeda

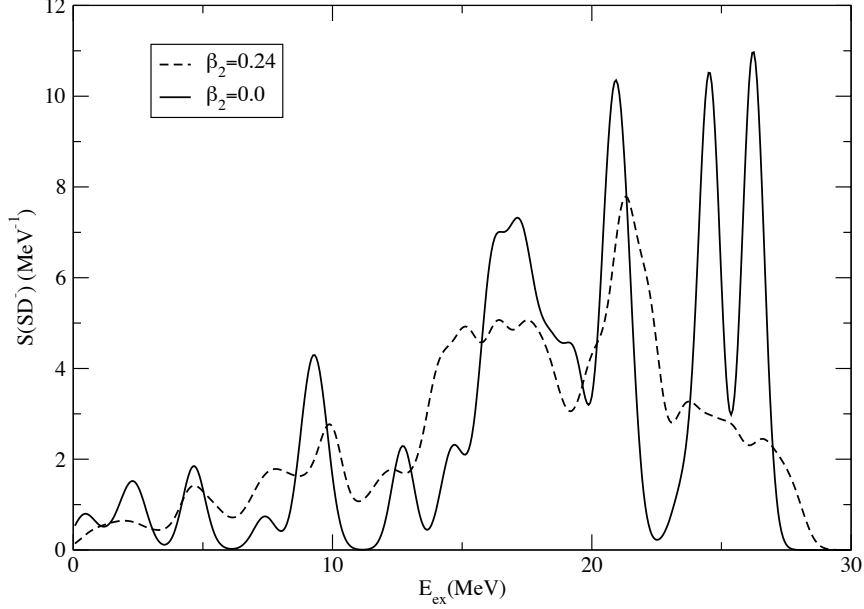


Figure 5.9: The same as fig.5.8 but for the case of ^{150}Nd .

sumrule[110]

$$\begin{aligned}
 S_{GT}^- - S_{GT}^+ &= \sum_{K=0,\pm 1} \sum_{p,n} |\langle p | \tau^+ \sigma_K | n \rangle|^2 (v_n^2 - v_p^2) \\
 &= 3(N - Z)
 \end{aligned} \tag{5.4}$$

and because the β^+ strength is suppressed as explained above, $S_{GT}^- \approx 3(N - Z)$. This explains the larger total GT strength for ^{150}Nd . We see here that for ^{150}Nd , the majority of the transition strength comes from the GT giant resonance. For β^+ strength of ^{150}Sm , we can also observe the resonance peak near the position of the GT giant resonance for β^- strength of ^{150}Nd which for the medium nucleus ^{76}Se is suppressed. And unlike the β^- transition for ^{150}Nd , one finds also comparable contributions from low energy states. When taking into considerations of quadrupole deformation, one finds similar changes as β^- transitions for ^{76}Ge and β^- transition for ^{76}Se . Due to the splits of the originally degenerated states, the shapes of the peaks are changed. They are much more fragmented.

Two sets of g_{pp} originating from different choices of the axial coupling constant g_A are used here. We see that for β^- transition, g_{pp} has almost negligible effect on the position and distribution of GT transitions. Especially, the change of g_{pp} does not change appreciably the position of the GT giant resonance. But for β^+ , for ^{76}Se , the increase of g_{pp} reduces the strength of lower energy excitation states while enhances that for high energy states. For ^{150}Sm , there are also such behaviors, but the effect is not so significant. In fig.5.6, for comparison, we also adopt different model spaces for calculations of ^{76}Ge and ^{76}Se : a full space from $0\hbar\omega$ shell to $5\hbar\omega$ shell and a smaller space from $2\hbar\omega$ to $4\hbar\omega$. The results come out that this truncations hardly affect the strength distributions.

To test the validity of our decision of choosing the same g_{ph} and g_{pp} for different multipole channels, we can calculate also the strength distributions for other transitions. As an exam-

ple, we calculate the Spin-Dipole(SD) transitions. The spin dipole transition has the form as $\beta_{SD}^-(K) = \sum_{pn} \langle p | \tau^- r^2 (\vec{\sigma} \times \vec{Y}_2)_K | n \rangle c_p^\dagger c_n$. The results are plotted in fig.5.8 for ^{76}Ge and fig.5.9 for ^{150}Nd , the solid lines are for the spherical nuclei and the dashed lines for deformed ones. These strength distributions include contributions from different projections of the 2^- intermediate states. Here we list only the results for the initial nuclei. Comparing with the GT strength distributions, one find a rich structure of resonances at the range of excitation energy from 10 – 25MeV for ^{76}Ge and 15 – 30MeV for heavy nucleus ^{150}Nd . There are more resonance peaks than that of GT transitions. The position of giant resonance is around the excitation energy of more than 20MeV for ^{76}Ge and ^{150}Nd . The sum of the strength is much smaller than that of GTR especially for heavy nuclei. If we take into consideration of the deformations, the same effects as that for GT transition apply. We see that some of the resonances will be split into more because of the breaking of degeneracy. The distributions become more smoothed and some peaks are wiped away.

5.2.2 NME for $2\nu\beta\beta$

In this section, we will discuss the NME for $2\nu\beta\beta$ in pn-QRPA calculation with account of the deformation. The NME is expressed in(4.24) in the previous chapter for the pn-QRPA method. From (4.24), we see that the NME depends on the overlap factors for different intermediate states and also the initial (β^-) and final legs (β^+) of the GT strengths as well as the energy denominators. The overlap factors depend on the overall BCS vacua overlap, in [29] we see that this overlap depends on the differences between the two quadrupole deformation parameters of the initial and final nuclei. So if there is a large difference in deformations during the decay process, the process is suppressed. Even for two spherical nuclei, the overlap factor is less than unity, as the BCS vacua for the two nuclei are definitely different. In table?? we list the BCS overlap factors between the initial and final nuclei for decays of the two nuclei ^{76}Ge and ^{150}Nd for both the spherical and deformed cases. The energy denominators are also important for the derivation of $2\nu\beta\beta$ -NME, we have redefined the energy denominators in (4.24). These definitions are different to the previous definitions of $\omega_{K,m_i,m_f} = (\omega_{m_i}^K + \omega_{m_f}^K)/2$ [129], and the comparisons between results obtained with these two definitions have been done by [29].

Table 5.4: Basic parameters for the two $2\nu\beta\beta$ processes derived from the $2\nu\beta\beta$ experiments. Here $T_{1/2}$ is the half life in years, NME I corresponds to $g_A = 1.25$ and NME II corresponds to $g_A = 0.94$. $E_{ex}(1^+)$ is the relative energy of the first 1^+ state to mean energy of ground states for the initial and final nuclei derived from the experiments.

Process	$T_{1/2}$ (year)	$2\nu\beta\beta$ NME		$E_{ex}(1^+)$ (keV)
		I	II	
$^{76}\text{Ge} \rightarrow ^{76}\text{Se} + 2e^- + 2\nu$	$2.5 \pm 0.1 \times 10^{21}$ [28]	0.15	0.27	1927.82
$^{150}\text{Nd} \rightarrow ^{150}\text{Sm} + 2e^- + 2\nu$	$8.2 \pm 0.9 \times 10^{18}$ [28]	0.07	0.12	1770.12

We have already studied the behaviors of the initial and final (β^\pm) legs for $\beta\beta$ decay. Now we come to the discussions of the $2\nu\beta\beta$ NME. The values of the NME can be extracted from the experimental half-lives by (3.4). The phase space factors for different nuclei are presented in [107].

Table 5.5: The values of the deformation parameter of Woods-Saxon mean field β_2 for initial and final nuclei fitted in the calculation to reproduce the experimental quadrupole moment. Also the fitted values of the p-p strength parameter g_{pp} are listed (with I for the values obtained with the bare axial vector coupling constant $g_A = 1.25$ and II for $g_A = 0.94$). For each case of ${}^{76}\text{Ge} \rightarrow {}^{76}\text{Se}$, the upper entry is obtained with a full space calculation and the lower one with a truncated space.

nuclei	β_{2i}	β_{2f}	$\langle BCS_i BCS_f \rangle$	g_{ppI}	g_{ppII}
${}^{76}\text{Ge} \rightarrow {}^{76}\text{Se}$	0.0	0.0	0.81	0.68	0.63
				0.78	0.71
	0.1	0.16	0.74	0.71	0.66
				0.82	0.74
${}^{150}\text{Nd} \rightarrow {}^{150}\text{Sm}$	0.0	0.0	0.86	1.01	0.99
	0.24	0.15	0.61	1.05	1.00

The NME's are presented in table.?? for the two nuclei concerned. One should be aware that here the coefficient g_A^4 in (3.4) have been taken into the phase space factor. For comparison, we adopt two values of the axial coupling constant, the bare one $g_A = 1.25$ and the quenched one $g_A = 0.94$. The different choices give us different values of NME in table.?. The fitting of the parameter g_{ph} has been done by adjusting the position of GT giant resonance. It is argued in [117] that $2\nu\beta\beta$ decay rate is especially suitable for the adjustment of g_{pp} , because it involves the same initial and final states as the $0\nu\beta\beta$ decay. So, with the $2\nu\beta\beta$ NME, we can fix the two parameters in our calculation.

$M_{GT}^{2\nu}$ for deformed nuclei were calculated first by [110] using the separable force. There instead of the renormalized strength g_{ph} and g_{pp} , they have the phenomenological constants κ and χ . And one finds the similar behaviors of NME with these interaction strengths, as that for the realistic force[29]. Because we have different single-particle mean field parameterization from[29], we recalculated $M_{GT}^{2\nu}$ and found not a large difference. In fig.5.10, we illustrated the NME's g_{pp} dependence for different nuclei without or with deformation, and the dashed lines for the truncated space with the same truncation as before. One finds the reduction of $M_{GT}^{2\nu}$ as the magnitude of g_{pp} increases. The increase of g_{pp} also accelerate this reduction. From the analyses in [130] for the sum rule, we see that for large values of g_{pp} , the GT resonance gives a large reductions to the NME, this is the reason for the rapid decreasing behavior at large g_{pp} for $M_{GT}^{2\nu}$. When g_{pp} is small, the negative contributions from the GTR are small and the reductions are not significant. And the experimental values of $M_{GT}^{2\nu}$ (horizontal lines in fig.5.10) usually lies in the region where the the curves drop rapidly. The large g_{pp} sensitivity of $M_{GT}^{2\nu}$ originates mainly from the transitions to the collective resonances.

Considering the deformation, one finds that the spherical curves drop faster with g_{pp} than the deformed ones. This means that the deformed results are more stable to the choice of g_{pp} . Deformation introduces the further reduction to $M_{GT}^{2\nu}$ by the BCS overlap factors. In fig.5.11, comparison between of contributions to $M_{GT}^{2\nu}$ from different K^π states are plotted for the deformed case. For small g_{pp} , the equalities of contributions from transitions to different K^π states are preserved, just like in the spherical case. But for larger g_{pp} , we find that deformation changes the behavior of

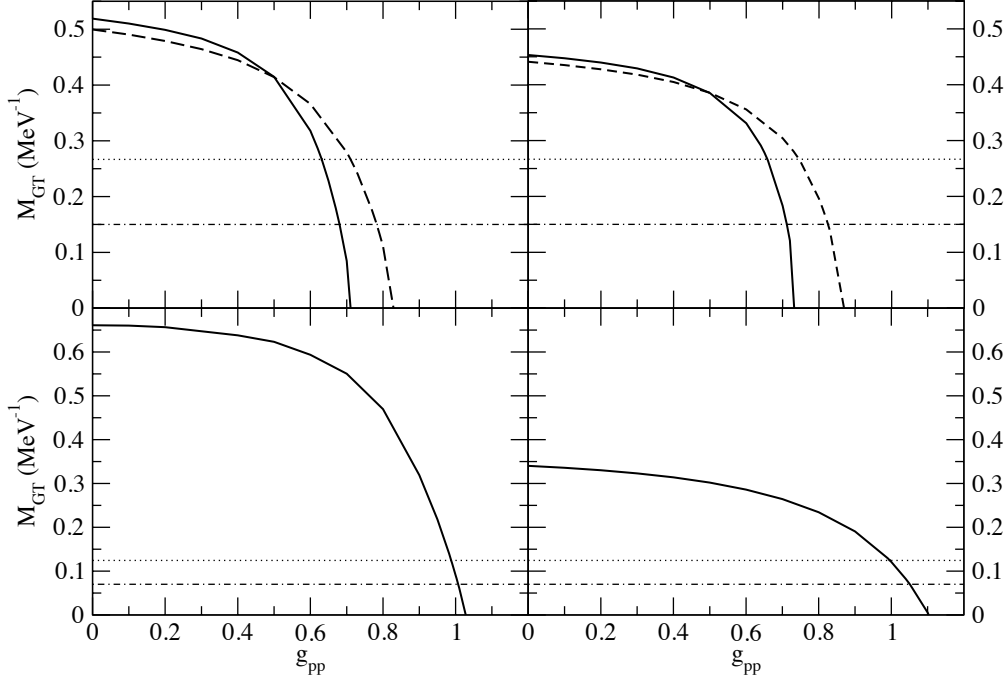


Figure 5.10: The dependence of the GT $2\nu\beta\beta$ NME on g_{pp} . Upper panels are for $^{76}\text{Ge} \rightarrow ^{76}\text{Se}$, with the left one for the spherical and the right one for the deformed cases. Solid lines are for the full $0 - 5\hbar\omega$ space. The dashed curves are obtained in the truncated $2 - 4\hbar\omega$ space. Lower panels are for $^{150}\text{Nd} \rightarrow ^{150}\text{Sm}$. The two horizontal lines in all graphs are the exp. $2\nu\beta\beta$ NMEs corresponding to the bare(dash-dotted lines) and quenched(dotted lines) g_A respectively.

the M_{GT} for different projection states drastically. The curve for $|0^+\rangle$ drops more rapidly than that for $|1^+\rangle$. This comes from the splitting of the GT resonances with different projections K^+ states in the deformed nuclei. From fig.5.11, we can draw the conclusion that the difference of contributions to $M_{GT}^{2\nu}$ for different projection states $|K\rangle$ emerges for large g_{pp} (at the region where its value sensitively affect the NME). The more sensitive the dependence of $M_{GT}^{2\nu}$ on g_{pp} is, the larger is the difference. This difference breaks the spherical symmetry in deformed nuclei.

In fig.5.10, we have results for both the full six-shell-space $0 - 5\hbar\omega$ and the truncated three-shell-space $2 - 4\hbar\omega$. Comparing these two curves, we can see that for the same value of NME, the truncated calculation may give a larger value of the fitted g_{pp} . This can be explained as following: for a larger space, the effect of the particle-particle interactions is enhanced, since more levels are involved, the ground states correlations are strengthened. So the value of g_{pp} for our solution is basis space size dependent. As for the value of g_A , since in our convention we have $(T_{1/2}^{2\nu})^{-1} = G^{2\nu}|M_{GT}^{2\nu}|^2$, which has incorporated the bare coupling constant $g_A = 1.25\text{MeV}$ inside the calculation of $G^{2\nu}$, so if we use different g_A , we get the corresponding NME as $M_{exp}^{2\nu}(g'_A) =$

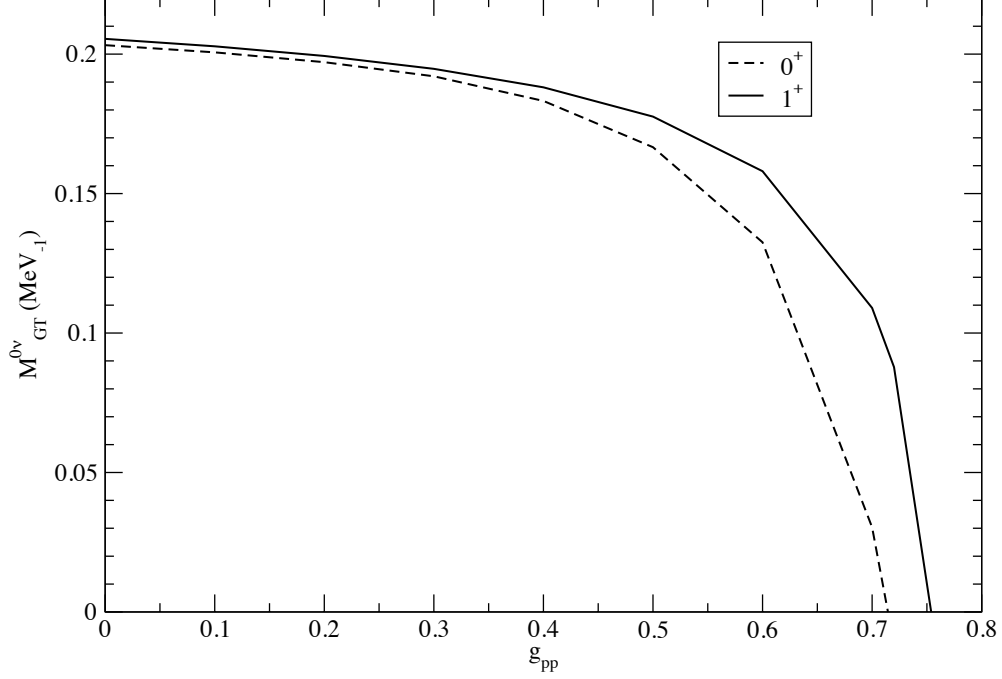


Figure 5.11: The dependence of the $2\nu\beta\beta$ GT NME on values of g_{pp} for $K^\pi = 1^+$ and $K^\pi = 0^+$ angular momentum projections for deformed ^{76}Ge nuclei. This graph shows the difference of $M_{GT}^{2\nu}$'s dependence on g_{pp} of the two projections which both belong to the same intermediate states with angular momentum 1^+ in the spherical limit.

$(g_A/g'_A)^2 M_{exp}^{2\nu}(g_A = 1.25)$. This will affect the fitted value of g_{pp} as we can see from the $M^{2\nu}(g_{pp})$ curves. Even with the quenched g_A value and consequently smaller NME, the corresponding value of g_{pp} still lies in the region where NME is sensitive to g_{pp} . In this sense, a better determination on the quenching factors is needed for the determinations of g_{pp} .

The adjustment of g_{pp} is done by fitting the experimental $M_{GT}^{2\nu}$, the results are listed in table???. Here we have the results for both the full space and truncated space for ^{76}Ge . Different g_A are adopted for both the cases without and with quenching. The deformation has also been taken into consideration. These values of g_{pp} are used in our following calculations for $0\nu\beta\beta$.

5.2.3 NME for $0\nu\beta\beta$

In present thesis, we calculate only the matrix elements for light Majorana neutrino mediating mechanism as the leading contribution for $0\nu\beta\beta$. The initial and final nuclei are in ground states, that means the decay is from 0^+ to 0^+ . Unlike $2\nu\beta\beta$ decay, in $0\nu\beta\beta$ decay more intermediate states of different multipoles rather than $K^\pi = 0^+, 1^+$ are involved. This is due to the mediating particles which can carry the angular momentum. Unlike in $2\nu\beta\beta$ decay, an *SSD*(Single State Dominance)

hypothesis is not available for $0\nu\beta\beta$ because of so many multipoles. So it is difficult to extract from experiments such as charge-exchange scattering experiments the values of $M^{0\nu}$ despite of some attempts[116]. The detailed expressions of the $0\nu\beta\beta$ NME are given in (4.27). One notices that if we neglect the energies of the intermediate states and the finite nucleon size, with only the first order nuclear currents, we will have from the inner loop momentum integration the Coulomb-like radial dependence of the neutrino potential $1/r$. In actual calculation, we divide the NME into two parts, the leading order part corresponding to $1/r$ and all the corrections mentioned above are added later. A third correction is incorporated later on, this is the short range Correlation (SRC) originating from the strong repulsive nature of the nuclear force.

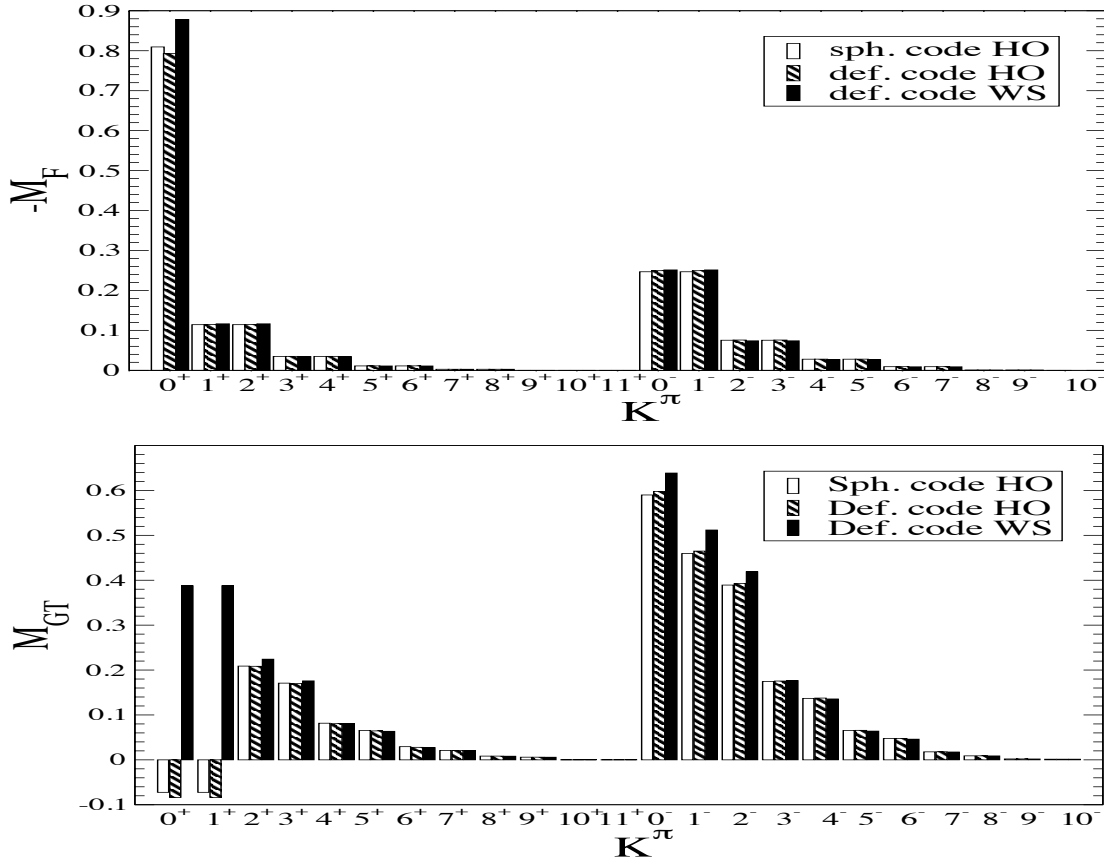


Figure 5.12: The partial contributions $M^{0\nu}(K^\pi)$ of different intrinsic intermediate states with projection and parity K^π to the total calculated $0\nu\beta\beta$ -decay NME for the cases of realistic deformation and in the spherical limit. In this illustrative figure only the leading, Coulomb-like, radial dependence of the neutrino potential is taken into account for comparison between different choices of the single-particle wave functions. Also, for simplicity, the BCS overlap factor is omitted in these results. The Fermi and the GT contributions are shown in the upper and lower panels, respectively. The three bars represent (from left to right) the results obtained with the spherical harmonic oscillator wave functions with the spherical code, with the harmonic oscillator and Woods-Saxon wave functions in the spherical limit with current code.

For axially deformed system, the angular momentum is not conserved. So when dealing these

deformed nuclei in the intrinsic frame, one needs to replace the angular momentum by other quantum numbers, the projections on z -axis K in our case. In order to compare our result with that of the previous calculations in spherical nuclei [81], we make the following decompositions. In spherical nuclei, the contributions of NME come from different projections of the intermediate states with the same angular momentum should be equal due to the spherical symmetry, this gives:

$$M^{0\nu}(0^+ \rightarrow (J^\pi, K) \rightarrow 0^+) = M^{0\nu}(0^+ \rightarrow (J^\pi, K') \rightarrow 0^+) \quad (5.5)$$

so we have $M^{0\nu}(J^\pi, K) = \frac{M^{0\nu}(J^\pi)}{2J+1}$, thus in the intrinsic system we have

$$M^{0\nu}(K^\pi) = \sum_{J \geq K} \frac{M^{0\nu}(J^\pi)}{2J+1} \quad (5.6)$$

Here J^π (angular momentum and parity) are multipoles of different intermediate states in the spherical nuclei. In this way, we can compare our results with the previous calculations in spherical pn-QRPA. For the F part, in spherical system, only intermediate states with 'natural parity' $\pi = (-1)^J$ will contribute, so in this case, we have the equality $M_F^{0\nu}(J^\pi; \pi \neq (-1)^J) = 0$, for example $0^-, 1^+$ etc. In the intrinsic frame for the spherical limit, this corresponds to the relations

$$M_F^{0\nu}(K^\pi; \pi = (-1)^K) = M_F^{0\nu}((K-1)^\pi) \quad (5.7)$$

this can be a basic examination of our code at the spherical limit. And another basic relation for the spherical calculations is that $M_{GT}^{0\nu}(J^\pi = 0^+) = 0$ (0^+ intermediate states will not contribute), this then gives

$$M_{GT}^{0\nu}(K^\pi = 0^+) = M_{GT}^{0\nu}(K^\pi = 1^+) \quad (5.8)$$

in intrinsic frame. In this sense, the multipoles J^π in the spherical system are now replaced by K^π in the intrinsic frame.

In order to test the reliability and consistency of our code, we make comparisons with previous results of the spherical QRPA [81, 117] which makes use of the spherical harmonic oscillator wave functions. So for a comparison, we substitute the Woods-Saxon wave function by the harmonic oscillator wave function in the spherical limit. The procedure is the following: In our calculations we expand the wave function over the deformed harmonic basis (see Appendix B). In the spherical limit we expect which then is equivalent to the spherical harmonic oscillator basis ($\omega_\perp = \omega_z = \omega_0$). For each state from the Woods-Saxon potential, we set the largest expansion coefficient to be unity and other coefficients be zero. So now the Woods-Saxon wave function is reduced to the spherical harmonic oscillator one. Using this reduced wave function in our code for the deformed nuclei, we try to reproduce the results obtained by previous calculations in spherical nuclei. In fig.5.12, we illustrate the final results of $0\nu\beta\beta$ NME ($M_F^{0\nu}$ and $M_{GT}^{0\nu}$) for ${}^{76}\text{Ge}$ in the leading order (the neutrino potential takes the form $H(r) = 1/r$). For different K^π , we have three bars in the graph, the first is obtained in the spherical basis by a transformation in Eq.(5.6), the second is calculated by our code with a harmonic oscillator wave-function in the spherical limit, and the third is obtained with the Woods-Saxon wave-functions also in the spherical limit. From the first two bars in fig.5.12, one sees the perfect agreement between the spherical and deformed codes for both the GT and F parts. Here we see that the relations (5.7) and (5.8) are fulfilled. These results connect

the calculations between the spherical and deformed codes, ensure us the consistency between them. This confirms the reliability of the generalization of pn-QRPA from the spherical system to the deformed one. The second and third bars in graph5.12 are results obtained with the harmonic oscillator and Woods-Saxon wave functions. This gives us a comparison of $M^{0\nu}$ between these two different wave function. Here the same parameters of g_{ph} and g_{pp} are used for both cases, we have a very good agreement on these results for $M^{0\nu}$ for all multipole K^π except the 0^+ and 1^+ states. The reason of this exception will be explained later. One can draw the conclusion that in the spherical limit, choices of HO or WS wave functions (or the mean fields) have limited effects on the general results of $M^{0\nu}$.

We could also have a look at the multipole decomposition of the NME's in the leading order in the spherical limit. We expect the results of contributions for high multipoles (larger K) to converge. This is the case in fig.5.12. Large proportion of the contributions comes from low multipoles such as 0^+ , 1^+ , 2^+ and 0^- , 1^- . The $M^{0\nu}$ decrease rapidly with the increase of K . We also see that for the intermediate states with K larger than 9, their contributions can be neglected in the calculations. This is due to the choice of our model space, for which the numbers of high K configurations are limited. In other words, these states come from the excitations to or from single-particle states far away from the Fermi surface. Their contributions to $M^{0\nu}$ are suppressed anyhow by the small occupation amplitude. Another observation here is that the contributions from intermediate states with negative parity are with nearly the same magnitude as from the states with positive parity. So in this sense, we must choose a moderate model space to include the intermediate states with negative parity in our calculations. One would expect the positive parity states contributions mainly come from excitations within the same shell, while the negative ones comes from the excitations between the neighboring shells. This will help us to choose the correct truncations of the model space.

By including the corrections from the form factors, the intermediate energies and high order nuclear currents, one gets in total the reductions of about 20% to $M_F^{0\nu}$ and 40% to $M_{GT}^{0\nu}$. In fig.5.13 (the white bars in the graph are the reductions from above corrections) and table.5.6, these results are illustrated. In our calculation, we neglect the contributions from the tensor part, as it is small compared to the GT and F parts(about 10% of the F part and 5% of the GT part [81]). For simplifications, we use the closure intermediate energy of $\bar{E} \approx 7MeV$ to replace excitation energies obtained from QRPA ($E_{K^\pi}^m - (E_i + E_f)/2$). This changes the energy denominators, and will surely introduce an error to the final result. But by comparing \bar{E} with the mean momentum of visual neutrino of $\sim 100MeV$, one expects this error to be small. The inclusion of these correction reduces the total magnitude for each multipole, but it doesn't change the general structure of these multipoles. The relations (5.7) and (5.8) for the spherical nuclei are fulfilled exactly.

Another important correction comes from the SRC (short-range correlations), which originate from the short-range repulsion of the realistic NN interaction. We find that if we use the conventional Jastrow type of corrections, then there is an overall reductions of NME about 15% (fig.5.13, the shadowed area) for both the F and the GT parts. This has nearly the same magnitude as that of the FNS (finite nucleon size) and high order currents corrections. But if we use modern version of Brückner CCM (coupled-cluster method) corrections[120], the suppressions to the NME is only about 5% as we see in table.5.6. So the choice of the SRC is important for the determinations of

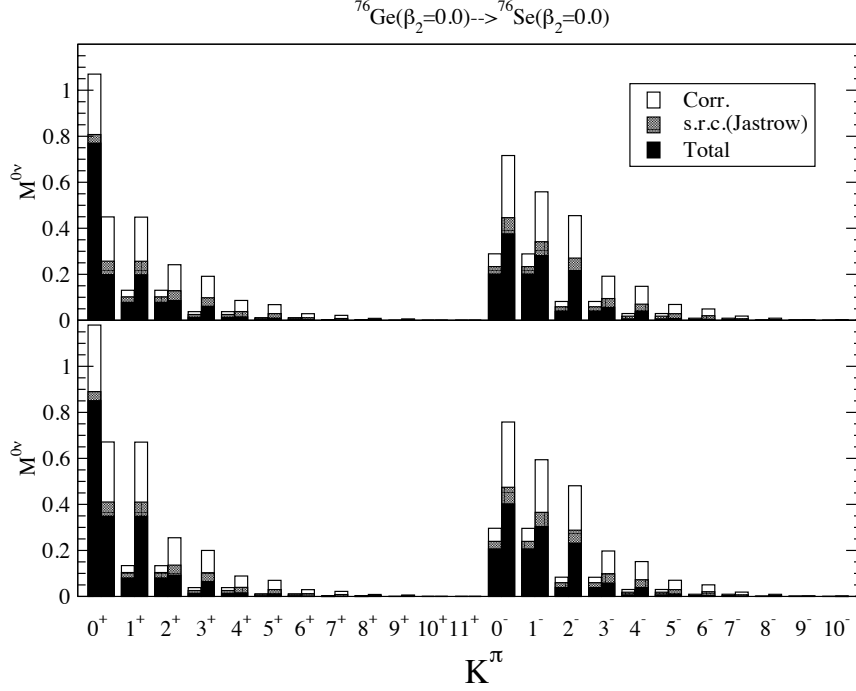


Figure 5.13: The NME for different multipole channels for the spherical case of ^{76}Ge with g_{pp} value corresponding to bare g_A (upper panel) and quenched one (lower panel). The white bars are subtracted from the total value and represent high order currents and finite nucleon size effects *etc.* The gray area is a reduction due to Jastrow SRC. The black bar is the results including all these corrections. For each multipole K^π , the left bar is for $-M_F^{0\nu}$ and right bar for $M_{GT}^{0\nu}$.

the $0\nu\beta\beta$ NME $M^{0\nu}$.

As ^{76}Ge has less protons and neutrons than heavy nuclei such as ^{150}Nd , a smaller model space is needed in our calculation. This nucleus is numerically easy to calculate with such a model space. We can check for this nucleus how different treatments will affect the final results and these results will give us rough estimations on the uncertainties in our calculations for ^{150}Nd . Calculations for ^{150}Nd are more time-consuming, and we have to make some approximations due to capacity of current computers.

In the following, we consider three different aspects of our calculation: Fig.5.14 for the consideration of deformations, fig.5.15 for different choices of model space and fig.5.16 for different choices of g_A , this also related with different choices of g_{pp} .

In fig.5.14, we see an excellent agreement between the deformed and the spherical nuclei if the BCS overlap factor of the ground states is not taken into consideration. This perfect agreement shows that the difference between the spherical and deformed calculations comes mainly from the overlaps of two ground states. The only exception comes from the 0^+ and 1^+ multipoles, the relations (5.8) is broken here, just as the inequality between the $K^\pi = 0^+$ and 1^+ in $2\nu\beta\beta$ decay. This is only the conclusions for the small deformations and for larger deformations such as that

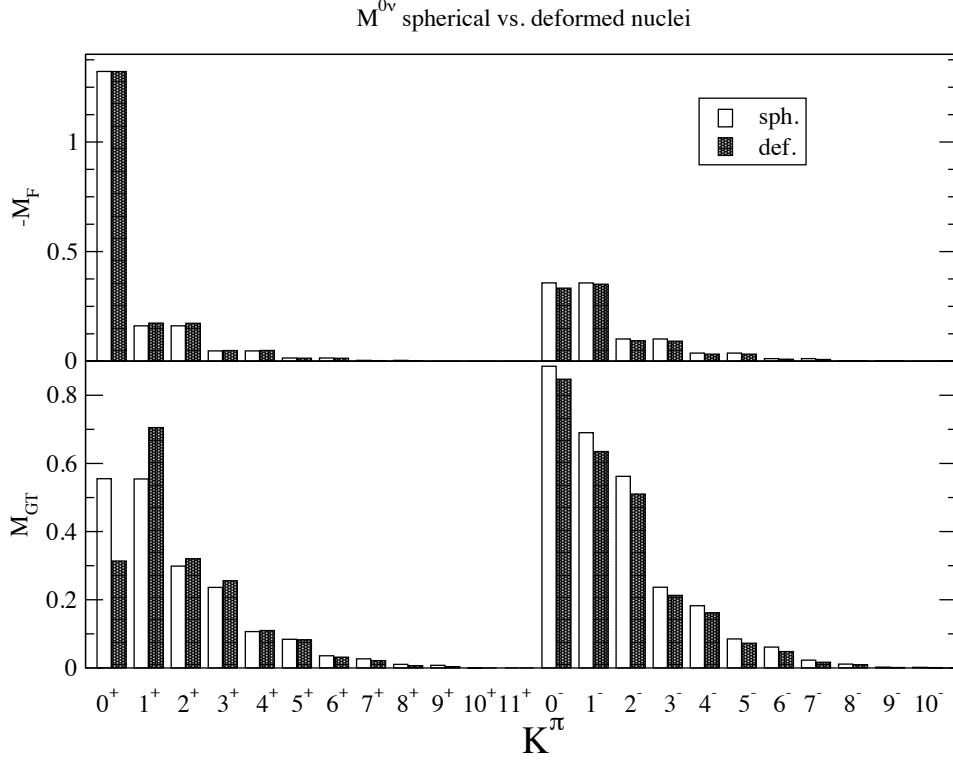


Figure 5.14: Comparisons between the $0\nu\beta\beta$ NME's for ^{76}Ge in leading order (no corrections included) for both spherical and deformed cases without considerations of the BCS overlap factors. The left bars are for spherical and right bars for the deformed cases with deformation parameters given in table??.

of ^{150}Nd , we will check later. For calculations of $^{76}\text{Ge} \rightarrow ^{76}\text{Se}$, the quadrupole deformations for both nuclei are very small. As one can see in fig.5.1, for values of deformation we adopted for our calculations, the levels are although non-degenerated, but not far from the degenerated spherical levels. So the transition strengths should be approximately the same for the same single states. Because we have an one-to-one correspondence for the model spaces for the spherical limit and the deformed case, one can obtain such a coincidence. But such a high coincidence is somehow out of our expectation.

For the calculations for ^{150}Nd , it is almost impossible to include all the levels due to the capacity of the computers. For these heavy $\beta\beta$ emitters with strong deformation, a truncation is always needed. One would wonder how the results may be changed with the introduction of these truncation, so we study here this effect of truncation for ^{76}Ge . Because ^{76}Ge is much lighter than ^{150}Nd , both a full and a truncated space calculations are possible. In fig.5.15, making the same truncation as for the $2\nu\beta\beta$ NME, we get a very good agreement between the full and truncated model space calculations. As we can see, the truncation brings some changes to the NME. There are only minor modifications to all the multipoles K^π . Those intermediate states which are excluded out by

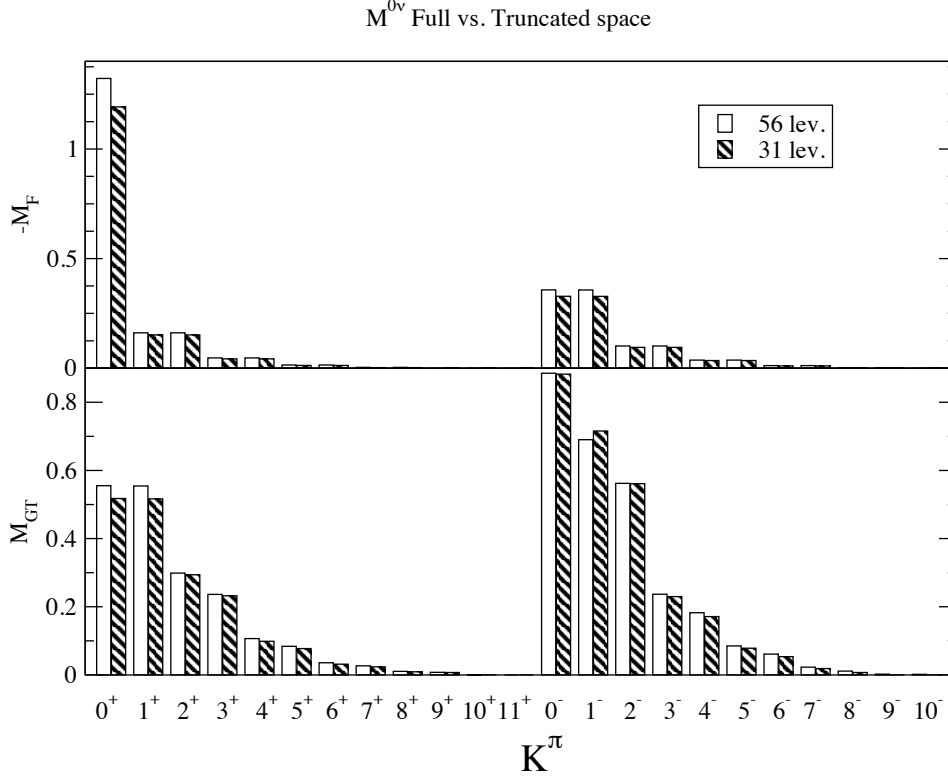


Figure 5.15: Comparisons between the $0\nu\beta\beta$ NME's for ^{76}Ge in leading order for different space without considerations of BCS overlap factors. The left bars are for a full $0 - 5\hbar\omega$ space and the right bars are results for a truncated $2 - 4\hbar\omega$ space.

our truncation gives very small contributions because of the suppressions by their low occupation amplitudes. As we have seen earlier, the truncations keep the occupation probabilities of neutrons and protons unchanged, and all the active levels (which is neither fully occupied nor empty) have already been included in our calculations. So in this sense, we should take all the active levels not far from the Fermi surface within the truncated space to avoid the loss of the NME while making truncations.

A third comparison has been done for the considerations of the quenching effects in the nuclei. In this case, we have different values of $M^{2\nu}$ for different g_A as shown in table.??, so different values of g_{pp} have been derived. In proceeding part, we will have detailed analyses on $M^{0\nu}$'s dependence on g_{pp} in a full region from 0 to the collapse limit. Here, in fig.5.16, one finds that there are slight changes for M_F and M_{GT} due to the different g_A . However, M_{GT} is more sensitive to g_A than M_F . As we will discuss later, the changes of the overall $M^{0\nu}$ may come largely from the values of g_A than from the changes from g_{pp} .

So we now check the dependence of the NME on g_{pp} in the leading order. As we have shown above, a truncation of the model space will not affect the values of $M^{0\nu}$ much, so we analyze this dependence within a truncated model space. This dependence for the spherical nuclei was studied

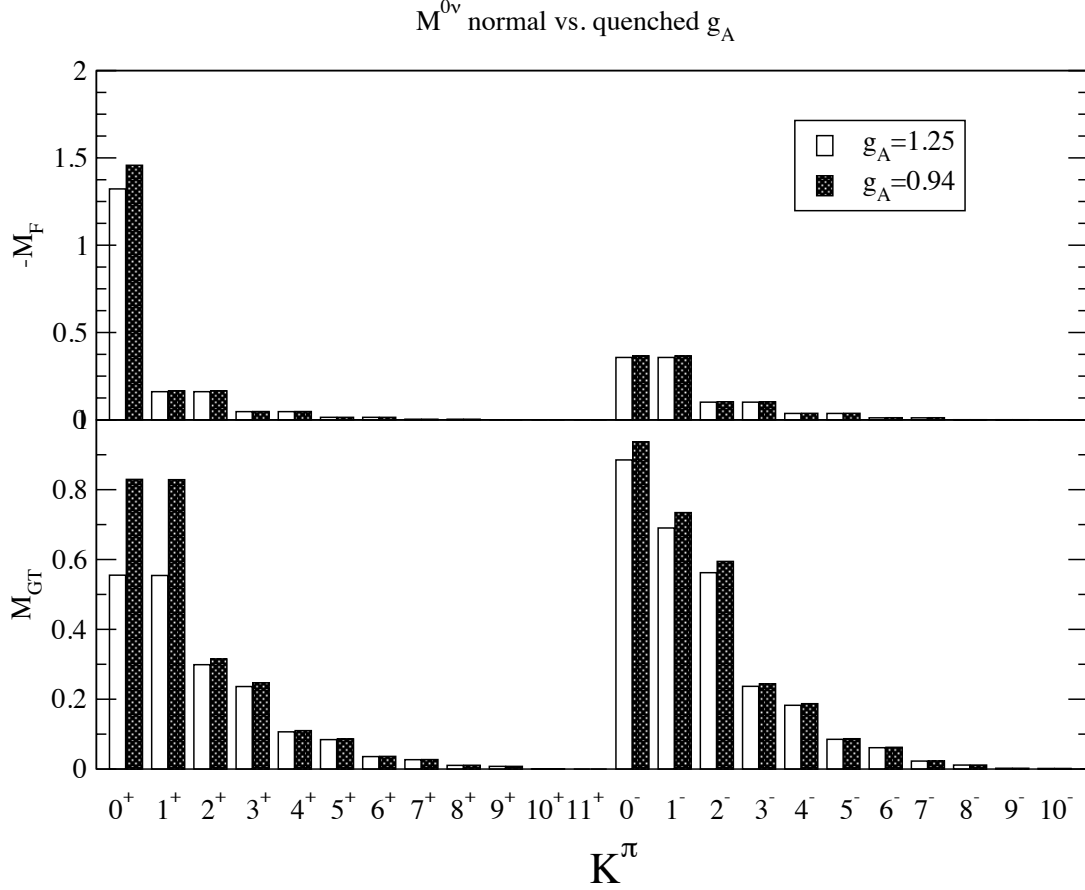


Figure 5.16: Comparisons between the $0\nu\beta\beta$ NME's for ^{76}Ge in leading order for normal and quenched g_A without considerations of the BCS overlap factors. For each multipole, the left bar is for $g_A = 1.25$ and right bar for $g_A = 0.94$.

in [117], their conclusion is that the contributions of $J^\pi = 1^+$ multipole for both modes of the $\beta\beta$ decay depend very sensitively on the strength of g_{pp} . In fig.5.17, the dependences of $M^{0\nu}(K^\pi)$ are plotted for the deformed nuclei. One finds that only the contributions from multipoles K^π of 0^+ and 1^+ of GT part depend sensitively on g_{pp} , and this is in accordance to conclusions of [117]. One also notices that the $M_{GT}^{0\nu}$ for multipoles 0^+ and 1^+ depend on g_{pp} less sensitive than $M_{GT}^{2\nu}$. This is because the $M_{GT}^{2\nu}$ elements for $K^\pi = 0^+$ and 1^+ involve only $J^\pi = 1^+$ states, but for $M_{GT}^{0\nu}$, many other J^π states are involved. As for the other multipoles, there is no such sensitivity. So when they all are added together, the sensitivity of 0^+ and 1^+ contributions are reduced. The reason of this sensitivity is that the Gamow-Teller correlations (spin one, isospin zero pairs) are very near the corresponding phase-transition in the $J^\pi = 1^+$ channel (corresponding to the collapse of the QRPA equation of motion) [117]. All the other multipoles J^π correspond to small amplitude of the collective motion, so there is no such phase transition and they are insensitive on g_{pp} . For deformed nuclei, one finds that the spherical limit gives a good approximation for the F part, as the relations (5.7) are fulfilled as g_{pp} changes. But for 0^+ and 1^+ of GT part, the relation (5.8) is broken, this is similar to the 0^+ and 1^+ contributions to $M_{GT}^{2\nu}$. And, again, the magnitude of this

symmetry breaking is related to the sensitivity of the NME on g_{pp} .

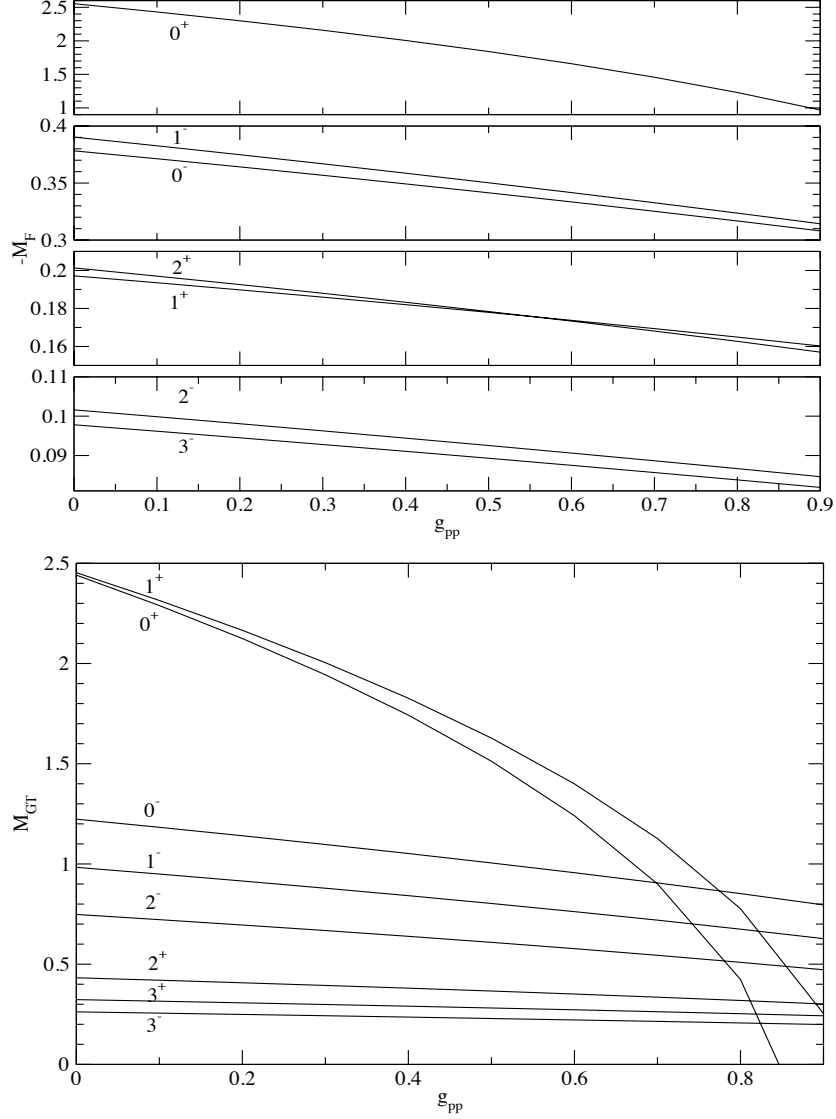


Figure 5.17: The dependence of the $0\nu\beta\beta$ NME's of ${}^{76}\text{Ge}$ on g_{pp} for different multipoles.

The final results are sums of the contributions of all multipoles, this is in contrast to the $2\nu\beta\beta$ case where one has only the contribution from the intermediate $J^\pi = 1^+$ states. These total NMEs of $M_F^{0\nu}$ and $M_{GT}^{0\nu}$ as functions of g_{pp} are plotted in fig.5.18. Because the 0^+ and 1^+ contributions are ones of the largest contributions of to the total $M_{GT}^{0\nu}$, we observe the changes of slope of the $M_{GT}^{0\nu}(g_{pp})$ curve. The curve $M_F^{0\nu}(g_{pp})$ has a nearly constant small slope. In the deformed case, $M_F^{0\nu}$ is less sensitive to g_{pp} than $M_{GT}^{0\nu}$.

The overall $0\nu\beta\beta$ NME in our convention has the form:

$$M^{0\nu}(g'_A) = (g'_A/g_A)^2[M_{GT}^{0\nu}(g'_A) - (g_V/g_A)^2M_F^{0\nu}(g'_A)] \quad (5.9)$$

here $g_A = 1.25$ is bare axial coupling constant for nucleons. It is commonly accepted that in the nuclear environment, this constant is quenched, but the detailed value is unknown. As $M^{2\nu}$

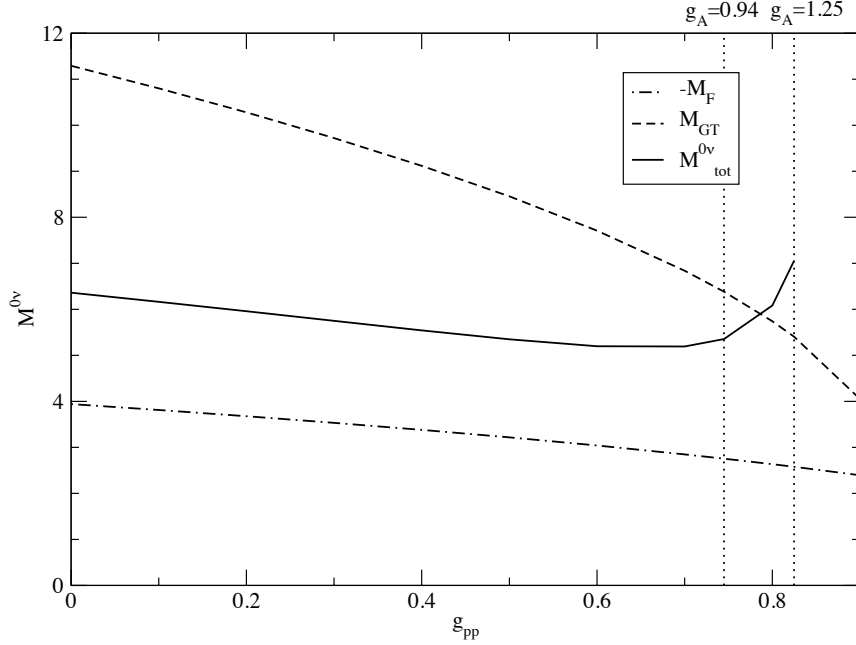


Figure 5.18: The total $M^{0\nu}$ as a function of g_{pp} . For each g_{pp} the experimental $M_{GT}^{2\nu}$ is fitted by a choice g_A . So along the curves g_A is changing. The two dotted vertical lines give the fit of g_{pp} for the values $g_A = 1.25$ and $g_A = 0.94$

depends also on the value of g_A , for different g_A 's, $M_{GT}^{2\nu}$ is different and it sensitively depends on g_{pp} , This means that our fitted values of g_{pp} depends also on the value of g_A . Now we can proceed our discussions in two-fold.

On one hand, let us set g_A to be a constant, and consider only the g_{pp} dependences of the $0\nu\beta\beta$ NME's. This is usually used in the occasion where the measured $2\nu\beta\beta$ half-lives are with large error bars. Then from the g_{pp} dependences of $M_F^{0\nu}$ and $M_{GT}^{0\nu}$ one can find that $M^{0\nu}$ is g_{pp} dependent, there may be a change of magnitude for 2 – 3 times before the collapse of the QRPA. But this dependence is not as sensitive as that of $M^{2\nu}$, and $M^{0\nu}$ are generally more stable against g_{pp} .

On the other hand, if there is a measured half-life $T^{2\nu}$ of the $\beta\beta$ emitter, one can get the $M_{GT}^{2\nu}$ as a function of g_A (as g_A is quenched in the nuclei and the exact value is still unclear). The fitted value of g_{pp} then become an indirect function of g_A from the functions of $M^{2\nu}(g_{pp})$. For ${}^{76}\text{Ge}$, we have the $M_{exp}^{2\nu}(g_A = 1.25) = 0.15\text{MeV}^{-1}$, while varying g_A , $M^{2\nu}$ changes, so does g_{pp} , this then changes $M_F^{0\nu}$ and $M_{GT}^{0\nu}$. We want to observe here how these changes of g_A will modify the final values of $M^{0\nu}$. In fig.5.18, we have illustrated this relation. This is obtained by following procedure: For different g_{pp} (from 0 to the value corresponding to $M_{GT}^{2\nu}$ with bare g_A), we calculate $M_{GT}^{2\nu}$ together with $M_F^{0\nu}$ and $M_{GT}^{0\nu}$. From the calculated $M_{GT}^{2\nu}$, we can get the corresponding g_A , with these g_A 's and the formula(5.9) we have the dependence of $M^{0\nu}$ on g_{pp} . The final results (illustrated in fig.5.18) are somehow unexpected: From this graph we find that $M^{0\nu}$ has less dependence on

g_{pp} than $M_{GT}^{0\nu}$. We have the maximum and minimum values of $M^{0\nu}$ when the $2\nu\beta\beta$ half-life of the nucleus is known, with an uncertain g_A . In this sense a particular choice of g_A does not have that significant effect on the determinations of $M^{0\nu}$ as one supposed to. If the $2\nu\beta\beta$ half-life is measured accurately, one can obtain $M^{0\nu}$ with an uncertainty of about 25% for different g_A . In the above discussion we considered the deformation effect for the leading order contribution to $M^{0\nu}$. In fig.5.13 and Table5.6, we show the results of deformed calculations for the overall $M^{0\nu}$ with all the corrections. The deformation haven't largely changed the multipole structures of the NME, but the overall magnitude has been reduced by the BCS overlaps. And we can generalize all the discussions applicable in the leading order to the full results. In particular, the same dependence on g_{pp} can be applied to the corrected NMEs.

Table 5.6: Different contributions to the total calculated NME's for $0\nu\beta\beta$ decay ${}^{76}\text{Ge}\rightarrow{}^{76}\text{Se}$. The BCS overlap is taken into account. The results for the $0\nu\beta\beta$ NME's are listed for the spherical ($\beta_2 = 0.0$) and deformed nuclei ($\beta_2 = 0.10$ for ${}^{76}\text{Ge}$ and $\beta_2 = 0.16$ for ${}^{76}\text{Se}$) and for bare axial coupling constant $g_A = 1.25$ and the quenched one $g_A = 0.94$. The table gives the Fermi part M_F , the Gamow-Teller part M_{GT} and the total $0\nu\beta\beta$ transition matrix elements. The different contributions are: the leading, coulomb like, contribution $M(1/r)$, of higher order currents and the finite nucleons size (eq. (3.9) to (3.12)) ΔM , the Jastrow SRC eq.(3.13) $\delta M(J)$ and Brückner SRC[117, 119] $\delta M(BCD)$ calculated with the Bonn CD force. The last two columns give the total final $0\nu\beta\beta$ matrix elements with Jastrow $tot(J)$ and with Brückner $tot(BCD)$ correlations for the Fermi M_F , the Gamow-Teller M_{GT} and the total contributions $M^{0\nu}$ defined in eq.(5.9). The calculations are done in a $6\hbar\omega$ space, $N=0$ to 5.

Full space $0 - 5\hbar\omega$								
β_2	g_A		$M(1/r)$	ΔM	$\delta M(J)$	$\delta M(BCD)$	tot(J)	tot(BCD)
0.0 (0.0)	1.25	M_F	-3.15	0.78	0.45	-0.09	-1.92	-2.47
		M_{GT}	6.37	-2.85	-1.01	0.20	2.52	3.72
		$M^{0\nu}$					3.75	5.30
	0.94	M_F	-3.31	0.82	0.46	-0.10	-2.03	-2.59
		M_{GT}	7.28	-3.15	-1.04	0.21	3.10	4.35
		$M^{0\nu}$					3.05	4.10
0.10 (0.16)	1.25	M_F	-2.83	0.69	0.40	-0.08	-1.74	-2.22
		M_{GT}	5.59	-2.49	-0.88	0.18	2.21	3.27
		$M^{0\nu}$					3.33	4.69
	0.94	M_F	-2.98	0.73	0.40	-0.18	-1.85	-2.34
		M_{GT}	7.69	-3.65	-1.47	0.27	2.83	3.93
		$M^{0\nu}$					2.77	3.70

There are systematic analyses of the uncertainties in the calculations of $M^{0\nu}$ by different nuclear structure theories [117]. We can follow these discussions and give some rough estimations on the uncertainties in our calculations. The uncertainties may arise from different aspects of the calculations, the first is the limitation of different methods adopted, this is hard to estimate, as different methods really differ a lot and different approximations are used. But the choices of model space in different methods may have similar effects, so in this sense, the small model space

Table 5.7: Different contributions to the total calculated NME's for $0\nu\beta\beta$ decay $^{76}\text{Ge}\rightarrow^{76}\text{Se}$. The BCS overlap is taken into account. The results are the same as in table5.6 but in a restricted model space $2 - 4\hbar\omega$.

Truncated space $2 - 4\hbar\omega$								
β_2	g_A		$M(1/r)$	ΔM	$\delta M(\text{J})$	$\delta M(\text{BCD})$	tot(J)	tot(BCD)
0.0 (0.0)	1.25	M_F	-2.89	0.71	0.42	-0.09	-1.76	-2.26
		M_{GT}	6.19	-2.72	-0.94	0.20	2.53	3.67
		$M^{0\nu}$					3.66	5.12
	0.94	M_F	-3.07	0.76	0.43	-0.09	-1.89	-2.40
		M_{GT}	7.12	-3.02	-0.96	0.21	3.14	4.31
		$M^{0\nu}$					2.98	3.97
0.10 (0.16)	1.25	M_F	-2.58	0.63	0.37	-0.08	-1.85	-2.34
		M_{GT}	5.41	-2.37	-0.81	0.17	2.22	3.21
		$M^{0\nu}$					3.23	4.50
	0.94	M_F	-2.75	0.67	0.38	-0.09	-1.71	-2.17
		M_{GT}	6.38	-2.68	-0.84	0.19	2.86	3.89
		$M^{0\nu}$					2.70	3.57

adopted by Nuclear Shell Model may bring a severe loss in the total transition strength of $0\nu\beta\beta$ decay. Then the different parameterizations and approximations of the same methods may bring also errors, these are listed in [117]. In this work for the deformed nuclei, we can also give some assessment on these errors from our calculations following the discussion in [117]:

i) The quasiparticle mean field may change the results slightly except $M_{GT}^{0\nu}$ for intermediate states 0^+ and 1^+ which are sensitive on g_{pp} . In our calculations we compared the Woods-Saxon potential and the Harmonic oscillators in the spherical limit, they differ only a little. Other mean fields may give the similar results;

ii) we have discussed g_{pp} dependence of the final results. One finds only contributions of GT part from the multipoles $K^\pi = 1^+$ and $K^\pi = 0^+$ are sensitive to g_{pp} , other multipoles evolve with g_{pp} steadily. In this sense, the experimental errors of the half-lives will bring the uncertainties to $M^{0\nu}$ mainly for multipoles (K^π) 0^+ and 1^+ . Because of the different magnitudes of g_{pp} sensitivities of $M^{0\nu}$ and $M^{2\nu}$, an uncertainty in the $2\nu\beta\beta$ half-life will produce a much smaller relative error bar $0\nu\beta\beta$ decay half-life.

iii) For certain values of $2\nu\beta\beta$ NME, $0\nu\beta\beta$ NME is also related with another parameter in our calculation, the axial vector coupling constant g_A , and we find that with the choices of different g_A , one may obtain an error of about 20% at the leading order. Here M_F change slightly and M_{GT} changes a bit with the change of g_A . But for the final NME, as the GT part depends also on the values of g_A which is also depends on $M^{2\nu}$, the effect of the change of M_{GT} is not significant in the overall NME $M^{0\nu}$. For the choices we made for the g_A values, in consideration of all the corrections, there is a 23% change in the spherical case and 21% for the deformed case. In this case the determination of the value of g_A can reduce the uncertainty of $M^{0\nu}$;

iv) The effect of the sizes of model spaces are also intensively discussed in this thesis. A truncation

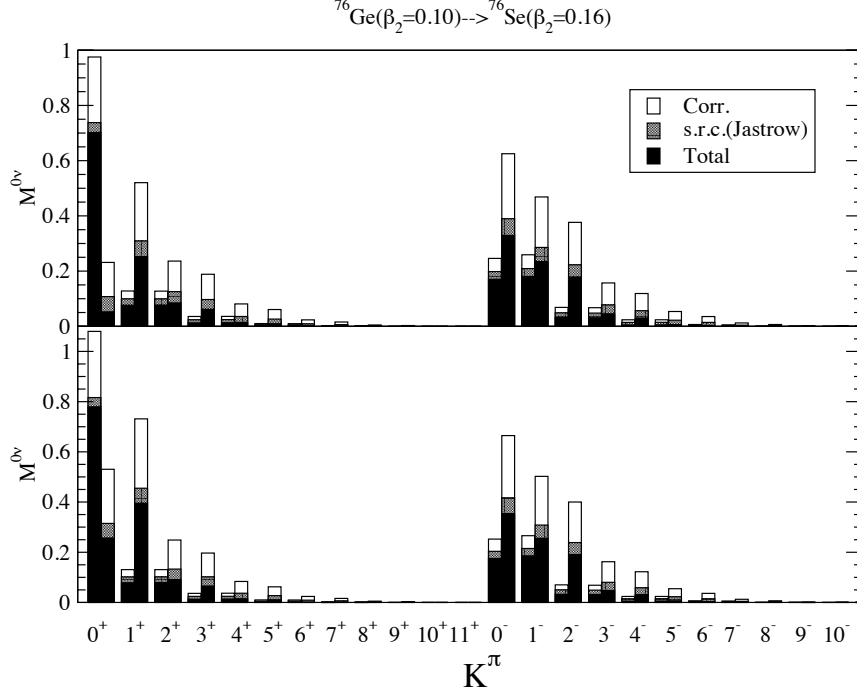


Figure 5.19: The NME's for different multipole channels for the deformed case of ${}^{76}\text{Ge}$ with the g_{pp} values fitted to the $2\nu\beta\beta$ decay with the bare g_A (upper panel) and the quenched one (lower panel). The results are the same as in fig.5.13 but allowing for deformations ($\beta_2 = 0.1$ in ${}^{76}\text{Ge}$ and $\beta_2 = 0.16$ in ${}^{76}\text{Se}$).

of the model space may also bring an error of about several percents to the final result. In the spherical case, from table 5.7, less than 5% if all the other parameters are the same, and with deformation, the errors are similar as listed in table 5.7. So even with a larger deformation, with suitable truncation, we expect the error to be within 10%;

v) It is estimated that using the closure energy to replace the intermediate energies, the error could be within 10% [117]. This is because the mediating neutrino's average momentum is of $\approx 100\text{MeV}$, considerably larger than the nuclear excitation energies which have a magnitude of $10 - 20\text{MeV}$;

vi) The higher order terms and the finite nucleon size give us a total correction of about 30% to the overall NME. So in this sense, the correct high order terms and correct form factors may be important for the determination of $M^{0\nu}$;

vii) The different choices of SRC, may change the value greatly, as can be seen in table 5.7, the Jastrow type gives a 15% reduction to the final $M^{0\nu}$ comparing to 5% to the Brückner CCM style SRC. In this sense a more accurate SRC is needed;

viii) The overlap factors of initial and final nuclei also reduce the NMEs, especially for the deformed nuclei. This suppression comes from the different BCS vacua of the initial and final nuclei. For the two nuclei with large deformation differences, this suppression is significant, can be as large as 40%. Even in the case that both the initial and final nuclei are spherical, a nearly 20% reduction

has been derived;

ix) the last important topic is the effect of the different shapes of the nuclei, deformation, which is the objective of this work. We have seen that the effect of deformation can reduce $M^{0\nu}$ largely, this signifies the importance of the deformed calculation for heavy nuclei since many of them are usually strongly deformed.

From above analyses, the importance and priorities of different approximations become clear. First, the effect of deformation affects most strongly the BCS vacua overlap between the ground states of the initial and final nuclei, we will check this again for the heavy deformations. In addition, all the corrections as the finite nucleon size, the higher order currents and SRC must be taken into account. As for the truncations, if we keep all the neighboring shells of the active shell, then small errors are expected. A suitable choice of g_A is also important for the final result.

To conclude of this discussion, we give the results of calculations for the deformed ${}^{76}\text{Ge}$, with the corresponding uncertainties. The results are listed in table5.6 and table5.7. The largest value is $M^{0\nu} = 4.69$ when we use the Brückner CCM SRC and ignore the quenching of g_A in nuclei. And the smallest value 2.70 is obtained when we make the truncations, use the Jastrow type SRC and take into consideration the quenching effect. All these different choices of parameters such as the SRC, the quenching *etc* give a total reduction of about 40%. And now we come to the calculations of ${}^{150}\text{Nd}$, following all the calculation results we obtained for ${}^{76}\text{Ge}$.

As an example we showed how the different uncertainties may arise from different approximations and assumptions used in the deformed calculations for ${}^{76}\text{Ge}$. And this can give us some insight into our calculations of ${}^{150}\text{Nd}$ which has more nucleons and a larger level space. In the deformed calculations, the enlargement of the level space makes the computational time increase drastically, so we need to choose suitable truncations for these calculation. From the above discussions we see that the effects of the far away single particle states can be indeed eliminated, or at least substantially reduced. So we make the truncation to drop the shells $0 - 3\hbar\omega$ from the full space $0 - 6\hbar\omega$. This reduces the total numbers of the single particle levels from 84 to 64 and saves a lot of computational time. In the following part, we will illustrate the results for $0\nu\beta\beta$ of ${}^{150}\text{Nd}$ which definitely is deformed and previous spherical calculations are with big deviations.

The input deformation parameters for our Woods-Saxon potential have been given in preceding section for ${}^{150}\text{Nd}$. For comparison, we make also the calculations in the spherical limit. We calculated two sets of results corresponding to the bare and quenched axial vector coupling constants g_A respectively. The contributions of different multipoles to NME are illustrated in fig.5.22 in the spherical limit, and fig.5.23 for the deformed case. They have the similar multipole structures as in the case of ${}^{76}\text{Ge}$, the low multipoles contribute more, and the high multipoles can be neglected in the calculations. The detailed results is illustrated in table.5.8 for sums of all the multipoles for the leading order contributions and different corrections. We see that in our calculation for ${}^{150}\text{Nd}$, the reduction from the high order terms of the nucleon currents and form factors is about 20% for $M_F^{0\nu}$ and 40% for $M_{GT}^{0\nu}$ respectively. These reductions produce about 30% overall reduction in the final $M^{0\nu}$. In addition, the SRC is important here, depending on which scheme we use we may have reductions varying from as large as 20% to less than 5%.

And as for ${}^{76}\text{Ge}$, we made several comparisons for different approximations in the calculation for ${}^{150}\text{Nd}$ in figs.5.20,5.21 at the leading order, to evaluate the uncertainties. First one is the

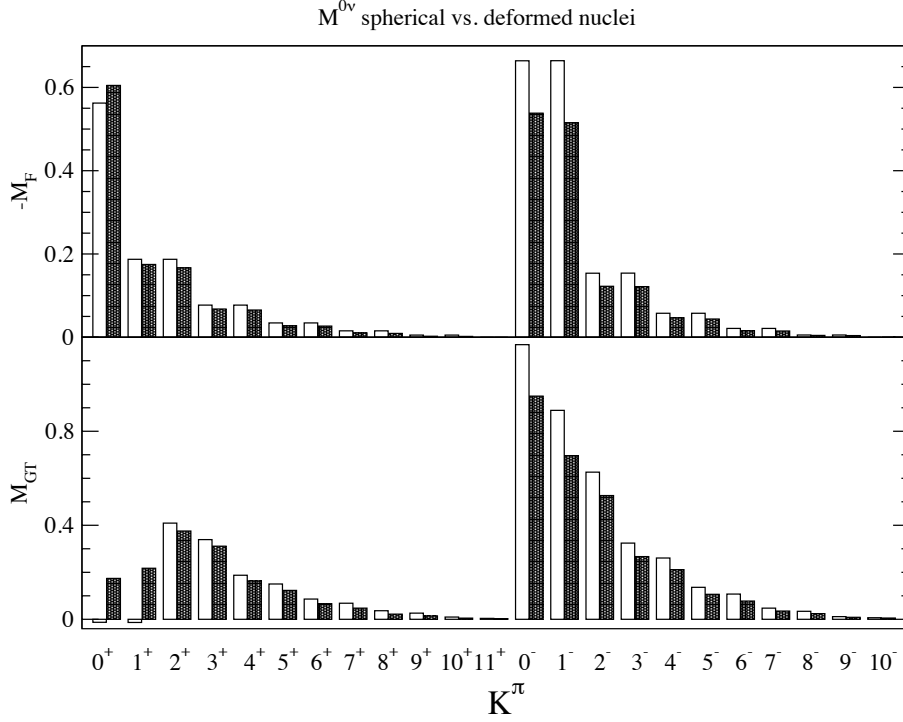


Figure 5.20: Comparisons between the NME's for $^{150}\text{Nd} \rightarrow ^{150}\text{Sm}$ in leading order for both spherical and deformed case without considerations of the BCS overlap factors. The left bars are for spherical and right bars for the deformed case with deformation parameters given in table.???. The upper panel is for the Fermi part while the lower panel shows the Gamow-Teller part (eq.(5.9)). K^π are for the intermediate states, *i.e.* for (pn) pair.

deformation, we see that for ^{150}Nd , the deformation may change the structure of NME, comparing with the case of ^{76}Ge . This may come from the larger deformation of ^{150}Nd , which is twice as large as that of ^{76}Ge . For such large deformation, the level scheme has changed greatly from that of the spherical case. This means that in heavily deformed nuclei, there is a bigger change of NME. It is different from the small deformation case where the NME of the single states is nearly the same as the corresponding ones in the spherical nuclei. If large suppressions from BCS overlap factors are not taken into consideration, we can have a reduction of 24%, of which the F part contributes a bit more than GT part. So in the heavily deformed nuclei, the importance of the choices of deformation parameters becomes much more crucial.

The g_{pp} dependence of $M^{0\nu}$ seems not so significant here for realistic $g_{pp} \sim 1$, and we believe that the similar behavior applies here as in the case of ^{76}Ge . One finds only small changes of multipoles 0^+ and 1^+ , for a change of g_{pp} for 0.02. The large change of $2\nu\beta\beta$ NME from the change of g_A is compensated by the sensitivity of $M_{GT}^{2\nu}$ to g_{pp} . Hence, with the different choices of g_A , $M_F^{0\nu}$ and $M_{GT}^{0\nu}$ can be viewed as constants. Under this assumption, the value of g_A we adopt may play a crucial role for the determination of the final $M^{0\nu}$ from Eq.(5.9).

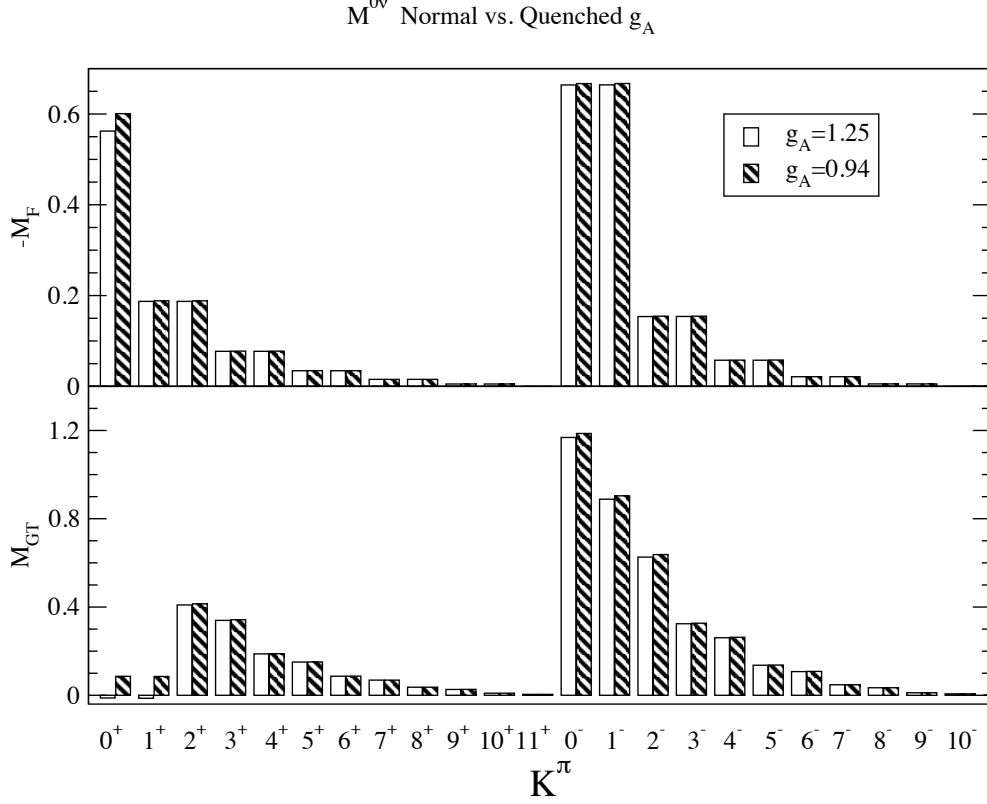


Figure 5.21: Comparison between the NME in the leading order for unquenched $g_A = 1.25$ and quenched $g_A = 0.94$, without considerations of the BCS overlap factors. The left bars are for $g_A = 1.25$ and right bars for $g_A = 0.94$. It corresponds to fig.5.16 for ${}^{76}\text{Ge}$.

Here we used a truncated space because a full space calculation is somehow unrealistic at present due to the limitation of the computers. From the experience of ${}^{76}\text{Ge}$ we expect that our truncation will at most bring an error of 10%, comparing with uncertainties brought by the deformation parameters and axial coupling constant, this is really a small error.

For the full consideration of all the corrections, the reductions stemming from the deformation for ${}^{150}\text{Nd}$ is about 40%. Noticing that the BCS overlap factors gives the reductions about 30%, we may conclude that in this case, the reductions of $M^{0\nu}$ largely comes from the BCS overlap factors. We also investigate the effect of the quenching of g_A , for the quenched axial vector coupling constant g_A , we have a reduction of about 30% for $M^{0\nu}$. This is because in the quenched case we have a smaller contribution from $M_{GT}^{0\nu}$ due to a smaller g_A . And the largest predicted value of $M^{0\nu}$ for ${}^{150}\text{Nd}$ in our calculation is 3.34, with the Brückner style SRC and bare g_A , while the smallest value is 1.79 with the Jastrow type SRC and quenched g_A , so the total uncertainty of 46%. And it is clear that Jastrow type SRC over reduced the results [119] and it is commonly accepted that there are quenching effects in the nuclei, with these assumptions, we would like to recommend the value 2.06 as the best value of our calculations.

In tabel5.9 the calculated NME $M^{0\nu}$ for ${}^{150}\text{Nd}$ is listed and compared with the calculation results by other approaches. One can see that the NME $M^{0\nu}$ of this work calculated with the neglect

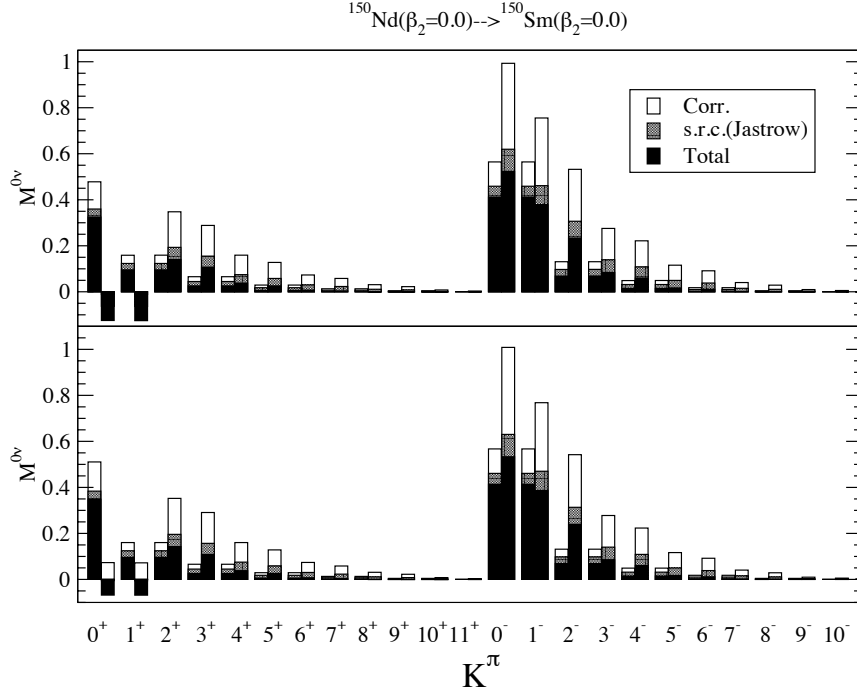


Figure 5.22: The $0\nu\beta\beta$ NME's in spherical nuclei for different multipole channels of ^{150}Nd with g_{pp} value fitted with the bare g_A (upper panel) and the quenched g_A (lower panel). It is similar to fig.5.13 for ^{76}Ge .

of deformation (column 3) agrees well with the previous ones of the spherical QRPA [117]. A small difference can have its origin in the somewhat different approximations involved (use of the Woods-Saxon single particle wave-functions and the BCS overlap factors, the different SRC and truncations of the model space). By including deformation (column 4), one gets a much smaller NME $M^{0\nu}$. The main origin of the suppression is given above, stemming from the BCS overlap factors as well as the quenching of g_A .

Our present NME $M^{0\nu}$ for ^{150}Nd , obtained within the state-of-the-art QRPA approach that accounts for nuclear deformation, and it has nearly the same magnitude as NME of other approaches (columns 5, 6, 7) when the quenching effect is taken into consideration. The $0\nu\beta\beta$ decay half life $T_{1/2}^{0\nu}$ corresponding to the effective Majorana neutrino mass $m_{\beta\beta} = 50\text{meV}$ gives a rough estimation of 10^{26} year, in agreement with the general results obtained by different methods.

5.3 Prospect of Neutrinoless Double Beta Decay

Although with the claim by [7], we till now don't have enough evidence for the existence of the $0\nu\beta\beta$. Till now we have just lower limits for the $0\nu\beta\beta$ half-lives for most of the candidate nuclei. We need more accurate experiments with improved measurements and detection technology to confirm or deny the possibility of the $0\nu\beta\beta$, we are still far from full understanding the whole

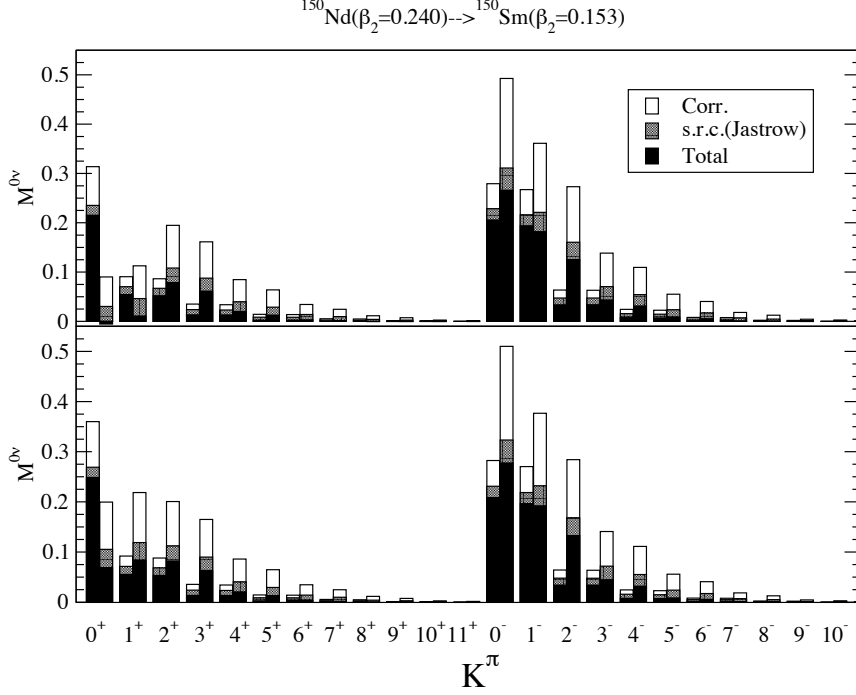


Figure 5.23: The $0\nu\beta\beta$ NME's for different multipole channels for the deformed case of ^{150}Nd with g_{pp} fitted with the bare g_A (upper panel) and quenched one (lower panel).

process both experimentally or theoretically. Even if the $0\nu\beta\beta$ is observed, a lot of work will be needed for identifying the underlying physics.

For the matrix element calculations of the deformed nuclei, we now developed the deformed pn-QRPA methods, together with previous versions of QRPA approaches, we can deal with nearly all the nuclei which decay with the $\beta\beta$ -decay. With several nuclear system measured and matrix elements $M^{0\nu}$ calculated for different mechanisms, in this case, we can determine which mechanism is dominant. This can also be determined by the comparisons of half-lives for decays to different final states such as the ground states or the 1^+ and 2^+ excitation states, but the observation of these decays may be difficult because of the large $2\nu\beta\beta$ background.

However, the determination of NME is not simple, a comparison of different methods may give us some clues, but till now the discrepancies among different models are still very large, especially that between the two main approach, QRPA and NSM. At the present stage, to close the gaps between them should be the most realistic and necessary, since we have no idea when one will discover the $0\nu\beta\beta$.

On the other hand, $0\nu\beta\beta$ can also be viewed as a good constraint on new physics beyond the SM. An apparent situation is the problems of the neutrino, we now have the difference of the masses squared as well the mixing angle measured from the oscillation experiments. But these values do not help us to answer questions like how small is neutrino mass and are they Majorana particles. Answers to these problem now wait the results from $0\nu\beta\beta$ as well as other experiments and observations,

Table 5.8: Different contributions to the total calculated NME's for $0\nu\beta\beta$ decay $^{150}\text{Nd}\rightarrow^{150}\text{Sm}$ for model space $4-6\hbar\omega$. The BCS overlap is taken into account. The different contributions are described in table5.6.

β_2	g_A		$M(1/r)$	ΔM	$\delta M(\text{J})$	$\delta M(\text{BCD})$	tot(J)	tot(BCD)
0.240 (0.153)	1.25	M_F	-2.09	0.51	0.33	-0.06	-1.25	-1.64
		M_{GT}	4.01	-1.86	-0.72	0.14	1.43	2.29
		$M^{0\nu}$					2.23	3.34
	0.94	M_F	-2.16	0.52	0.33	-0.06	-1.30	-1.70
		M_{GT}	4.44	-2.00	-0.73	0.14	1.71	2.58
		$M^{0\nu}$					1.79	2.06
0.0 (0.0)	1.25	M_F	-4.07	0.99	0.67	-0.13	-2.41	-3.21
		M_{GT}	7.35	-3.54	-1.46	0.26	2.36	4.07
		$M^{0\nu}$					3.90	6.12
	0.94	M_F	-4.12	1.00	0.68	-0.13	-2.44	-3.25
		M_{GT}	7.69	-3.65	-1.47	0.27	2.58	4.31
		$M^{0\nu}$					3.01	4.50

Table 5.9: The matrix elements $M^{0\nu}$ for the $0\nu\beta\beta$ decay $^{150}\text{Nd}\rightarrow^{150}\text{Sm}$ calculated in different models. The final result of this work obtained with account of deformation is given in column 4. A result with neglect of deformation is also listed for comparison with the earlier result of Ref. [117]. The corresponding half-lives $T_{1/2}^{0\nu}$ (in the unit of 10^{25} years) for an assumed effective Majorana neutrino mass $\langle m_{\beta\beta} \rangle = 50$ meV are also shown.

	QRPA [117]	def. QRPA(sph.)	def. QRPA	pseudo-SU(3) [25]	PHFB [26]	IBM-2 [27]
$M^{0\nu}$	5.17	6.12	2.06	1.57	1.61	2.32
$T_{1/2}^{0\nu}$	1.72	1.23	10.8	18.7	17.7	8.54

the improvement of the precision of the experiments will bring us either the definite answers or further constraints. Further, we may wonder why are neutrinos Dirac or Majorana particles, why are their masses so tiny, *etc.* All these underlying problems require experimental determinations of the $0\nu\beta\beta$. In this sense, the discovery of the $0\nu\beta\beta$ will trigger a new era of physics together with experiments such at the LHC and other high energy accelerators.

Chapter 6

Summary and Conclusions

The absolute neutrino mass scale and the nature of neutrino (whether it is Majorana particle, *i.e.* it is its own antiparticle) have long been important questions in particle physics since the observation of the neutrino oscillations. The former question can be answered by different experiments and observations. The single beta decay can give the anti-electron-neutrino mass. The current running experiment for this task is the KATRIN in Karlsruhe with sensitivity of about 0.2 to 0.3 eV. From the study of the cosmic microwave radiation spectrum as well as the study of the large scale structure in the universe, one can get a limit on the sum of the neutrino masses of about 1.6eV from Sloan Digital Sky Survey(SDSS). And one can also extract this mass scale from the neutrinoless double beta decay experiment, from the so-called effective neutrino mass. However, only the latter experiments can reveal the Majorana nature of the neutrinos and can answer the second question of the neutrino physics. Hence, the neutrinoless double beta decay experiments have crucial importance in the neutrino physics and for new physics beyond the Standard Model (SM).

Double beta decay is a rare decay with a half-life much longer than the age of our universe. It was proposed by Maria Goeppert-Mayer in 1935, only one year after the Fermi weak interaction theory was formulated. It originates from the nuclear pairing (the protons and neutrons get paired by the residual interaction) which tends to lower the ground states of the even-even nuclei and makes them more stable than the odd-odd ones with the same nucleon numbers. The decay is thus from even-even nucleus to another even-even one with a larger binding energy, with a change of nucleus electric charge by two units. To conserve the electric charge, two electrons are emitted. According to the number of the emitted neutrinos, one can divide this decay into two types: If the lepton number is conserved, then two anti-electron-neutrinos are emitted, $(A, Z) \rightarrow (A, Z + 2) + 2e^- + 2\bar{\nu}_e$, this process is called the two neutrino double beta decay; Otherwise, if there is no neutrinos presented in the final state, $(A, Z) \rightarrow (A, Z + 2) + 2e^-$, the lepton number is violated by two units, this decay is called the neutrinoless double beta decay. The two neutrino double beta decay has been observed by different experiments, for different double beta decay emitters, its half-life lies in a range from 10^{18} to 10^{21} years. But currently, there is no confirmed evidence for the existence of neutrinoless double beta decay despite the highly contesting result from Klapdor-Kleingrothaus group for ^{76}Ge .

From the above descriptions, one finds that neutrinoless double beta decay is a weak process with the lepton number being violated. One of the origins of such violation is the Majorana nature of the neutrinos, a Majorana mass term in the Lagrangian violates the lepton number conservation. This is forbidden in the SM. But with a simple addition to the SM such as a basic type I see-saw with both Dirac and Majorana mass terms, this violation can be achieved. And in some other new physics models such as Grand Unification Theory (GUT), this violation is obtained automatically from the interactions of fermions with the extra gauge bosons such as in the SO(10) GUT. There may be also other origins of this violation, such as that coming from the R-parity violated SUSY, where the violated lepton number is accompanied by the violated R-parity. For these different possible underlying mechanisms, one prefers the basic mechanism with a simple addition of see-saw, and it is supposed to be a dominant one with the contributions from the light neutrinos being overwhelming.

As mentioned above, the neutrinoless double beta decay implies the Majorana nature of the neutrinos. If this process is truly mediated by a light virtual neutrino, one can extract the effective neutrino mass from the measured half-life, but only if the nuclear matrix element (NME) is precisely determined. The NME is closely related to nuclear physics, it describes the nuclear transitions of the double beta decay process. The theoretical calculation of the NME for the two-neutrino double beta decay can be a good cross check for the reliability of the calculated many-body wave functions used in the neutrinoless double beta decay NME. The nucleus is a very complicated many-body system, and to deal with such a system, one needs nuclear many-body theories. One of such theories which is frequently often used in the calculations of NME is the Quasiparticle Random Phase Approximation (QRPA). The QRPA methods use the mean field approximation to get the single particle wave functions and solve the BCS pairing equations in the basis of these s.p. states to construct the ground states of the initial and final nuclei. With the proton-neutron (pn) excitations mixed by the residual interactions, one constructs the excited states in the intermediate nucleus. The method has been shown to be capable of successfully describing the double beta decay processes provided the particle-particle residual interaction is included along with the usual particle-hole one. On the other hand, the calculated nuclear matrix elements for the double beta decay, both for the two-neutrino and neutrinoless modes, turned out to be sensitive to the value of the particle-particle interaction strength.

Of the different double beta decay emitters, ^{150}Nd has the largest phase space and hence the largest decay rate and the relatively shortest half-life of about 10^{25} years in the spherical QRPA calculation (for the effective neutrino mass of 50 meV). So it could be the emitter with the largest discovery potential of neutrinoless beta decay. But in contrast to other emitters, most of which are spherical, it is heavily deformed. Most of the previous calculations of neutrinoless double beta decay NME were done for the spherical case only. So one needs to develop the QRPA approach to deal with the deformation. The deformed QRPA to treat the two neutrino double beta decay was developed by Tübingen group. The deformed Woods-Saxon wave functions with the phenomenological residual interactions are used and the Gamow-Teller-Resonance (GTR) and the two neutrino double beta decay NME are successfully described. However, using the phenomenological forces for calculating the neutrinoless double beta decay amplitude would immediately rise the problem of how to fix the numerous strength parameters of the forces in different J^π channels. So the realistic NN forces

have been included into this calculation by Tübingen group to replace the phenomenological forces. In order to perform the deformed QRPA calculations, the main effects of the deformation on the ground state properties have to be clarified. Pairing interactions for protons and neutrons in the even-even nuclei have to be described. The BCS equations were solved self-consistently to obtain the occupation probabilities which enter the QRPA equations, and also to obtain gap parameters as well as the chemical potentials for protons and neutrons. As a two-body interaction, the nuclear G-matrix was used which is a solution of Bethe-Goldstone equation for the Bonn-CD one boson exchange potential. The deformed G-matrix elements are obtained from a decomposition over the spherical ones, the decomposition coefficients are calculated by space overlap integrals between the single particle basis of spherical harmonic oscillator and the deformed wave functions. The single particle states of the deformed basis are calculated in a deformed axially-symmetric Woods-Saxon potential. The same G-matrix elements are also used for the residual interaction which mixes the pn excitations. By solving the QRPA equations, one can get the wave functions for the states of the intermediate nucleus. There are two parameters in this model, the renormalized particle-hole strength g_{ph} and the renormalized particle-particle strength g_{pp} , they are determined by the GTR position and the NME of two neutrino double beta decay. This adjustment was first done for the realistic forces in Mohamed Saleh Yousef's work by Tübingen group. For the first time, they developed the deformed QRPA by including the realistic forces and calculated the GTR and the two neutrino double beta decay NME within the deformed QRPA frame.

The topic of this thesis is to apply the deformed QRPA with the realistic forces to the calculations of the neutrinoless double beta decay. Following the previous works in Tübingen group done by M. S. Yousef, we determine the free parameters of our QRPA calculation by adjusting the position of GTR (for g_{ph}) and fitting the two neutrino double beta decay NME (for g_{pp}). The two-neutrino double beta decay is governed by the Gamow-Teller (GT) matrix elements connecting the final and initial nucleus with the intermediate states. Then, with the fixed parameters, we calculated also the Spin-Dipole (SD) transitions to verify the reliability of our method. Then we come to the final calculation of the neutrinoless double beta decay NME.

Before calculation for ^{150}Nd , we first calculated the NME for ^{76}Ge as it is light and a smaller model space is needed. These make this nucleus numerically easier for the calculations. Also this nucleus is well studied by previous calculations with a spherical treatment. So, a comparison between the deformed and spherical QRPA methods has been done with the deformations in the deformed QRPA set to be zero (The spherical limit). At the leading order, one gets a perfect agreements between the NME's of these two calculations for both the Fermi (F) part and Gamow-Teller (GT) part for all the multipoles J^π or K^π (here π is the parity, and J and K are the total angular momentum and its projections on the symmetry axis respectively), which implies a good consistency between the current deformed extension of the QRPA and the original spherical one. If deformation is taken into account, one finds a reduction of the neutrinoless double beta decay NME, which comes mainly from the BCS overlap between the ground states of the initial and final nuclei. This BCS overlap depends on the difference between the deformations of the initial and final nuclei, but one finds that even in the spherical limit, this overlap factor is less than unity. In this thesis we also assess the different uncertainties which may arise from different approximations adopted. The size of the model space will not affect the final results if one includes the active shell

(where the Fermi level lies in) and its neighbors in the calculations. The two-neutrino double beta decay NME depends sensitively on g_{pp} , because only the multipole $J^\pi = 1^+$ is involved in this calculation. But for neutrinoless double beta decay more multipoles are involved, and the NME dependence on g_{pp} is not very sensitive. Different choices of the axial vector coupling constant g_A can affect the final results by as large as 20% because of these dependences on g_{pp} . The high order currents and the finite nucleon size give all together a reduction of about 40% in the GT part and 20% in the F part. This gives a reduction to the overall NME by 30%. And different choices of Short-Range-Correlation (SRC) may give a reduction from about 5% (Brückner CCM) to 20% (Jastrow).

Coming to ^{150}Nd , one gets similar results. Here for the reality of current computers, we truncated the model spaces, and use a space $4 - 6\hbar\omega$ with shells with principal number $N = 4, 6$. Now one has much larger deformations with a larger deformation difference, hence the reduction from the BCS overlap is much larger, the BCS overlap is about 0.6. So a large reduction from the deformation is expected compared with previous results with the spherical calculations. Similar reductions from the high order currents and the finite nucleon size as well as the SRC are obtained, these give an overall reduction for about 30% if one uses the Brückner CCM SRC, or about 40% if the Jastrow SRC is adopted. One finds that our method gives a larger NME than other methods and a corresponding half-life of about 10^{25-26} years for $m_{\beta\beta} = 50\text{eV}$ (depending on the actual quenching effect of the axial vector coupling constant and the adopted SRC). This makes ^{150}Nd still the favorite among the neutrinoless double beta decay candidates.

The future of the double beta decay is promising. It is not only a big challenge but also a huge chance for both the theorists and the experimentalists. Strong double beta programs in both particles and nuclear physics are under way. The detection technology also develops rapidly, making the sensitivity of the experiments higher and higher.

Chapter 7

Zusammenfassung

Neutrino-Oszillationen haben gezeigt, dass Neutrinos Masse besitzen. Die Neutrino-Oszillationen können uns jedoch keine Information über die absoluten Massen liefern weil sie nur die Differenzen der Massenquadrate der Neutrinos und die Mischungsmatrix zwischen den Massen- und Flavor-Eigenzuständen geben. Im Neutrino-Sektor gibt es noch viele offene Probleme:

1. Ist das Neutrino ein Dirac- oder Majorana-Teilchen, d.h. ist es verschieden oder identisch mit dem Antiteilchen?
2. Was ist die absolute Skala der Neutrinomassen?
3. Ist die Massen-Hierarchie der Neutrinos die natürliche (1-2-3) oder ist sie invertiert (3-2-1)?
4. Was ist die Dirac-Phase, die bei drei Generationen der Neutrinos in der Transformation z.B. im Element (1,3) von Massen-zu Flavor-Neutrinos auftreten kann?
5. Was sind die beiden Majorana-Phasen?

Die absolute Skala der Neutrinomassen lässt sich in folgenden Experimenten bestimmen:

1. Einfacher Betazerfall, z.B. im Tritium-Zerfall mit dem sehr kleinen Q-Wert 18,6 keV. Hier liegt die Obergrenze für die Elektron-Neutrinomasse bei 2,3 eV im Mainz und Troitsk-Experiment. KATRIN-Experiment in Karlsruhe wird die obere Grenze bis 0,3 eV reduzieren.

2. Eine Zweite Möglichkeit entsteht durch die Untersuchung der Massenverteilung im Universum. Bei der Strukturbildung sorgen massive Neutrinos dafür, dass mit zunehmender Summe der Massen der drei Neutrinos die Wahrscheinlichkeit für Galaxien bei kleineren Abständen reduziert wird. Das gemessene "Power"-Spektrum der Massenverteilung legt für eine obere Grenze der Summe der drei Neutrinomassen einen Wert von 1 bis 2 eV nahe. Die Zuverlässigkeit dieser Grenze ist aber eng verbunden mit unserem Verständnis der Strukturformation im Universum, wo es auch noch viele offene Fragen gibt.

3. Die dritte Möglichkeit der Festlegung der absoluten Neutrinomasse benutzt den neutrinolosen Doppelten Betazerfall. Hierzu müssen die Übergangsmatrixelemente zuverlässig bekannt sein. Die entsprechende Berechnung wird in dieser Dissertation zum ersten Mal mit realistischen Nukleon-Nukleon-Kräften (das neueste Bonn CD-Potential) in deformierten Kernen durchgeführt.

Der neutrinolose Doppelte Betazerfall ist im Standard-Modell verboten. In Großvereinheitlichten Theorien (GUT's) und in Supersymmetrischen Modellen (SUSY) ist er jedoch erlaubt. In diesen Theorien ist das Neutrino ein Majorana-Teilchen und besitzt Masse. Bisher gibt es nur obere

Grenzen für den neutrinolosen doppelten Betazerfall, abgesehen von einer Messung in ^{76}Ge von Klapdor-Kleingrothaus und seinen Hiedelberger Mitarbeitern, die jedoch von dem Rest der Kollaboration und allen anderen Experten auf dem Gebiet des Doppelten Betazerfalls angezweifelt wird.

Um aus den Übergangswahrscheinlichkeiten die Majorana-Masse zu bestimmen sind die Übergangsmatrixelemente genau so wichtig wie die Daten.

Die Berechnungen der Übergangsmatrixelemente für den neutrinolosen doppelten Betazerfall wurden bisher mit realistischen NN-Kräften nur im sphärischen Fall durchgeführt. Der Zerfall von ^{150}Nd mit einem sehr großen Phasenraum und daher einer großen Übergangswahrscheinlichkeiten und einer relativ "kurzen" Lebensdauer in der Gegend von etwa 10^{25} Jahren (abhängig von der unbekanntem Neutrinomasse) verspricht mit sphärischen Rechnungen die beste Aussicht auf die Entdeckung des neutrinolosen Doppelten Betazerfalls.

^{150}Nd ist aber deformiert, und jede realistische Berechnung vom Übergangsmatrixelement muss die starke Deformation des Kerns berücksichtigen. In dieser Doktorarbeit werden die benötigten Vielteilchenwellenfunktionen der Kerne im Rahmen der Quasi-Teilchen-Random Phase-Näherung (QRPA) berechnet. Zuerst, müssen die Einteilchen-Nukleon-Wellenfunktionen der Protonen und Neutronen in einem deformierten Woods-Saxon-Potential berechnet werden. Diese deformierten Nukleonwellenfunktionen werden dann in eine sphärische Basis entwickelt, in der dann die Nukleon-Nukleon-Matrixelemente der Bonn CD-Kraft im Rahmen der Brückner Theorie durch Lösen der relativistischen Bethe-Salpeter-Gleichung (halb auf der Energieschale) mit Pauli-Operator berechnet werden. Hierzu sind mehrfaches Umkoppeln der Drehimpulse für den Spin und den Bahndrehimpuls und entsprechende Schritte auch im Isospin-Raum notwendig. Am Ende hat man nun die Zweikörpermatrixelemente der realistischen NN-Wechselwirkung in der deformierten Basis und kann diese zusammen mit den Einteilchenenergien in die entsprechende QRPA Gleichungen einsetzen. Die gleiche Transformation wird auch mit den Zweikörpermatrixelementen des Neutrinopotenzials gemacht.

Mit der QRPA Lösung für Vielteilchenwellenfunktionen werden die Übergangsmatrixelemente für den Doppelten Betazerfall in den Systemen $^{76}\text{Ge} \rightarrow ^{76}\text{Se}$ und $^{150}\text{Nd} \rightarrow ^{150}\text{Sm}$ berechnet. Zum Test der Qualität dieses Elements ist die Berechnung des entsprechenden deformierten Zwei-Neutrino Übergangsmatrixelements notwendig. Es wurde zuerst in Tübingen in der Doktorarbeit von Mohamed Saleh Yousef gemacht. Durch dieser Rechnung erfährt man dass eine leichte Renormierung der Teilchen-Teilchen und Teilchen-Loch Wechselwirkungen benötigt ist um die relevanten experimentellen Daten anzupassen. Die Gamow-Teller-Resonanz (GTR) könnte in ihre Position in Zwischenkern durch eine Renormierung der Teilchen-Loch-Matrixelemente angepasst werden (solch eine Anpassung ist jedoch in der Regel nicht notwendig, da schon die nackten Brückner-G-Matrixelemente die experimentelle Lage der GTR fast genau wiedergeben). Die Renormierungsfaktor der Teilchen-Teilchen-Wechselwirkung ist für ^{150}Nd $g_{pp} \approx 1$. Das heißt die nackte Brückner-G-Matrixelemente sind schon ziemlich genau in den QRPA Rechnungen.

Im Vergleich zu früheren sphärischen Berechnungen ist da in dieser Doktorarbeit berechnete Übergangsmatrixelement für den neutrinolosen doppelten Betazerfall $^{150}\text{Nd} \rightarrow ^{150}\text{Sm}$ ziemlich stark, um ca. 40%, reduziert. Das ist der Effekt der starken Deformation, und je grösser der Unterschied zwischen den Deformationen im Anfangs- und Endkern wird, desto stärker wird die Reduktion.

Diese Beobachtung stimmt mit den Resultaten anderer Methoden überein. Trotz der Reduktion, zeigen die Resultate dieser Arbeit, dass der neutrinolose doppelte Betazerfall für $^{150}\text{Nd} \rightarrow ^{150}\text{Sm}$ eine der besten Empfindlichkeiten für die Majorana Neutrinomasse hat.

Appendix A

Brief Introduction to Superfield Formulation

To construct the supersymmetry multiplets, we can introduce the so-called superspace coordinate which is Grassmann number behaving like a spinor. we introduce a left Weyl spinor coordinator θ_α and its complex conjugate $\bar{\theta}^{\dot{\alpha}} = (\theta_\alpha)^\dagger$, satisfying $[x^\mu, \theta_\alpha] = \{\theta_\alpha, \theta_\beta\} = \{\theta_\alpha, \bar{\theta}^{\dot{\beta}}\} = \{\bar{\theta}^{\dot{\alpha}}, \bar{\theta}^{\dot{\beta}}\} = 0$, with these coordinates we can define the Superderivatives:

$$D_\alpha \equiv \frac{\partial}{\partial \theta^\alpha} + i\sigma_{\alpha\dot{\alpha}}^\mu \bar{\theta}^{\dot{\alpha}} \partial_\mu \quad \bar{D}_{\dot{\alpha}} \equiv -\frac{\partial}{\partial \bar{\theta}^{\dot{\alpha}}} - i\theta^\alpha \sigma_{\alpha\dot{\alpha}}^\mu \partial_\mu \quad (\text{A.1})$$

a general superfield can be defined as a function of superspace coordinates, the expansion on θ and $\bar{\theta}$ reads:

$$\begin{aligned} S(x, \theta, \bar{\theta}) &= \phi(x) + \theta\psi(x) + \bar{\theta}\bar{\chi}(x) + \bar{\theta}\bar{\sigma}^\mu\theta A_\mu(x) + \theta\theta f(x) + \bar{\theta}\bar{\theta}g^*(x) \\ &+ i\theta\theta\bar{\theta}\bar{\lambda}(x) - i\bar{\theta}\bar{\theta}\theta\theta\rho(x) + \frac{1}{2}\theta\theta\bar{\theta}\bar{\theta}D(x) \end{aligned} \quad (\text{A.2})$$

Under the superfield approach, the infinitesimal supersymmetric transformation has the form:

$$\delta S = (\xi Q + \bar{\xi}\bar{Q})S \quad (\text{A.3})$$

Here the supercharge is actually the same we defined before. But now it has the form:

$$Q_\alpha = \frac{\partial}{\partial \theta^\alpha} - i\sigma_{\alpha\dot{\alpha}}^\mu \bar{\theta}^{\dot{\alpha}} \partial_\mu \quad \bar{Q}_{\dot{\alpha}} = \frac{\partial}{\partial \bar{\theta}^{\dot{\alpha}}} + i\theta^\alpha \sigma_{\alpha\dot{\alpha}}^\mu \partial_\mu \quad (\text{A.4})$$

So the supercharges has just a different of sign with the superderivatives.

The general superfield can be reduced to several different irreducible superfields: the chiral superfield and the vector ones with a special case the gauge superfield.

The chiral superfield Φ obeys the relation:

$$\bar{D}_{\dot{\alpha}}\Phi = 0 \quad (\text{A.5})$$

This is the left chiral superfield and the right one is just its complex conjugate of the left one. By solving the equation, we may have Φ expended in the superfield as:

$$\Phi(x, \theta, \bar{\theta}) = \phi(x_+) + \sqrt{2}\theta\psi(x_+) + \theta\theta F(x_+) \quad (\text{A.6})$$

Here the composite coordinate defined as $x_{\pm}^{\mu} = x^{\mu} \pm i\theta\sigma^{\mu}\bar{\theta}$. Here ϕ and ψ are scalar and left Weyl spinor field respectively and F auxiliary field.

The vector superfield V is obtained by imposing the condition on the general superfield

$$V = V^{\dagger} \quad (\text{A.7})$$

This requires $\chi = \psi$, $g = f$ and $\rho = \lambda$. We are more interested in the gauge superfield since it is related to the gauge theory. Gauge superfield is a special vector superfield where V is in the representation of the gauge algebra under the transformation

$$e^V \rightarrow e^{V'} = e^{-i\Lambda^{\dagger}} e^V e^{i\Lambda} \quad (\text{A.8})$$

Where Λ may be also superfields transform under gauge group. There are extra degrees of freedom in the gauge theory, and the usual way is to choose a particular gauge to remove these extra degrees of freedom. In SUSY gauge theory, the commonly used one is the Wess-Zumino gauge, which set $\chi = \psi = f = g = \phi = 0$, leaving the gauge superfield with the form:

$$V(x, \theta, \bar{\theta}) = \bar{\theta}\bar{\sigma}^{\mu}\theta A_{\mu}(x) + i\theta\theta\bar{\theta}\bar{\lambda}(x) - i\bar{\theta}\bar{\theta}\theta\lambda(x) + \frac{1}{2}\theta\theta\bar{\theta}\bar{\theta}D(x) \quad (\text{A.9})$$

A_{μ} is the gauge field. And a new particle λ , the gaugino, is introduced. Here D again is the auxiliary field.

We can construct the Lagrangian from the superfield by integrating over the superspace. From the expression of the superfield and properties of the superspace coordinates, only F and D terms are non-vanishing after the integration. Because the superfield is supersymmetric invariant, the Lagrangian is automatically invariant, this is simpler than constructing the Lagrangian directly and add the terms from the multiplets by hand. In the following, we show several examples of constructing the supersymmetric invariant Lagrangian.

We call any complex analytical functions $f(\Phi)$ depending on the left chiral superfield Φ^i (or the right one but not on both) the superpotential, which itself is a left (right) chiral superfield. We can construct the Lagrangian from the F -term of the superpotential's superspace integrations:

$$\mathcal{L}_f = \int d^2\theta f(\Phi^i) + \int d^2\bar{\theta} \bar{f}(\bar{\Phi}^i) = [f(\Phi^i)]_F + [\bar{f}(\bar{\Phi}^i)]_{\bar{F}} \quad (\text{A.10})$$

This part correspond to the fermion and Higgs kinetic terms as well as fermion Yukawa couplings in the SM, and of course after the integration on superspace coordinate we can have more interaction such as which between Higgsino and sfermions.

Following the normal definition for gauge field, the gauge field strength is defined out of the gauge superfield as

$$W_{\alpha} = -\frac{1}{4}\bar{D}\bar{D}(e^{-V}D_{\alpha}e^V) \quad (\text{A.11})$$

The kinetic terms of gauge field can be constructed as

$$\mathcal{L}_G = \int d^2\theta \tau_{cc'}(\Phi^i)W^cW^{c'} + c.c. = (\tau_{cc'}(\Phi^i)W^cW^{c'})_F + c.c. \quad (\text{A.12})$$

And the gauge-fermion interactions can be construct from the so called "Kähler potential":

$$\mathcal{L}_K = \int d^2\theta \int d^2\bar{\theta} K(e^V\Phi^i, (\Phi^i)^{\dagger}) = K(e^V\Phi^i, (\Phi^i)^{\dagger})_D \quad (\text{A.13})$$

With these potentials, we can construct the gauge theories which we need.

Appendix B

Nuclear Mean Field

B.1 Nuclear Mean Field Potential for deformed nuclei

In this part, we briefly introduce the mean field potentials and wave functions we use in our work.

B.1.1 Harmonic Oscillators

The Harmonic Oscillator potentials are commonly used in quantum mechanics. For spherical nuclei, it has the general form as 3-dimensional isotropic Harmonic oscillator:

$$V(r) = -V_0[1 - (\frac{r}{R_0})^2] = \frac{m}{2}\omega_0^2(r^2 - R_0^2) \quad (\text{B.1})$$

Here V_0 is the potential-well depth. R_0 is the nuclei radius. The Harmonic oscillator potential gives the energy eigenvalues $\epsilon_N = \hbar\omega_0(N + 3/2) - V_0$, here $N = 2n_r + l$ is the principal quantum number with n_r the radial quantum number and l the orbital angular momentum. The normalized wave function for fermions can be written as:

$$|Nl\Lambda\Sigma\rangle = |Nl\Lambda\rangle|\Sigma\rangle = \psi_{n_r l}(r)\psi_l^\Lambda(\theta, \phi)\chi(\Sigma) \quad (\text{B.2})$$

Here Λ is the z -projection of l , and Σ the spin with the spin wave function χ , the angular function is just $\psi_l^\Lambda(\theta, \phi) = Y_{l\Lambda}(\theta, \phi)$ the spherical harmonic function. The radial part of the wave function can be expressed as:

$$\psi_{n_r}^l(r) = C_{n_r l} \nu^{\frac{l}{2}} e^{-\frac{\nu}{2}} L_{n_r}^{(l+\frac{1}{2})}(\nu) \quad (\text{B.3})$$

$\nu \equiv \frac{r^2}{b_0^2}$ is the dimensionless coordinate with $b_0 = \sqrt{\frac{\hbar}{m\omega_0}}$ the oscillation length, $L_{n_r}^l(\nu^2)$ are the associate Laguerre polynomials, the normalization constant $C_{n_r l} = (\frac{2n_r!}{(n_r+l+1/2)!b_0^3})^{\frac{1}{2}}$.

For the deformed case, the spherical symmetry is no longer valid. But in our case, the axial symmetry remains, then the harmonic oscillator potential may have the form in cylindrical coordinates (ρ, z, ϕ) as:

$$V = -V_0 + \frac{m}{2}(\omega_\perp^2 \rho^2 + \omega_z^2 z^2) \quad (\text{B.4})$$

From the solution of schrödinger equation, we can get the single particle energy as $\epsilon_N = \hbar\omega_\perp(2n_\rho + \Lambda + 1) + \hbar\omega_z(n_z + 1)$. λ and Σ are the projections of the orbital and spin angular momentum on the z axis. The principal quantum number is defined in this case as $N = n_z + 2n_\rho + |\Lambda|$ with n_z the

axis quantum number, n_ρ radial quantum number. The projection of total angular momentum on the z axis is $K = \Lambda + \Sigma$, the parity of the level may be defined as $\pi = (-1)^N$. The wave function of the deformed nuclei can be described as:

$$|Nn_z\Lambda\Sigma\rangle = |Nn_z\Lambda\rangle|\Sigma\rangle = \psi_{n_\rho}^{|\Lambda|}(\rho)\psi_{n_z}(z)\frac{e^{i\Lambda\phi}}{\sqrt{2\pi}}\chi(\Sigma) \quad (\text{B.5})$$

The radial function $\psi_{n_\rho}^{|\Lambda|}$ is in the form:

$$\psi_{n_\rho}^{|\Lambda|}(\rho) = C_{n_\rho}^{|\Lambda|}(\eta) \quad (\text{B.6})$$

with $\eta = (\rho/b_\perp)^2$ a dimensionless coordinate, here b_\perp defined as before $b_\perp = \sqrt{\frac{\hbar}{m\omega_\perp}}$ is the oscillation length for motion perpendicular to z axis, with the normalization constant $C_{n_\rho}^{|\Lambda|} = \left(\frac{2n_\rho!}{(n_\rho+|\Lambda|)!b_\perp^2}\right)^{\frac{1}{2}}$ and $L_{n_\rho|\Lambda|}$ the associate Laguerre polynomial. The axial wave function ψ_{n_z} is written in the similar manner with a dimensionless variable $\xi \equiv z/b_z$, b_z the axial oscillation length with the form $b_z = \sqrt{\frac{\hbar}{m\omega_z}}$:

$$\psi_{n_z} = C_{n_z} e^{-\frac{\xi^2}{2}} H_{n_z}(\xi) \quad (\text{B.7})$$

Here the normalization constant $C_{n_z} = (\sqrt{\pi}2^{n_z}n_z!b_z)^{-\frac{1}{2}}$, H_{n_z} is the Hermite polynomial.

In our calculation, we frequently use the transformation between the spherical and deformed systems. So we need to decompose the deformed harmonic oscillator over the spherical ones as:

$$|Nn_z\Lambda\rangle = \sum_{n_r l} A_{Nn_z\Lambda}^{N'l} |N'l\Lambda\rangle \quad (\text{B.8})$$

The spatial overlap coefficient $A_{Nn_z\Lambda}^{N'l}$ is an integral which can be calculated numerically in the spherical system as:

$$A_{Nn_z\Lambda}^{N'l} = \sqrt{2\pi} \int_0^\infty \left[\int_0^\pi \psi_{n_\rho}^{|\Lambda|}(r \sin \theta) \psi_{n_z}(r \cos \theta) Y_{l\Lambda}^*(\theta, \phi = 0) \sin \theta d\theta \right] \psi_{n_r l}(r) r^2 dr \quad (\text{B.9})$$

B.2 Deformed Woods-Saxon Potential

In this section we will introduce the single particle wave functions for deformed Woods-Saxon potential with the spin-orbit and other interaction. It is composed of three parts: the centrifugal potential, the spin-orbit interactions and the coulomb interactions which only affect the protons. The centrifugal potential has the form as:

$$V_{w.s.}(r, \theta, \phi) = \frac{V_0}{1 + \exp[(r - R(\theta, \phi))/a(\theta, \phi)]} \quad (\text{B.10})$$

Here V_0 is the depth of the potential well and $R(\theta, \phi)$ is the nuclear radius which may be expressed as [101] $R(\theta, \phi) = R_0\{1 + \beta_2\sqrt{\frac{5}{16\pi}}f(\theta, \phi)\}$, $f(\theta, \phi)$ is an angular function expressed in [118], this shows us the dependence of the potential on the shapes of the nuclei, and the surface diffuseness $a(\theta, \phi)$ has similar angular dependence [118] $a(\theta, \phi) = a_0F(\theta, \phi)$, and we should notice that we have different parameters for protons and neutrons especially the depth of the potential well because of the coulomb corrections.

The spin-orbit interactions have the form:

$$V_{s.o.}(r, \theta, \phi) = 2\left(\frac{\hbar}{m_\pi c}\right)^2 \vec{\nabla} \frac{V_{s.o.}}{1 + \exp[(r - R_{s.o.}(r, \theta, \phi))/a_{s.o.}(r, \theta, \phi)]} \cdot [\vec{\sigma} \times \vec{p}] \quad (\text{B.11})$$

With $V_{s.o.}$ the depth of the spin-orbit potential. $R_{s.o.}$ and $a_{s.o.}$ have the similar form as R and a respectively.

The last part is coulomb potentials which can only have effect on the protons, which has the form:

$$V_c = \int \frac{\rho(r, \theta, \phi)}{1 + \exp[(r' - R_c(r, \theta, \phi))/a_c(r, \theta, \phi)]} \frac{1}{|r - r'|} d^3 r' \quad (\text{B.12})$$

Here ρ is the charge density distribution, and once again R_c and a_c the similar form. And all the radius can be written in the form $R = rA^{1/3}$.

With the radial and spin-orbit potential (for proton also the coulomb potential), we can solve the Shrödinger equation, noticing that the Wood-Saxon Potential is shape dependent (on the quadrupole deformation β_2 and Hexadecupole deformation β_4 , we usually neglect the latter since it contribute less to the solution). We expand the solution on the deformed harmonic basis. In the deformed system, angular momentum J is not a good quantum number. But the projection on the symmetry axis is, also are the parity and the energy. For single particle state $|\tau\Omega_\tau\rangle$ with energy ϵ_τ , one has the state expanded on the deformed harmonic oscillator basis as:

$$|\tau\Omega_\tau\rangle = \sum_{Nn_z\Sigma} b_{Nn_z\Sigma} |Nn_z\Lambda_\tau = \Omega_\tau - \Sigma\rangle |\Sigma\rangle \quad (\text{B.13})$$

Bibliography

- [1] S. L. Glashow, J. Iliopoulos and L. Maiani, Phys. Rev. D **2**, 1285 (1970).
- [2] S. Weinberg, Phys. Rev. Lett. **19**, 1264 (1967).
- [3] D. J. Gross and F. Wilczek, Phys. Rev. D **8**, 3633 (1973).
- [4] R. P. Feynman, Phys. Rev. **76**, 769 (1949).
- [5] J. S. Schwinger, Phys. Rev. **82**, 914 (1951).
- [6] P. W. Higgs, Phys. Rev. Lett. **13**, 508 (1964).
- [7] H. V. Klapdor-Kleingrothaus, A. Dietz, H. L. Harney and I. V. Krivosheina, Mod. Phys. Lett. A **16**, 2409 (2001) [arXiv:hep-ph/0201231].
- [8] M. Mayer, Phys. Rev. Lett. **48**, 512 (1935).
- [9] M. A. Luty, Phys. Rev. D **45**, 455 (1992).
- [10] R. N. Mohapatra and G. Senjanovic, Phys. Rev. Lett. **44**, 912 (1980).
- [11] H. Georgi and S. L. Glashow, Phys. Rev. Lett. **32**, 438 (1974).
- [12] S. Rajpoot, Phys. Rev. D **22**, 2244 (1980).
- [13] N. Arkani-Hamed, S. Dimopoulos and G. R. Dvali, Phys. Lett. B **429**, 263 (1998) [arXiv:hep-ph/9803315].
- [14] N. Arkani-Hamed, S. Dimopoulos, G. R. Dvali and J. March-Russell, Phys. Rev. D **65**, 024032 (2002) [arXiv:hep-ph/9811448].
- [15] M. F. Sohnius, Phys. Rept. **128**, 39 (1985).
- [16] K. A. Brueckner, Phys. Rev. **97**, 1353 (1955).
- [17] D. Gogny, *Proc. of the International Conference on Nuclear Physics*, München, 1973 (North Holland, Amsterdam, 1973).
- [18] H. S. Koehler, Nucl. Phys. A **258**, 301 (1976).
- [19] J. Retamosa, E. Caurier and F. Nowacki, Phys. Rev. C **51**, 371 (1995).

- [20] P. Vogel and M. R. Zirnbauer, Phys. Rev. Lett. **57**, 3148 (1986).
- [21] J. Toivanen and J. Suhonen, Phys. Rev. Lett. **75**, 410 (1995).
- [22] J. Toivanen and J. Suhonen, Phys. Rev. C **55**, 2314 (1997).
- [23] J. Schwieger, F. Simkovic and A. Faessler, Nucl. Phys. A **600**, 179 (1996) [arXiv:nucl-th/9602032].
- [24] V. Rodin and A. Faessler, Phys. Rev. C **66**, 051303 (2002) [arXiv:nucl-th/0205072].
- [25] J. G. Hirsch, O. Castanos and P. O. Hess, Nucl. Phys. A **582**, 124 (1995) [arXiv:nucl-th/9407022].
- [26] R. Chandra, J. Singh, P. K. Rath, P. K. Raina and J. G. Hirsch, Eur. Phys. J. A **23**, 223 (2005) [arXiv:nucl-th/0405074]; S. Singh, R. Chandra, P. K. Rath, P. K. Raina and J. G. Hirsch, Eur. Phys. J. A **33**, 375 (2007) [arXiv:0706.4357 [nucl-th]]; K. Chaturvedi, R. Chandra, P. K. Rath, P. K. Raina and J. G. Hirsch, Phys. Rev. C **78**, 054302 (2008).
- [27] J. Barea and F. Iachello, Phys. Rev. C **79**, 044301 (2009).
- [28] A. S. Barabash, Ph. Hubert, A. Nachab and V. Umatov, J. Phys. Conf. Ser. **203**, 012130 (2010).
- [29] M. S. Yousef, V. Rodin, A. Faessler and F. Simkovic, Phys. Rev. C **79**, 014314 (2009) [arXiv:0806.0964 [nucl-th]].
- [30] W. Pauli, "Brief an die Gruppe der Radioactiven..", Zürich, 4 Dezember, 1930.
- [31] F. Reines and C. L. Cowan, Phys. Rev. **92**, 830 (1953); C. L. Cowan, F. Reines, F. B. Harrison, H. W. Kruse and A. D. McGuire, Science **124**, 103 (1956).
- [32] C. Rubbia, Rev. Mod. Phys. **57**, 699 (1985).
- [33] B. Pontecorvo, Sov. Phys. JETP **6**, 429 (1957) [Zh. Eksp. Teor. Fiz. **33**, 549 (1957)].
- [34] N. Cabibbo, Phys. Rev. Lett. **10**, 531 (1963).
- [35] M. Kobayashi and T. Maskawa, Prog. Theor. Phys. **49**, 652 (1973).
- [36] Z. Maki, M. Nakagawa and S. Sakata, Prog. Theor. Phys. **28**, 870 (1962).
- [37] S. F. King, Rept. Prog. Phys. **67**, 107 (2004) [arXiv:hep-ph/0310204].
- [38] K. Nakamura [Particle Data Group], J. Phys. G **37** (2010) 075021.
- [39] P. Minkowski, Phys. Lett. B **67**, 421 (1977).
- [40] R. N. Mohapatra and G. Senjanovic, Phys. Rev. D **23**, 165 (1981).
- [41] R. N. Mohapatra and J. W. F. Valle, Phys. Rev. D **34**, 1642 (1986).
- [42] M. C. Gonzalez-Garcia and Y. Nir, Rev. Mod. Phys. **75**, 345 (2003) [arXiv:hep-ph/0202058].

- [43] J. Goldstone, *Nuovo Cim.* **19**, 154 (1961).
- [44] Y. Nambu, *Phys. Rev. Lett.* **4** (1960) 380.
- [45] J. Goldstone, A. Salam and S. Weinberg, *Phys. Rev.* **127**, 965 (1962).
- [46] J. Schechter and J. W. F. Valle, *Phys. Rev. D* **25**, 774 (1982).
- [47] Y. Chikashige, R. N. Mohapatra and R. D. Peccei, *Phys. Rev. Lett.* **45**, 1926 (1980).
- [48] P. Bamert, C. P. Burgess and R. N. Mohapatra, *Nucl. Phys. B* **449**, 25 (1995) [arXiv:hep-ph/9412365].
- [49] H. Fritzsch and P. Minkowski, *Annals Phys.* **93**, 193 (1975).
- [50] M. Gell-Mann, P. Ramond and R. Slansky, *Rev. Mod. Phys.* **50**, 721 (1978).
- [51] H. Georgi and D. V. Nanopoulos, *Phys. Lett. B* **82**, 392 (1979).
- [52] M. S. Chanowitz, J. R. Ellis and M. K. Gaillard, *Nucl. Phys. B* **128**, 506 (1977).
- [53] J. C. Pati and A. Salam, *Phys. Rev. D* **10**, 275 (1974) [Erratum-ibid. *D* **11**, 703 (1975)].
- [54] J. C. Pati, S. Rajpoot and A. Salam, *Phys. Rev. D* **17**, 131 (1978).
- [55] T. Nakano and K. Nishijima, *Prog. Theor. Phys.* **10**, 581 (1953).
- [56] L. Randall and R. Sundrum, *Phys. Rev. Lett.* **83**, 3370 (1999) [arXiv:hep-ph/9905221].
- [57] S. Weinberg, *Phys. Lett. B* **143**, 97 (1984).
- [58] A. Pilaftsis, *Phys. Rev. D* **60**, 105023 (1999) [arXiv:hep-ph/9906265].
- [59] G. Bhattacharyya, H. V. Klapdor-Kleingrothaus, H. Pas and A. Pilaftsis, *Phys. Rev. D* **67**, 113001 (2003) [arXiv:hep-ph/0212169].
- [60] K. R. Dienes, E. Dudas and T. Gherghetta, *Nucl. Phys. B* **557**, 25 (1999) [arXiv:hep-ph/9811428].
- [61] S. R. Coleman and J. Mandula, *Phys. Rev.* **159** (1967) 1251.
- [62] R. Haag, J. T. Lopuszanski and M. Sohnius, *Nucl. Phys. B* **88**, 257 (1975).
- [63] S. P. Martin, arXiv:hep-ph/9709356.
- [64] P. Fayet and J. Iliopoulos, *Phys. Lett. B* **51** (1974) 461.
- [65] L. O'Raiheartaigh, *Nucl. Phys. B* **96**, 331 (1975).
- [66] E. Cremmer, S. Ferrara, L. Girardello and A. Van Proeyen, *Nucl. Phys. B* **212**, 413 (1983).
- [67] M. Dine and W. Fischler, *Phys. Lett. B* **110**, 227 (1982).
- [68] M. Dine and A. E. Nelson, *Phys. Rev. D* **48**, 1277 (1993) [arXiv:hep-ph/9303230].

- [69] V. A. Rubakov and M. E. Shaposhnikov, *Phys. Lett. B* **125** (1983) 136.
- [70] G. R. Farrar and P. Fayet, *Phys. Lett. B* **76**, 575 (1978).
- [71] S. Dimopoulos and H. Georgi, *Nucl. Phys. B* **193**, 150 (1981).
- [72] A. Masiero and J. W. F. Valle, *Phys. Lett. B* **251**, 273 (1990).
- [73] M. Hirsch, H. V. Klapdor-Kleingrothaus and S. G. Kovalenko, *Phys. Rev. Lett.* **75**, 17 (1995);
M. Hirsch, H. V. Klapdor-Kleingrothaus and S. G. Kovalenko, *Phys. Rev. D* **53**, 1329 (1996)
[arXiv:hep-ph/9502385].
- [74] J. D. Vergados, *Phys. Lett. B* **184**, 55 (1987).
- [75] H. E. Haber and G. L. Kane, *Phys. Rept.* **117**, 75 (1985).
- [76] J. Erler and P. Langacker, *Phys. Rev. D* **52**, 441 (1995) [arXiv:hep-ph/9411203].
- [77] S. L. Adler, E. W. Colglazier, J. B. Healy, I. Karliner, J. Lieberman, Y. J. Ng and H. S. Tsao,
Phys. Rev. D **11**, 3309 (1975).
- [78] A. Faessler, S. Kovalenko, F. Simkovic and J. Schwieger, *Phys. Rev. Lett.* **78**, 183 (1997)
[arXiv:hep-ph/9612357].
- [79] A. Faessler, T. Gutsche, S. Kovalenko and F. Simkovic, *Phys. Rev. D* **77**, 113012 (2008)
[arXiv:0710.3199 [hep-ph]].
- [80] A. Faessler, S. Kovalenko and F. Simkovic, *Phys. Rev. D* **58**, 055004 (1998) [arXiv:hep-ph/9712535].
- [81] F. Simkovic, G. Pantis, J. D. Vergados and A. Faessler, *Phys. Rev. C* **60**, 055502 (1999)
[arXiv:hep-ph/9905509].
- [82] J. D. Vergados, *Phys. Rev. C* **24**, 640 (1981).
- [83] J. D. Vergados, *Phys. Rev. D* **25**, 914 (1982).
- [84] J. D. Vergados, *Phys. Rept.* **133**, 1 (1986).
- [85] K-C. Chou, *Soviet Physics JETP* **12**, 492(1961).
- [86] J. Bernstein, S. Fubini, M. Gell-Mann and W. Thirring, *Nuovo Cimento* **17**,757(1960).
- [87] G. Prezeau, M. Ramsey-Musolf and P. Vogel, *Phys. Rev. D* **68**, 034016 (2003) [arXiv:hep-ph/0303205].
- [88] M. Doi, T. Kotani, H. Nishiura, K. Okuda and E. Takasugi, *Phys. Lett. B* **103**, 219 (1981)
[Erratum-ibid. **113B**, 513 (1982)].
- [89] M. Doi, T. Kotani and E. Takasugi, *Prog. Theor. Phys. Suppl.* **83**, 1 (1985).
- [90] M. Doi, T. Kotani, H. Nishiura and E. Takasugi, *Prog. Theor. Phys.* **69**, 602 (1983).

- [91] M. Doi, T. Kotani, H. Nishiura, K. Okuda and E. Takasugi, *Prog. Theor. Phys.* **66**, 1739 (1981) [Erratum-ibid. **68**, 347 (1982)]; M. Doi, T. Kotani, H. Nishiura, K. Okuda and E. Takasugi, *Prog. Theor. Phys.* **66**, 1765 (1981) [Erratum-ibid. **68**, 348 (1982)].
- [92] G. A. Miller and J. E. Spencer, *Annals Phys.* **100**, 562 (1976).
- [93] M. Hjorth-Jensen, T. T. S. Kuo and E. Osnes, *Phys. Rept.* **261**, 125 (1995).
- [94] W. C. Haxton and G. J. Stephenson, *Prog. Part. Nucl. Phys.* **12** (1984) 409.
- [95] A. N. Kamal and J. N. Ng, *Phys. Rev. D* **20**, 2269 (1979).
- [96] G. K. Leontaris and J. D. Vergados, *Nucl. Phys. B* **224**, 137 (1983).
- [97] T. Tomoda, *Rept. Prog. Phys.* **54**, 53 (1991).
- [98] D. J. Rowe, *Rev. Mod. Phys.* **40**, 153 (1968).
- [99] G. E. Brown, J. A. Evans and D. J. Thouless, *Nucl. Phys.* **24**, 1(1961).
- [100] M. Baranger, *Phys. Rev.* **120**, 957(1960).
- [101] P. Ring and P. Schuck, *The Nuclear Many-Body Problem*(Springer-Verlag, New York, 1980).
- [102] C. P. Burgess and J. M. Cline, *Phys. Rev. D* **49**, 5925 (1994) [arXiv:hep-ph/9307316].
- [103] H. Primakoff and S. P. Rosen, *Phys. Rev.* **184**, 1925 (1969).
- [104] A. Faessler and F. Simkovic, *J. Phys. G* **24**, 2139 (1998) [arXiv:hep-ph/9901215].
- [105] J. Bardeen, L. N. Cooper and J. R. Schrieffer, *Phys. Rev.* **106**, 162 (1957); J. Bardeen, L. N. Cooper and J. R. Schrieffer, *Phys. Rev.* **108** (1957) 1175.
- [106] F. Simkovic, L. Pacearescu and A. Faessler, *Nucl. Phys. A* **733**, 321 (2004) [arXiv:nucl-th/0308037].
- [107] G. Pantis, F. Simkovic, J. D. Vergados and A. Faessler, *Phys. Rev. C* **53**, 695 (1996) [arXiv:nucl-th/9612036].
- [108] A. A. Raduta, F. Simkovic and A. Faessler, *J. Phys. G* **26**, 793 (2000).
- [109] J. Schwieger, F. Simkovic, A. Faessler and W. A. Kaminski, *Phys. Rev. C* **57**, 1738 (1998).
- [110] L. Pacearescu, V. Rodin, F. Simkovic and A. Faessler, *Phys. Rev. C* **68**, 064310 (2003) [Erratum-ibid. **C 75**, 059902 (2007)] [arXiv:nucl-th/0308035].
- [111] M. S. Yousef, *PhD Thesis*, University Tübingen(2009).
- [112] E. Caurier, G. Martinez-Pinedo, F. Nowacki, A. Poves and A. P. Zuker, *Rev. Mod. Phys.* **77**, 427 (2005) [arXiv:nucl-th/0402046].
- [113] E. Caurier, F. Nowacki, A. Poves and J. Retamosa, *Phys. Rev. Lett.* **77**, 1954 (1996).
- [114] B. A. Brown, *Prog. Part. Nucl. Phys.* **47**, 517(2001).

- [115] E. Caurier and F. Nowacki, *Acta. Phys. Polon. B* **30**, 705(1999).
- [116] V. Rodin and A. Faessler, *Phys. Rev. C* **80**, 041302 (2009) [arXiv:0906.1759 [nucl-th]].
- [117] V. A. Rodin, A. Faessler, F. Simkovic and P. Vogel, *Nucl. Phys. A* **766** (2006) 107 [Erratum-
ibid. A **793** (2007) 213] [arXiv:0706.4304 [nucl-th]].
- [118] Y. Tanaka, Y. Oda, F. Petrovich and R. K. Sheline, *Phys. Lett. B* **83**, 279(1979).
- [119] F. Simkovic, A. Faessler, V. Rodin, P. Vogel and J. Engel, *Phys. Rev. C* **77**, 045503 (2008)
[arXiv:0710.2055 [nucl-th]].
- [120] F. Simkovic, A. Faessler, H. Muther, V. Rodin and M. Stauf, *Phys. Rev. C* **79**, 055501 (2009)
[arXiv:0902.0331 [nucl-th]].
- [121] R. Nojarov, Z. Bochnacki and A. Faessler *Z. Phys. A* **324**, 289(1986).
- [122] R. Machleidt, K. Holinde and C. Elster, *Phys. Rept.* **149**, 1 (1987).
- [123] G. Audi and A. H. Wapstra, *Nucl. Phys. A* **595**, 409 (1995); G. Augid, O. Bersillon, J. Blachot
and A. H. Wapstra, *Nucl. Phys. A* **624**, 1 (1997).
- [124] P. Raghavan, *At. Data Nucl. Data Tabl.* **42**, 189(1989).
- [125] S. Raman, C. W. G. Nestor and P. Tikkanen, *Atom. Data Nucl. Data Tabl.* **78**, 1 (2001).
- [126] G. A. Lalazissis, S. Raman and P. Ring, *Atom. Data Nucl. Data Tabl.* **71**, 1 (1999).
- [127] P. Möller and J. R. Nix, *Nucl. Phys. A* **520**, 369(1990).
- [128] P. Sarriguren, E. Moya de Guerra and A. Escuderos, *Nucl. Phys. A* **658**, 13 (1999)
[arXiv:nucl-th/9907085].
- [129] R. Alvarez-Rodriguez, P. Sarriguren, E. Moya de Guerra, L. Pacearescu, A. Faessler and
F. Simkovic, *Phys. Rev. C* **70**, 064309 (2004) [arXiv:nucl-th/0411039].
- [130] D. Fang, A. Faessler, V. Rodin, M. S. Yousef and F. Simkovic, *Phys. Rev. C* **81**, 037303
(2010) [arXiv:0910.3090 [nucl-th]].

Acknowledgements

First of all, I would like to give my greatest appreciation to my supervisor, Prof. Dr. Dr. mult. h.c. Amand Fäßler for giving me this opportunity to work as a PhD student under his guidance and support, thanks for his valuable advices on my research and helpful discussions and corrections on my thesis. Under his supervision, I can make the transformation from a student to a researcher.

Sincere acknowledgement would be given to Dr. Vadim Rodin for his kindness and assistance on helping me finish this work of $\beta\beta$ -decay, his useful discussions and comments have key importance for my achievement of these calculations. I appreciate his help for me to overcome all these obstacles during my developments of codes and the literatures of this thesis.

I would like also to thank Prof. Fedor Simkovic for helpful discussions and comments during this process.

I would also like to thank my friends and colleagues in this institute for their kind help during my stay here, especially to Dr. Y.L. Ma, Dr. M. S. Youssef, Dr. P. Gorygorov, Prof. Y.P. Yan, Dr. A. Escuderos and all others, for their useful discussions on both science and other topics.

Special thanks to all my Chinese friends here in Tübingen, they make me really enjoy my stay here and make me away from homesick, particularly to people as following: Dr. J.W. Liu, Dr. Zh.Y. Zhang, Mr. T. Li, Ms. Y. X. Zhang, Mr. T. Wei, *etc.*

Finally, all my thanks to my family, my parents, for their giving birth to me, for their continuing support in heart and soul on my study and research, without them I cannot be whom I am right now. It's a pity that my father cannot witness all these works I have done during my PhD study, as a traffic accident deprived his life years before my study here, *r.i.p.* my beloved father, you will always be with me.